SHORT NOTES ON ALASKAN GEOLOGY 1993

Professional Report 113

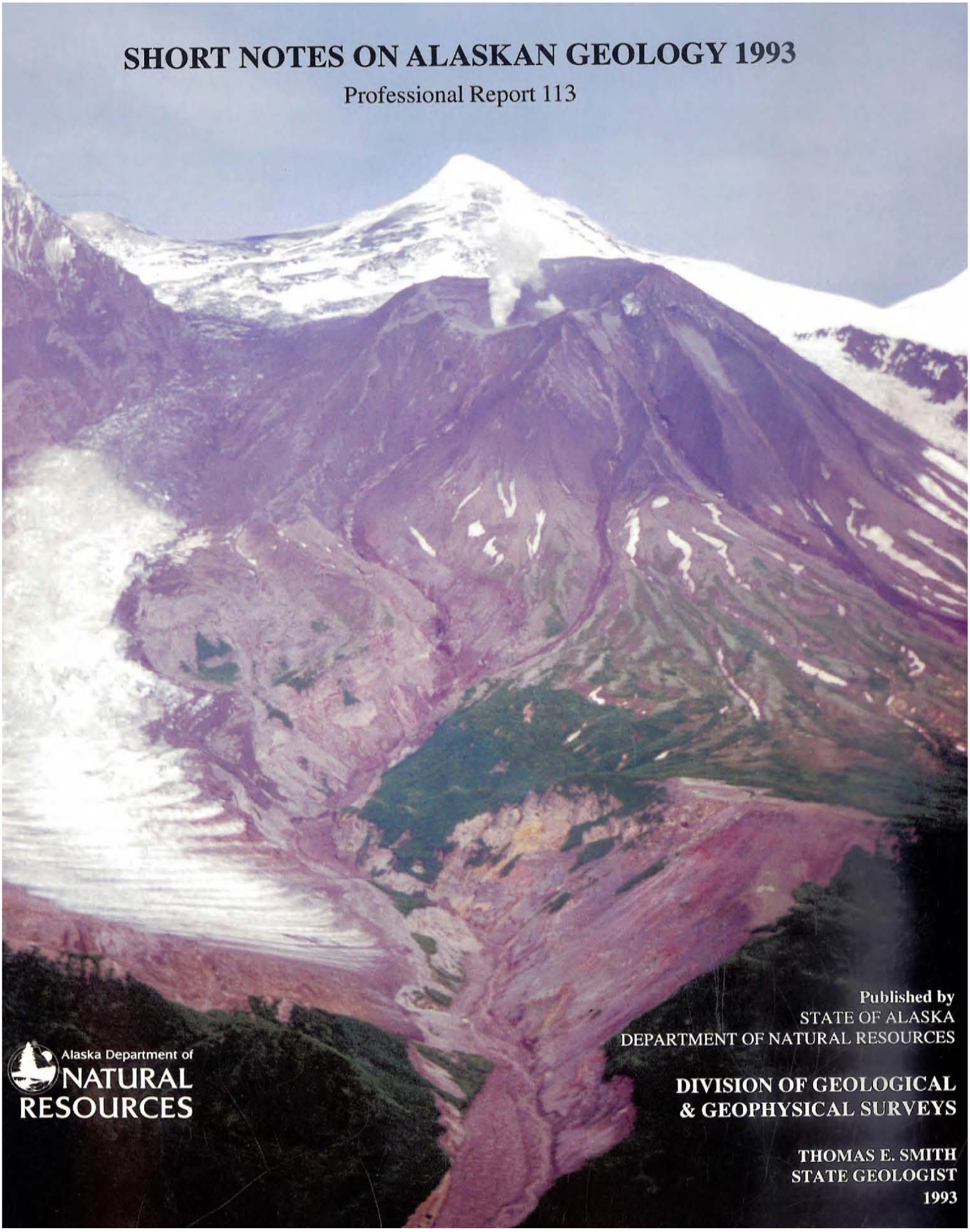

Published by
STATE OF ALASKA
DEPARTMENT OF NATURAL RESOURCES

DIVISION OF GEOLOGICAL
& GEOPHYSICAL SURVEYS

THOMAS E. SMITH
STATE GEOLOGIST

1993

Alaska Department of
NATURAL
RESOURCES

EDITORIAL POLICY

"Short Notes on Alaskan Geology" is a collection of brief contributions describing recent geological investigations of limited scope. This publication is widely distributed to a state, national, and international audience that represents industry, academia, government agencies, and the general public. Manuscripts are accepted for consideration with the understanding that they have not been previously published and are not being submitted for publication elsewhere, that all persons listed as authors have given their approval for submission of the paper, and that any person cited as a source of personal communication has approved such a citation. Authors are encouraged to suggest appropriate reviewers and provide reviewer's telephone numbers.

SUBMISSION OF MANUSCRIPTS

Authors should submit three paper copies of their draft manuscripts to Short Notes Editor, Alaska Division of Geological and Geophysical Surveys, 794 University Avenue, Suite 200, Fairbanks, Alaska 99709-3645. Contributors should retain one copy of all materials submitted. DGGS is not responsible for materials lost in the mail. In general, articles are limited to about 10 manuscript pages (approximately 2,000 words of text), including references, figures, and tables.

All draft manuscripts will be examined and approved by the DGGS editor and at least two reviewers. After technical reviews are completed, copies of review forms and reviewed manuscript pages will be returned to the author for revision (if required) and resubmittal. Conflicts between reviewers and authors must be resolved to the satisfaction of the DGGS editor before final acceptance of manuscripts. Final submittals must be provided as double-spaced paper copy and on high-density PC diskette (Microsoft Word or Word Perfect). Questions should be directed to the DGGS editor 907-474-7147. Major changes by the author—whether scientific or editorial—are not permitted after the manuscript is in galley form.

TEXT PREPARATION

Manuscripts should be double spaced with 1-inch margins on all sides. The title page should include the title of the article and the name(s) and affiliation(s) of the author(s). Because of the brevity of Short Notes articles, tables of contents, lists of illustrations, and abstracts are not needed. Words to be printed in italics should be typed in italics.

Specific guidelines for units of measure, abbreviations, and references are provided in *Suggestions to Authors of Reports of the United States Geological Survey* (7th edition)" or *Government Printing Office Style Manual 1973*. Potential authors are also encouraged to consult the latest issue of Short Notes for information.

PREPARATION OF ILLUSTRATIONS

All figures should be provided in camera-ready form. Computer-generated illustrations are acceptable. Line figures are generally published in black and white, but color art may be accepted with the understanding that the author will pay additional costs (color separation and printing) for colored figures. Current page-cost information can be obtained from the DGGS editor. Maximum size for figures is 6.5 by 8.5 inches. Large foldouts are not accepted.

SHORT NOTES ON ALASKAN GEOLOGY 1993

Edited by Diana N. Solie and Fran Tannian
Cover design by Ann-Lillian C. Schell

Professional Report 113

Recent research on Alaskan geology

Fairbanks, Alaska
1993

STATE OF ALASKA
Walter J. Hickel, *Governor*

DEPARTMENT OF
NATURAL RESOURCES
Glenn A. Olds, *Commissioner*

DIVISION OF GEOLOGICAL &
GEOPHYSICAL SURVEYS
Thomas E. Smith, *State Geologist*

Division of Geological & Geophysical Surveys publications may be inspected at the following locations. Address mail orders to the Fairbanks office.

Alaska Division of Geological &
Geophysical Surveys
Attn: Publications
794 University Avenue, Suite 200
Fairbanks, Alaska 99709-3645

Department of Natural Resources
Public Information Center
3601 C Street, Suite 200
Anchorage, Alaska 99510

This publication, released by the Division of Geological & Geophysical Surveys, was produced and printed in Anchorage, Alaska by A.T. Publishing & Printing, Inc., at a cost of $6 per copy. Publication is required by Alaska Statute 41, "to determine the potential of Alaskan land for production of metals, minerals, fuels, and geothermal resources; the location and supplies of groundwater and construction materials; the potential geologic hazards to buildings, roads, bridges, and other installations and structures; and shall conduct such other surveys and investigations as will advance knowledge of the geology of Alaska."

FOREWORD

The Division of Geological & Geophysical Surveys (DGGS) is pleased to continue the series *Short Notes on Alaskan Geology*. This unique source of brief but informative papers on a wide variety of topics related to geology in Alaska represents the works of earth scientists in state and federal agencies, universities, and industry. Because of their brevity and limited scope, many of the papers in this series might not be appropriate for publication in journals with more national and international focus. Nonetheless, the subject matter is very useful to those interested in learning more about the geology of Alaska. The *Short Notes* series is intended to serve as the medium through which these papers can be made available to the geologic community.

This 1993 volume, the seventh in the series, is the second in a renewed commitment by DGGS to the *Short Notes* series. After a hiatus of several years, *Short Notes on Alaskan Geology 1991* was published, due in large part to the energies of Dr. Richard D. Reger, who undertook the editorial task. We now continue with this volume, establishing a new biennial pattern for the series. This new timeframe will allow potential authors to anticipate manuscript submittal deadlines and thus increase the number of papers for consideration in each volume. Biennial publication generates realistic demands on the editorial and production staff and on publishing costs. Instructions for contributing authors that are printed inside the front cover are intended to encourage future contributions from inside and outside of DGGS. We are hoping for ever greater interest from the entire earth science community and increased participation in this unique series.

Thomas E. Smith
State Geologist

Erratum The back cover caption should read:

Thick buried peat layers are laterally extensive beneath the salt marsh at Chickaloon Bay and are exposed in meander banks along the Chickaloon River and other streams crossing the marsh. At location 92-17 (lower photograph), rooted wood from the top of the uppermost buried peat layer has a calibrated radiocarbon age of 0-259 yr B.P. and was probably submerged and buried as a result of subsidence during the 1964 event. Peat from the top of the second buried peat layer (at shovel tip) has a calibrated age of 761-1,060 yr B.P. and was probably buried as a result of the previous great earthquake. Photos by R.A. Combellick.

CONTENTS

Front cover: *Northward view of Crater Peak on June 28, 1992, the day after a moderate eruption deposited 50 million m^3 of ash as far north as Manley Hot Springs, 420 km downwind. Note that ash covers the snow on only the upper half of the cone, a result of the strong southerly winds during the eruption. A narrow, dark debris flow, also formed on June 27, descends the southeast flank. This eruption was the first of three from Crater Peak during the summer of 1992. On August 18 the second eruption deposited 3 mm of ash on Anchorage 125 km to the east and closed the airport for a day. On September 17 the third eruption deposited ash on Palmer and Wasilla and as far east as Beaver Creek in the Yukon Territory. All told, 210 million m^3 of ash were erupted, equivalent to 80 million m^3 of magma.*

The prominent gully on the south flank of Crater Peak was formed during the previous eruption in 1953. At that time debris flows generated by the melting of snow and ice filled the crater and partially dammed the Chakachatna River. Crater Peak is a 2,309-m-high andesitic cone that occupies the southern breach in a 5-by 6-km horseshoe-shaped caldera that formed during catastrophic destruction of the ancestral Mount Spurr stratovolcano in late Pleistocene time. The current summit of Mount Spurr (the high summit behind Crater Peak) is a 3,374-m-high dacitic dome in the center of the caldera. Photo by Diana N. Solie.

MISSISSIPPIAN TERRIGENOUS CLASTIC AND VOLCANICLASTIC ROCKS OF THE ELLESMERIAN SEQUENCE, UPPER SHEENJEK RIVER AREA, EASTERN BROOKS RANGE, ALASKA

by
Arlene V. Anderson,[1] C.G. Mull,[2] and R. Keith Crowder[1]

INTRODUCTION

In the upper headwaters of the Kongakut River southwest of Bathtub Ridge in the eastern Brooks Range, detailed field studies have identified a thick section of Middle Devonian and Lower Mississippian clastic deposits (Anderson,1991; Anderson, Crowder, and Wallace, 1991; Anderson and Wallace, 1991; Anderson, Wallace, and Mull, 1992). These rocks were divided into two unconformity-bounded depositional sequences that are interpreted as the basal rift deposits of the Ellesmerian sequence. Nonmarine, terrigenous-clastic deposits of the upper depositional sequence correlate with the Kekiktuk Conglomerate, a widespread Lower Mississippian clastic unit in the northeastern Brooks Range. Reiser and others (1980) originally recognized the lower depositional sequence, which consists of shallow-marine and nonmarine clastic rocks which they dated as Middle(?) Devonian. This sequence apparently crops out only in the eastern Brooks Range. A low-angle unconformity separates the two depositional sequences.

A reconnaissance survey in 1991 traced the lateral distribution of the two depositional sequences westward and evaluated the significance of a reported greenstone interval (Mull, unpublished field notes, 1971) in the clastic sequence. The survey began in the upper Kongakut River area and extended 20 km west to the upper Sheenjek River drainage (fig. 1). In 1971, Mull traversed a ridge and canyon on the southwest side of the upper Sheenjek River (fig. 2, traverse 1); the 1991 traverse was made 5 km farther west (fig. 2, traverse 2). This report discusses some of the results of the reconnaissance and documents the presence of a thick interval of volcaniclastic rocks interbedded with the Mississippian clastic rocks in the upper Sheenjek River area.

[1]Tectonics and Sedimentation Research Group, Geophysical Institute & Department of Geology & Geophysics, University of Alaska, Fairbanks, Alaska 99775.
[2]Alaska Division of Geological & Geophysical Surveys, Fairbanks, Alaska 99709-3645.

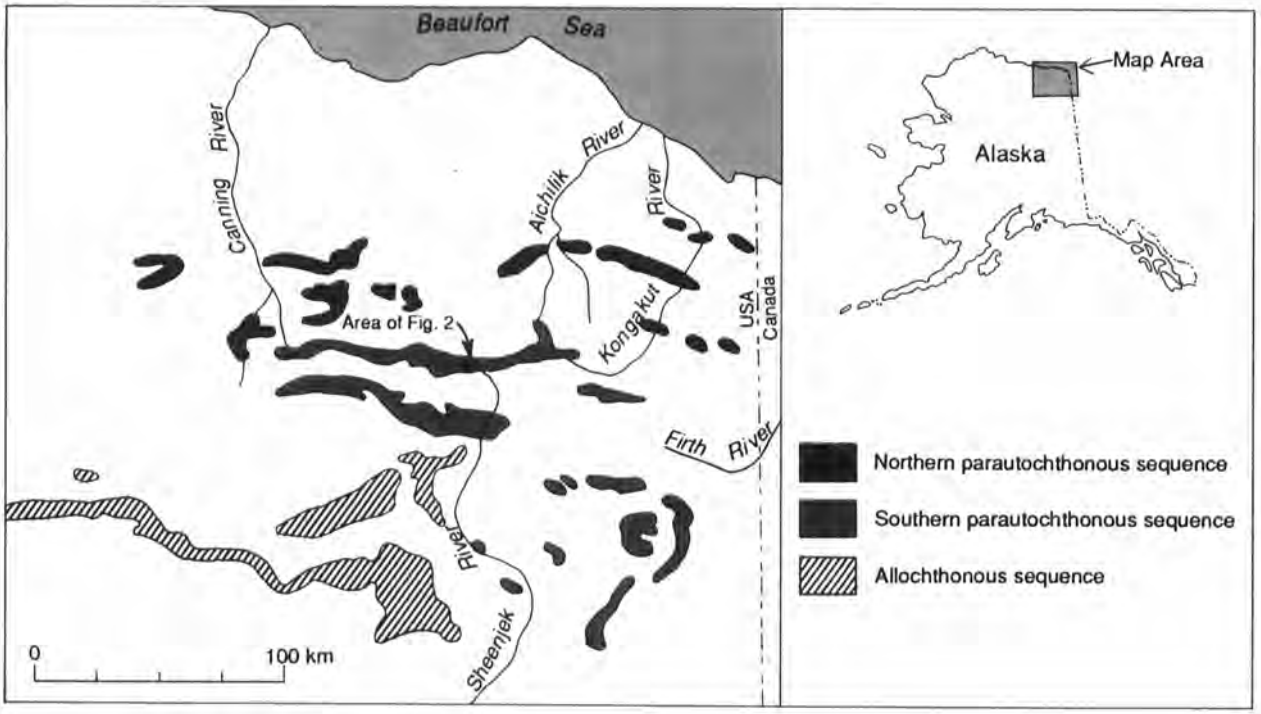

Figure 1. *Devonian to Mississippian terrigenous clastic deposits in eastern Brooks Range.*

DESCRIPTION OF UPPER SHEENJEK RIVER SUCCESSION

The stratigraphic succession on the southwest side of the upper Sheenjek River was partially described along two traverses separated by about 5 km (fig. 2, traverses 1 and 2). Figure 3 schematically illustrates the generalized stratigraphic succession at traverse 2. At both localities, the rocks traversed are overlain by the Lower Mississippian Kayak Shale and the cliff-forming carbonate rocks of the Mississippian-Lower Pennsylvanian Lisburne Group. Below the Kayak Shale, the stratigraphic succession consists of three lithologic units: Unit A, at the base, which consists mainly of massive conglomerate; Unit B, a middle assemblage composed mainly of basaltic volcaniclastic rocks; and Unit C, an upper assemblage of terrigenous clastic rocks. All the resistant units dip uniformly about 20° S. The upper and lower contacts of the volcaniclastic unit are sharp and apparently conformable with the underlying and overlying nonvolcanic, terrigenous-clastic rocks.

UNIT A

Unit A overlies a prominent bench that marks the position of a major thrust fault that can be traced along the north end of several ridges on the south side of the upper Sheenjek River valley. The lower part of unit A consists of a recessive-weathering interval of probable siltstone that is overlain by 80 m of interbedded shale and pebble-granule conglomerate beds organized in a series of 2- to 6-m-thick fining-upward cycles. These well-bedded deposits are abruptly overlain by a thick unbroken unit of about 100 m of poorly organized chert-pebble conglomerate and coarse-grained sandstone with internal large-scale, channeled erosion surfaces. Clasts in the conglomerate are mainly subrounded white, gray, and black chert and subordinate green and red chert. The unit represents an abrupt change from the more thinly bedded character of the underlying rocks. The contact with the overlying volcanic rocks of Unit B is a 1-m-thick covered interval, but the beds above and below the contact appear to be conformable, and there is no evidence of a fault within the covered interval. There is no indication of a baked zone at the top of the clastic rocks below the covered interval.

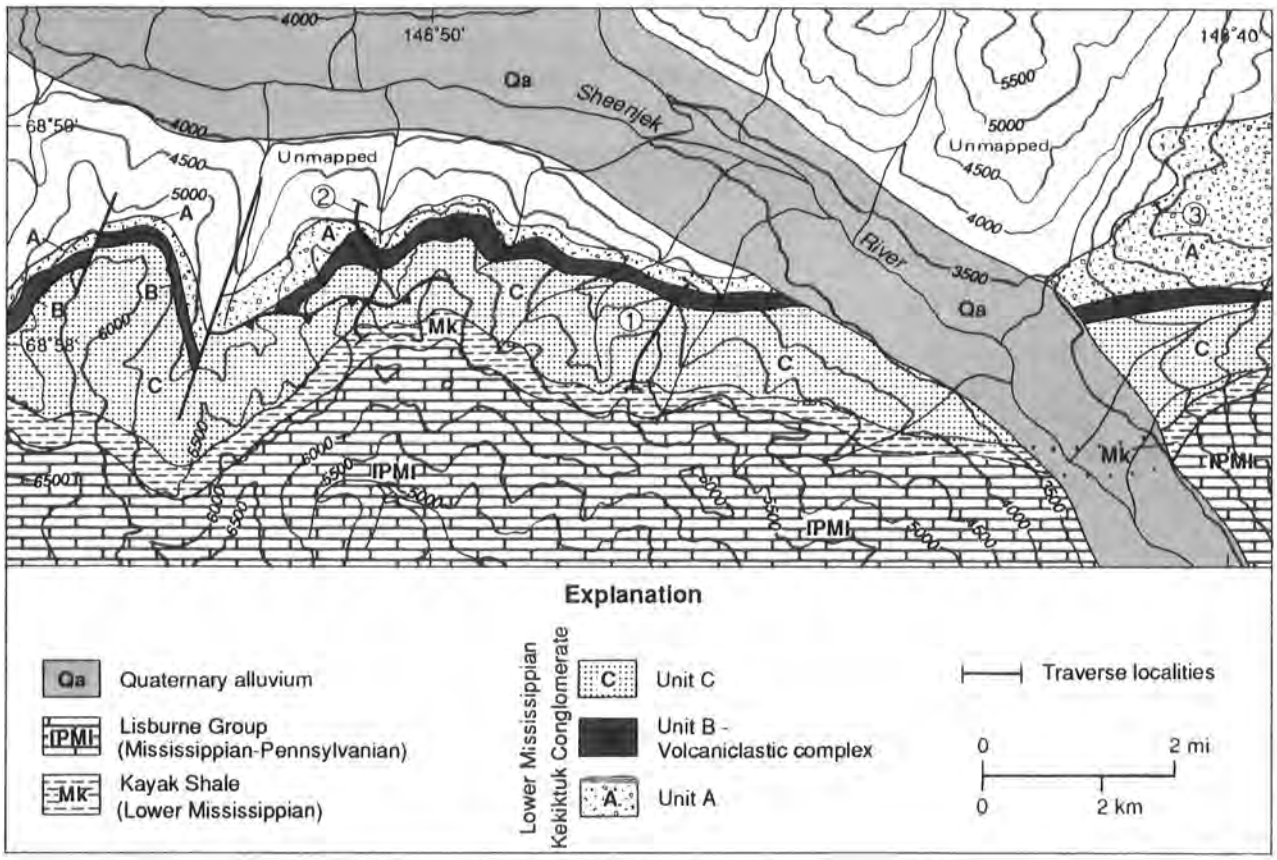

Figure 2. *Location and stratigraphic relationships of volcaniclastic rocks in the upper Sheenjek River valley.*

UNIT B

Unit B consists of about 100 m of basaltic volcaniclastic rocks. The unit forms distinctive steep, resistant, greenish-brown-weathering slopes and cliffs that can be traced easily along the north faces of the ridges that flank the south side of the upper Sheenjek River in the map area (fig. 2). In the area of traverse 2, this resistant unit is high on the ridges, but, because of regional dip, along strike to the east the volcaniclastic unit is progressively lower and closer to the valley bottom. Along traverse 2, above an apparently sharp basal contact, the lower beds of the volcaniclastic unit are dark green, fine grained, and relatively homogeneous. In places the basal 2-3 cm of the beds are graded and contain coarse basaltic fragments in a fine-grained matrix. The upper part of the unit consists of poorly sorted volcaniclastic rocks that include both unsorted, matrix-supported volcanic breccia with angular clasts to 20 cm and unsorted, rounded to subrounded volcanic clasts to 70 cm (fig. 4). Petrographic study shows that some clasts are composed of clinopyroxene phenocrysts in a fine-grained altered olivine-rich groundmass. These deposits appear to have a pyroclastic origin but may exhibit some reworking.

Along traverse 1 (fig. 2), unit B forms low resistant spurs on the north faces of the ridges near the valley bottom. The unit is about 15 m thick and consists entirely of dark-green, fine-grained schistose volcaniclastic rock.

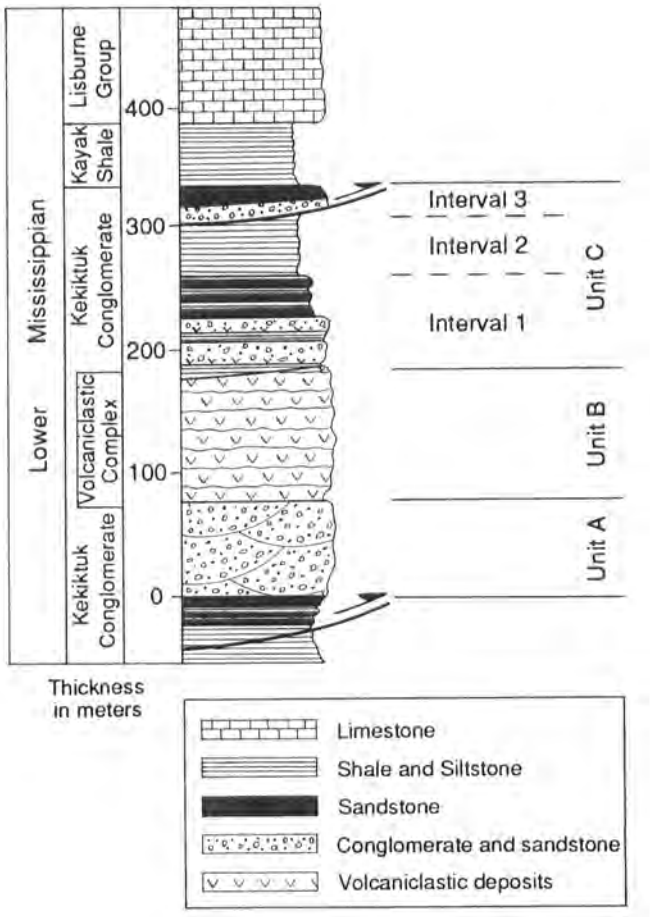

Figure 3. *Generalized stratigraphic succession at traverse 2.*

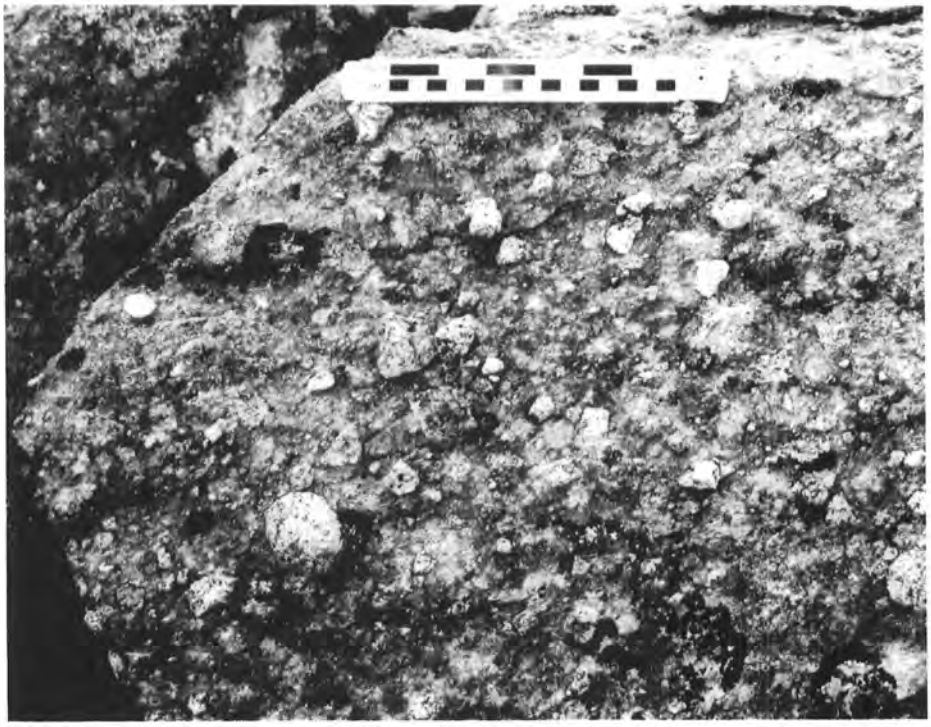

Figure 4. *Volcaniclastic rocks of unit B, 15 cm scale.*

In general, the volcaniclastic rocks become progressively thinner and finer grained eastward from the area of traverse 2.

Two rock samples of unit B were submitted to Paul Layer of the Geophysical Institute Geochronology Laboratory, University of Alaska Fairbanks, for whole-rock $^{40}Ar/^{39}Ar$ analysis. One sample, a volcanic breccia, was unsuitable for dating. The second sample, (91A-68B), an altered, very-fine grained volcanic rock, yielded a plateau age of 80 Ma. There is no evidence of any thermal event affecting the sample after 80 Ma. Inasmuch as the volcanic rocks are interbedded with rocks of Mississippian age, we interpret this date to be a reset age caused by cooling after either a low-grade metamorphic event (regional or local) or deep burial. No dates in the range of 80 Ma are known elsewhere in the eastern Brooks Range, and the significance of this single date in the Sheenjek River valley is unknown.

Unit C

Unit C is a succession of terrigenous-clastic deposits that overlies the volcaniclastic deposits of Unit B at an apparently sharp contact and that conformably underlies the Kayak Shale. The unit is divided into three intervals, from bottom to top: C-1, C-2, and C-3. Interval C-1, about 75 m thick, is a generally thinning- and fining-upward interval. The lower part contains two thick massive 3- to 4 m- thick beds of pebble to cobble conglomerate. The lower parts of both beds are poorly sorted volcanic and chert clasts that appear to have been deposited as debris flows; both beds grade upward into dominantly chert-pebble conglomerate. The upper part of the interval C-1 contains a series of well-bedded fining-upward successions of quartzose sandstone. Interval C-1 is overlain by an interval of 50 m of fine-grained sandstone, siltstone, and shale. The shale forms interval C-2, a dominantly recessive unit that contains scattered fragments of plant fossils and anthracite. Unit C-3 consists of about 25 m of resistant chert-pebble conglomerate and quartz sandstone, and, based upon lithologic similarity and map relationships, Unit C-3 appears to be a thrust-faulted repetition of part of Unit C-1. Along traverse 1, non-age diagnostic smooth-shelled linguloid brachiopods were noted in sandstones that may occupy the stratigraphic position of interval of C-1 or C-2.

CORRELATIONS

The terrigenous clastic rocks that underlie the Kayak Shale in both the Kongakuk River area and the upper Sheenjek River area appear to have the same general organization and character. However, the upper Sheenjek River succession differs from that in the Kongakut River area because of the presence of the thick, massive, poorly sorted conglomerate interval (unit A) and overlying volcaniclastic rocks (unit B) within the section. Based on lithology and stratigraphic position below the Kayak Shale, the terrigenous clastic deposits of intervals C-1 and C-3 correlate with the upper part of the Kekiktuk Conglomerate. Interval C-2 appears to be lower Kayak Shale overlying upper Kekiktuk Conglomerate of unit C1.

In the upper Kongakut River area, the base of the Kekiktuk Conglomerate is marked by a sharp contact and a low-angle unconformity that truncates the underlying Middle to Upper(?) Devonian Ulungarat Formation (Anderson, 1991); a similar relationship is exposed in a cliff on the northeast side of the Sheenjek River at the east edge of the map in figure 2, traverse 3. Here the base of the Kekiktuk Conglomerate (unit A) is a thick, massive, cliff-forming conglomerate about 100 m thick that truncates the Ulungarat Formation at a sharp contact (fig. 5). Locally on the northeast side of the Sheenjek River, this massive conglomerate unit is overlain by a thin inconspicuous section of the volcaniclastic unit (T.E. Moore, oral commun., 1992). On the basis of these relationships and the stratigraphic position below the Kayak Shale, we interpret units A and C to correlate with the Kekiktuk Conglomerate. On the basis of its apparent stratigraphic position above the basal Kekiktuk on the northeast side of the Sheenjek River and along the south side of the valley, the volcaniclastic unit seems to be an important part of the Kekiktuk succession in the upper Sheenjek area.

Distribution of Volcaniclastic Rocks

The volcaniclastic unit has been traced along strike for about 10 km, but its extent both to the east and west of the map area (fig. 1) is unknown. The extent of volcaniclastic rocks within the Kekiktuk to the south is also unknown. However, in the area of Double Mountain, about 40 km south of the map area, conspicuous green- and yellow-weathering schistose volcanic rocks are apparently interbedded with thick sections of coarse conglomerate and quartzite of unknown age. Future detailed studies in the area may show that the volcaniclastic rocks can serve as a correlation marker in the southeastern Brooks Range.

Figure 5. *Basal Kekiktuk Conglomerate unconformably overlying Middle Devonian Ulungarat Formation on northeast side of upper Sheenjek River (fig. 1, traverse 3).*

TECTONIC SIGNIFICANCE

The abrupt lateral and vertical variability of the parautochthonous succession of Middle Devonian and Lower Mississippian terrigenous clastic rocks in northern Alaska has been interpreted to reflect basal rift deposition during formation of the Ellesmerian south-facing continental margin of Arctic Alaska (Anderson, Wallace, and Mull, 1992; and Moore and others, 1992). Interbedded mafic volcanic rocks have not previously been reported within the parautochthonous nonmarine Devonian to Mississippian clastic succession in northern Alaska. Volcaniclastic deposits are reported interbedded within parautochthonous carbonate rocks of the Lisburne Group 175 km northwest of the Sheenjek River area (Keller and others, 1961; Brosgé and others, 1979; Robinson and others, 1989). Extrusive volcanic rocks are also present in an allochthonous Lower Mississippian succession in the Endicott Mountains of the central Brooks Range (Mull, unpublished field notes, 1990, 1992.)

Mafic volcanic rocks interbedded with fluvial and lacustrine sediments are characteristic of the first evolutionary stage of a rifted continental margin (Miall, 1984). The presence of such rocks in the Sheenjek River area thus supports a rift interpretation for the evolution of the late Paleozoic continental margin of northern Alaska. However, understanding of the details and timing of this evolution awaits further study of the stratigraphic relationships in the Sheenjek River area and other areas in the eastern Brooks Range.

ACKNOWLEDGMENTS

We thank C.J. Nye and W.K. Wallace for their helpful comments and thoughtful critique of a preliminary version of this paper. This work was supported by the Tectonics and Sedimentation Research Group, Geophysical Institute, University of Alaska Fairbanks, with funding from Amoco Production Company, ARCO Alaska, Inc., BP Exploration (Alaska) Inc., Chevron USA, Inc, Conoco Inc., Elf Exploration Inc., Exxon Company, USA, Japan National Oil Corporation, Mobil Exploration and Producing U.S. Inc., Murphy Exploration and Production Company, Phillips Petroleum Company, Shell Western Exploration & Production Inc., Texaco Inc., and Union Oil Company of California.

REFERENCES CITED

Anderson, A.V., 1991, Ulungarat Formation, type section of a new formation, headwaters of the Kongakut River, eastern Brooks Range: Alaska Division of Geological and Geophysical Surveys Public Data-File 91-4, 27 p.

Anderson, A.V. and Wallace, W.K., 1991, Middle Devonian to Early Mississippian stratigraphic record of the formation of a passive continental margin in northeastern Alaska: Geological Society of America Abstracts with Programs, v. 23, no. 5, p. 436.

Anderson, A.V., Crowder, R.K., and Wallace, W.K., 1991, Parautochthonous Middle Devonian rocks: Earliest record of the Ellesmerian Sequence in northeastern Alaska: Geological Society of America Abstracts with Programs, v. 23, no. 2, p. 3.

Anderson, A.V., Wallace, W.K., and Mull, C.G., 1992, Stratigraphic variation across a mid-Paleozoic rift-basin margin, Endicott Group, eastern Brooks Range, Alaska: Geological Society of America Abstracts with Program, v. 24, no. 5, p. 3.

Brosgé, W.P., Reiser, H.N., Dutro, J.T., Jr., and Detterman, R.L., 1979, Bedrock geologic map of the Philip Smith Mountains Quadrangle, Alaska: U.S. Geological Survey Miscellaneous Field Studies MF-879B, 2 sheets, scale 1:250,000.

Keller, A.S., Morris, R.H., and Detterman, R.L., 1961, Geology of the Shaviovik and Sagavanirktok Rivers Region, Alaska: U.S. Geological Survey Professional Paper 303D, 222 p.

Miall, Andrew D., 1984, Principles of sedimentary basin analysis: New York, Springer-Verlag, 490 p.

Moore, T.E., Wallace, W.K., Bird, K.J., Karl, S.M., Mull, C.G., and Dillon, J.T., 1992, Stratigraphy, structure, and geologic synthesis of northern Alaska: U.S.Geological Survey Open-File Report 92-330, 183 p.

Robinson, M.S., Imm, T.A., and Clough, J.G., 1989, Measured stratigraphic section of volcanic rocks in the Lisburne Group, Ivishak River area, Arctic National Wildlife Refuge: Alaska Division of Geological & Geophysical Surveys Public Data-File 89-26A, 4 p.

Reiser, H.N., Brosgé, W.P., Dutro, J.T., Jr., and Detterman, R.L., 1980, Geologic map of the Demarcation Point Quadrangle, Alaska: U.S. Geological Survey Miscellaneous Geologic Investigations Map I-1133, scale 1:250,000.

THE PENULTIMATE GREAT EARTHQUAKE IN SOUTHCENTRAL ALASKA: EVIDENCE FROM A BURIED FOREST NEAR GIRDWOOD

by
Rodney A. Combellick[1]

INTRODUCTION

Determining the potential for future great earthquakes (Richter magnitude about 8 or 9) requires knowing how often they have occurred in the past. In the Anchorage, Alaska, region, only one great earthquake has occurred during historic time. This event, the great 1964 Alaska earthquake (M_w=9.2), was accompanied by tectonic uplift and subsidence that affected an area of more than 140,000 km^2 along 800 km of the Alaska-Aleutian subduction zone (fig. 1) (Plafker, 1969). Historic records and instrument monitoring show that no other great earthquake ruptured this segment, roughly between Kodiak and Cape Suckling, for at least 180 yr before the 1964 event (Sykes and others, 1980). However, there is no reason to doubt the inevitability of future earthquakes similar to the 1964 event. Adjacent areas of the Alaska-Aleutian arc have ruptured during at least one and, in some cases, during several great earthquakes throughout historic time. Considering that about 11 percent of the world's earthquakes have occurred in Alaska, including three of the ten largest events (Davies, 1984), the potential for future great earthquakes in the region is clearly high.

Given the limitations of instrument and historic records to resolve the recurrence times of great earthquakes, only geologic investigation can disclose the long-term record of sudden tectonic changes and earthquake effects. Recent geologic studies show that recurrence intervals for great earthquakes in this region range from about 400 to 1,300 yr (Plafker and others, 1992). My purpose in this paper is to present evidence from a coastal marsh near Girdwood that the penultimate, or second to last, great earthquake in the Anchorage region occurred between about 700 and 900 yr ago. This evidence comes from a layer of high-marsh peat[2] and rooted trees that were submerged by subsidence, probably killed by salt-water intake, and buried by postseismic deposition of intertidal silt and clay. I present preliminary evidence that subsidence was substantial and sudden (coseismic), and suggest that this subsidence at Girdwood probably coincided with subsidence at Portage, Chickaloon Bay, Palmer Hay Flats, and Goose Bay and with uplift at Copper River Delta. If such a large area was deformed during a single event, it must have been a great earthquake similar to the 1964 event.

VERTICAL CHANGES DURING AND AFTER THE 1964 EARTHQUAKE

The 1964 earthquake released accumulated stresses on the Alaska-Aleutian subduction zone, where the North American and Pacific plates converge at about 6 cm/yr (DeMets and others, 1990). The associated pattern of uplift and subsidence (fig. 1) resulted from regional crustal warping and from displacements on subsurface portions of the northwest-dipping Aleutian megathrust and subsidiary reverse faults (Plafker, 1969). Downwarp of as much as 2 m occurred over an elongate region including Kodiak Island, Kenai Peninsula, most of Cook Inlet, and Copper River Basin. Uplift as much as 11.3 m occurred seaward of the subsidence zone in an elongate region including Middleton Island, Montague Island, most of Prince William Sound, and Copper River Delta. Superimposed on this pattern of coseismic deformation is regional interseismic subsidence (Plafker and others, 1992). The long-term net vertical displacement is the sum of coseismic and interseismic displacements. Therefore, some areas undergo coseismic and long-term subsidence (upper Cook Inlet), others coseismic and long-term uplift (Middleton Island), and still others coseismic uplift and long-term subsidence (Copper River Delta) or coseismic uplift and long-term stability (Montague Island).

Postearthquake changes have restored much of the subsided area of Turnagain Arm (fig. 2) to near pre-earthquake conditions. Subsidence totaled as much as 2.4 m at Portage, including about 1.6 m of regional tectonic subsidence and 0.8 m of local surficial compaction (McCulloch and Bonilla, 1970). During the decade following the earthquake, as much as 0.55 m of rebound occurred along Turnagain Arm (Brown and others, 1977). Additionally, intertidal silt deposition began in submerged areas immediately following the earthquake and by 1980 had nearly restored the tidal flats to pre-earthquake levels (Bartsch-Winkler and Garrow, 1982). In the Portage area, Ovenshine and others (1976) mapped this deposit as the

[1]Alaska Division of Geological & Geophysical Surveys, 794 University Avenue, Suite 200, Fairbanks, Alaska 99709-3645.

[2]In this paper, *high marsh* refers to the vegetated upper portion of the intertidal zone that is primarily influenced by terrestrial conditions (infrequently flooded by salt water). *Low marsh* refers to a topographically lower part of the intertidal zone that is primarily influenced by marine conditions (flooded at least daily by salt water).

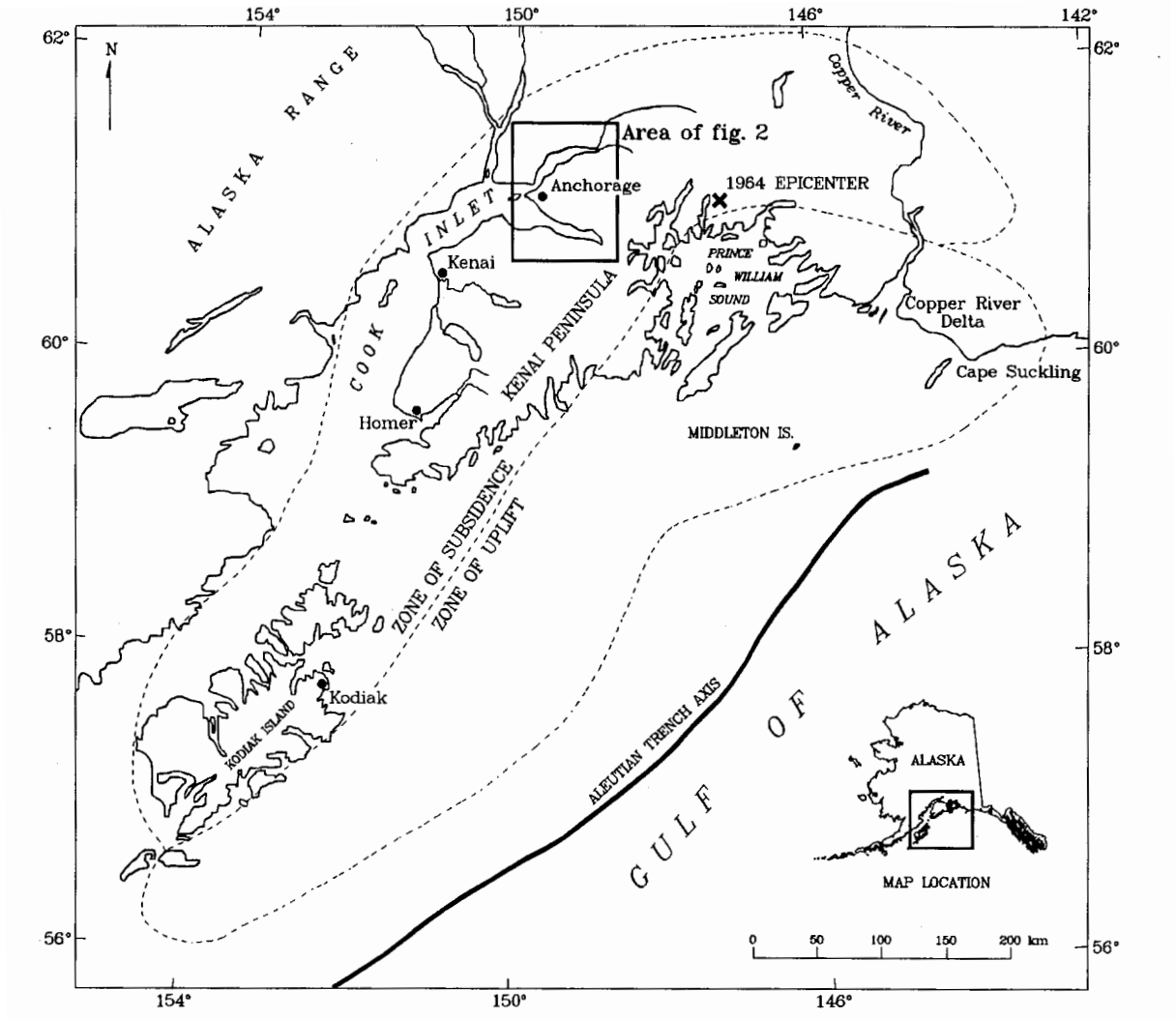

Figure 1. *Region affected by vertical tectonic displacement during the great Alaska earthquake of 1964 (modified from Plafker, 1969, fig. 3).*

Placer River Silt. An equivalent but thinner deposit is present at Girdwood. This postearthquake silt overlies grasses, mosses, herbaceous plants, peat, and root systems of spruce and cottonwood trees on the high marsh that was submerged in the Portage and Girdwood areas during the earthquake.

PALEOSEISMOLOGY AND RADIOCARBON DATING

Determining the effects and timing of prehistoric earthquakes depends on (1) correct interpretation of the geologic evidence of earthquakes and (2) accurate dating of the affected rocks or sediments (Allen, 1986). In the case of subduction-zone earthquakes like the 1964 Alaska event, the geologic evidence is usually related to sudden coastal uplift or subsidence (Plafker and Rubin, 1978; Lajoie, 1986) but may also be related to shaking effects, such as liquefaction (Obermeier and others, 1985).

Radiocarbon dating can provide a minimum or maximum age for an earthquake recorded in coastal sediments if organic material overlies or underlies the earthquake-related horizon. If organic material predating and postdating the horizon can be obtained, the age of the event can be bracketed. Alternatively, if it can be shown that the dated organisms died as a result of the earthquake, then the age of the youngest tissue approximates (very closely postdates) the age of the event.

Several sources of error make radiocarbon dating a relatively crude method for dating earthquakes and even less reliable for determining whether earthquake effects observed at different locations are attributable to a single

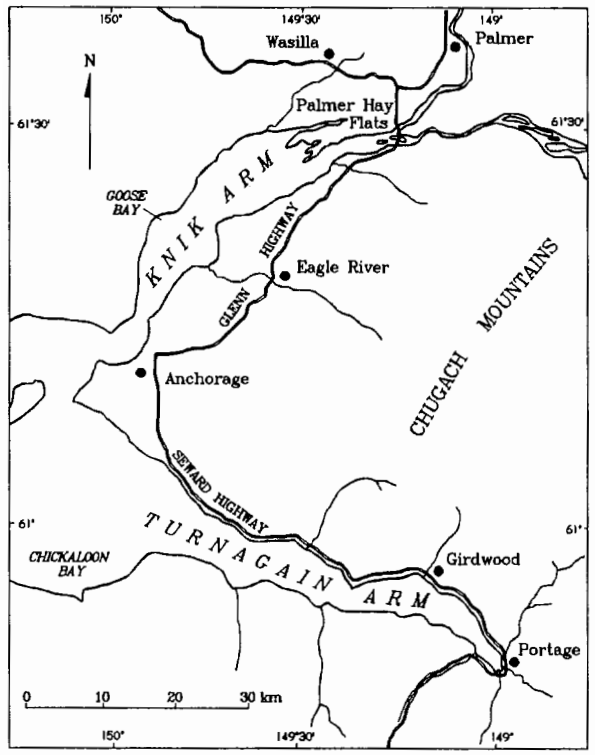

Figure 2. *Anchorage region and portion of upper Cook Inlet, including study area in vicinity of Turnagain and Knik Arms (see fig. 1 for map location).*

event (Atwater and others, 1991). Bulk samples of organic material, such as peat, may predate or postdate the event by many years. Contamination by younger roots, detrital organic material, or bacterial decomposition can introduce significant error. Quoted laboratory errors on reported ages are normally at least several decades and may be understated because of unknown analytical errors (Scott and others, 1990). Different laboratories analyzing splits of the same or stratigraphically equivalent Holocene samples have reported ages that fail to overlap even at two standard deviations and may differ by up to 700 yr (Nelson, 1992). Finally, because of natural variation of ^{14}C con-tent of atmospheric carbon through time, calibration to calendar years using dendrochronology is not linear and can result in a radiocarbon age yielding several possible calendar ages (Stuiver and Quay, 1980; Stuiver and Becker, 1986).

Despite these problems, conventional radiocarbon dating is a useful tool for determining approximate ages of earthquakes and their average recurrence interval. In some circumstances, high-precision radiocarbon dating of very carefully selected and prepared materials can provide ages with quoted errors on the order of one or two decades (Atwater and others, 1991).

REGIONAL STUDIES

Numerous studies have documented repeated sudden vertical tectonic displacements in southcentral Alaska during the past 5,000 yr, or late Holocene (Plafker and Rubin, 1967, 1978; Plafker, 1969; Plafker and others, 1992; Combellick, 1986, 1991; Bartsch-Winkler and Schmoll, 1987, 1992). Although the timing of all events is not yet clear, the distribution of prehistoric uplift and subsidence appears consistent with the pattern of 1964 deformation.

Radiocarbon dating of submerged peat layers in estuarine sediments of upper Cook Inlet indicates that the area probably subsided coseismically six to eight times during the 4,700 yr prior to the 1964 event, implying recurrence times on the order of 600 to 800 yr (Combellick, 1991). Elevated terraces on Middleton Island record five pre-1964 uplifts during the past 4,300 radiocarbon yr (Plafker and Rubin, 1978), or 4,900 calendar yr. The most recent uplift preserved by Middleton Island terraces was about 1,300 yr ago. At Copper River Delta, which undergoes net long-term subsidence punctuated by coseismic uplift, buried peat and forest layers record four pre-1964 uplifts during the past 3,000 yr (Plafker and others, 1992). The most recent event represented in the Copper River Delta sequence was about 800 yr ago.

Karlstrom (1964) dated and briefly described a buried forest layer in tidal sediments at Girdwood and recognized that it recorded a period of lower relative sea level. He obtained an age of 700 ± 250 radiocarbon yr (510-920 calendar yr) for wood from a rooted stump at about 0.8 m below the pre-1964 surface and 2,800 ± 180 yr (2,759-3,207 calendar yr) for wood from a peat layer about 4 m lower in the section. Karlstrom, whose report was prepared prior to the 1964 earthquake, did not attribute burial of the forest layer to possible coseismic subsidence.

Plafker (1969) used Karlstrom's dates to infer a regional average subsidence rate of 2-30 cm per century between 700 and 2,800 radiocarbon yr ago. He also concluded that gradual tectonic submergence prevailed in Prince William Sound as much as 1,180 yr prior to the 1964 earthquake. Plafker and Rubin (1978) inferred that the lowest elevated terrace at Middleton Island (fig. 1), dated at 1,360 radio-carbon yr, represented the last coseismic uplift in the region prior to 1964. However, Plafker and others (1992), reported new evidence of widespread coseismic uplift with a calibrated age of 665-895 yr in the Copper River Delta.

BURIED FOREST LAYERS AT GIRDWOOD

Erosion by waves and tidal currents has exposed two peat layers with rooted tree stumps along coastal banks at Girdwood (fig. A3). Trees rooted in the uppermost layer were killed as a result of submergence during the 1964 earthquake, probably by saltwater intake. Many of these dead trees remain standing but their root systems are partially or completely buried beneath postearthquake silt (equivalent to Placer River Silt) up to several tens of cm thick. Patches of bark remain on above-ground portions of some of the trees and are commonly well preserved on buried portions of the trunks.

Stumps rooted in the lower layer are broken or eroded to heights of less than 1 m and encased in about 1 m of gray clayey silt between the upper and lower forest layers. None of the lower stumps protrude through the modern marsh surface. No bark remains on the specimens I observed from the lower layer except for very few small, loosely attached patches. The lower stumps are rooted in a layer of mossy and woody peat 10-15 cm thick, which has been partly removed by tidal and wave erosion where the stumps crop out at the base of the bank (fig. 3B). This lower layer of rooted stumps is probably the same layer that Karlstrom (1964) dated at 700 ± 250 radiocarbon yr.

Several lines of evidence indicate that the lower forest layer was submerged and buried as a result of sudden subsidence: (1) the contact between the peat layer and overlying mud is very sharp, indicating rapid burial, as with the 1964 layer; (2) outer growth rings of the buried stumps are continuous and as wide as or wider than inner rings, indicating healthy growth until death, comparable to that observed in coastal Washington by Atwater and Yamaguchi (1991); and (3) the lower part of the overlying mud layer contains below-ground stems of the halophytic plant *Triglochin maritimum*, indicating submergence to a lower level in the intertidal zone. In southwestern Washington, where diurnal tide range is about 3 m, *T. maritimum* is dominant only in low-marsh areas that are 0.5-2.0 m or more below the typical high-marsh surface (Atwater, 1987). In upper Cook Inlet, where diurnal tide range is about 10 m, *T. maritimum* may indicate greater than 2-m depth below the high-marsh elevation. The overlying mud layer shows a gradual upward increase in roots, grass stems, and other plant material and grades into the overlying peat, suggesting a gradual return to the high-marsh environment.

Although alternating layers of peat and intertidal mud can be produced by nonseismic processes (Nelson and Personius, in press), the sharp peat-mud contact, presence of *T. maritimum* in mud above the contact, apparent sudden death of rooted trees, and gradual mud-peat transition are strong evidence of coseismic subsidence followed by gradual uplift or sedimentation that returned the tidal flat to high-marsh conditions. Still lacking, however, is convincing evidence of strong ground shaking in the form of liquefaction features associated with burial of the peat. This evidence may be very difficult to find; a 1991 reconnaissance of several km of tidal- and river-bank exposures in the Portage area, where liquefaction was extensive during the 1964 earthquake (McCulloch and Bonilla, 1970), revealed only a few sand dikes penetrating the 1964 soil (B. Atwater and R. Combellick, unpub. data, 1991). Locating similar evidence of ground shaking during previous events will be even more difficult because previous coseismic subsidence is interpreted mainly from borehole samples (Combellick, 1991).

Radiocarbon Ages

My estimate for age of burial of the lower forest layer at Girdwood is based on radiocarbon dating of three wood samples and three peat samples. The wood samples were collected from the outermost 10 to 25 growth rings of three rooted tree stumps. Because bark was not present on the sampled stumps, these may not be the last growth rings added before death. However, the well-preserved condition of the stumps, nearly continuous outermost rings, and smoothness of the outer surface suggest that few or no growth rings have been lost to decomposition. Considering the potential sources of error in conventional radiocarbon dating, the exact position of the dated wood relative to the outermost ring at time of death is probably insignificant. If my assumption is correct that these trees were growing normally at the time of submergence and died quickly as a result of submergence, the average age of these outer rings should predate the time of the event by no more than a few years. The potential for contamination of wood samples with older or younger organic material is far less than for peat samples. Therefore, the wood samples should provide a more reliable age estimate for submergence.

Two of the peat samples were collected from the upper 2-3 cm of the peat layer exposed near the rooted stumps, immediately below the abrupt contact between the peat and overlying tidal mud. The third peat sample was collected from an equivalent stratigraphic position in a nearby borehole (Combellick, 1991, table 2, sample TA1-12.8). If the peat is composed primarily of plant material that was growing at or shortly before submergence, these samples should provide a closely limiting maximum age for the event. However, possible contamination by older plant matter or younger roots may introduce unknown errors.

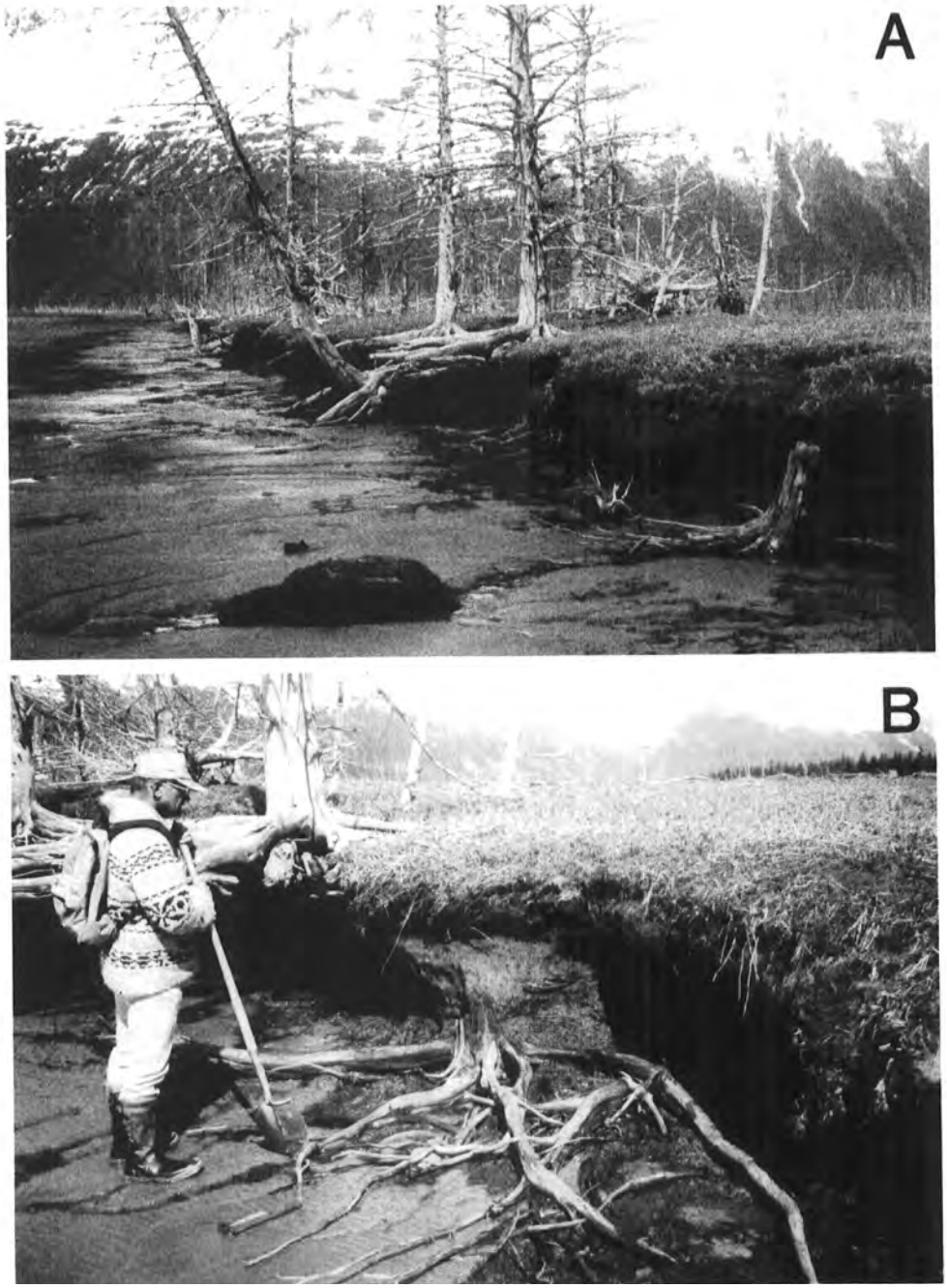

Figure 3. *Erosion has exposed root systems of two generations of dead spruce trees in coastal banks along upper Turnagain Arm near Girdwood. (7A) View of standing trees that probably died from salt-water intake following submergence during the 1964 earthquake. The roots of these trees and other contemporaneous vegetation were buried by postearthquake deposition of intertidal silt. Stumps along the base of the bank are rooted in an older peat layer, which is buried beneath about 1 m of intertidal silt. (7B) Closeup of older rooted stump showing intertidal mud that buried the root system and associated peat layer (erosion has removed much of the peat). Death of these older trees and burial of the peat layer within which they are rooted probably resulted from subsidence during the previous great earthquake (1991 photographs).*

Two commercial laboratories performed the radiocarbon dating using standard pretreatment and gas-proportional counting techniques. Reported radiocarbon ages (fig. 4) include a correction for natural $^{13}C/^{12}C$ isotopic fractionation and are referenced to A.D. 1950. Calibration to calendar years was based on tree-ring data of Stuiver and Becker (1986) and was performed using a computer program by Stuiver and Reimer (1986). The laboratories did not provide specific error multipliers to account for non-counting analytical errors, so I used a conservative value of 2 for all calibrated ages. Although this has the effect of doubling the quoted standard deviation, the probability that the true sample age is within the calibrated age range remains at 68 percent. This is because the quoted standard deviation may not be large enough to account for all sources of laboratory error (Stuiver and Pearson, 1986).

The weighted average age of the wood samples is 926 ± 35 radiocarbon yr, which gives possible calibrated ages of 799, 810, 830, 856, and 909 yr and an error range probably within the interval 744-946 yr B.P. at 68 percent confidence (fig. 4). The calibrated age range is greater than the uncalibrated range because of multiple intercepts in the calibration curve and greater rate of change of calibrated age versus radiocarbon age during this period (fig. 5).

Ages of the peat samples (fig. 4) are consistent with the wood ages but show greater variation, probably because of the longer period spanned by each peat sample and, in the case of sample 91-1-1, possible contamination by younger organic material.

REGIONAL CORRELATION AND DISCUSSION

Buried peat layers with characteristics similar to the lower Girdwood forest layer, but without observed rooted stumps, occupy an equivalent stratigraphic position in estuarine sediments at Portage and Palmer Hay Flats (Combellick, 1991) and at Chickaloon Bay and Goose Bay (this study) (fig. 2). Samples from the tops of the peat layers yielded ages that are consistent with the ages of wood and peat samples from the lower Girdwood forest layer (fig. 4). The reported 665-895-yr calibrated age for coseismic uplift in the Copper River Delta area (Plafker and others, 1992) is also consistent with the wood and peat ages in upper Cook Inlet.

These data do not prove that vertical displacement was coeval in all areas; if the dated deposits were produced by events separated by only a few years or decades, these events cannot be resolved by conventional radiocarbon dating. However, because the current body of paleoseismic evidence indicates an average recurrence interval of 600-800 yr for great earthquakes in this region, it is reasonable to presume that the dated deposits represent a single event.

If vertical displacement was coeval, the minimum magnitude of this earthquake can be roughly estimated using an empirical relationship between magnitude of subduction-zone earthquakes and length of measurable deformation (West and McCrumb, 1988). Considering that deformation zones are elongated parallel to the trench axis, the deformation associated with the earthquake must have exceeded the 300-km distance between upper Cook Inlet and Copper River Delta because this line is roughly perpendicular to the trench axis. According to the graphic relationship of West and McCrumb (1988, fig. 1), the minimum earthquake magnitude for a 300-km-long zone of deformation is about 7.8.

High-precision dating involving much longer counting periods could provide radiocarbon ages with standard deviations on the order of one or two decades (Stuiver and Becker, 1986; Atwater and others, 1991). However, this technique may not improve resolution of the calendar age of the earthquake because of apparent wide variability of atmospheric ^{14}C between about 750 and 900 yr B.P. (A.D. 1050-1200). The resulting calibration curve (fig. 5) shows that radiocarbon ages between about 860 and 960 yr give multiple calibrated ages between 750 and 925 yr. As Atwater and others (1991) have demonstrated, it may be possible to precisely date older rings of rooted stumps, thereby obtaining radiocarbon ages on a steeper portion of the calibration curve (greater than 960 radiocarbon yr B.P.) where there are fewer multiple intercepts. Subtracting the number of growth rings between the sampled portion and the outer surface would then yield more precise calibrated ages for the samples. This method could help determine whether sudden vertical displacements in this region between 700 and 900 yr ago resulted from multiple great earthquakes.

SUMMARY AND CONCLUSIONS

The last great earthquake that caused tectonic deformation in the Anchorage region prior to 1964 probably occurred between 700 and 900 yr ago. This inferred earthquake caused vertical shoreline changes extending at least from upper Cook Inlet to the Copper River Delta. Evidence of these changes appears in tidewater banks at Girdwood, where a layer of peat and rooted tree stumps exposed about 1.7 m below the modern coastal high marsh is buried beneath intertidal mud. The abrupt upper contact of the peat, apparent sudden death of the trees, and presence of halophytic plant fossils in mud above the contact indicate submergence into the low-marsh environment more rapidly than would be expected as a result

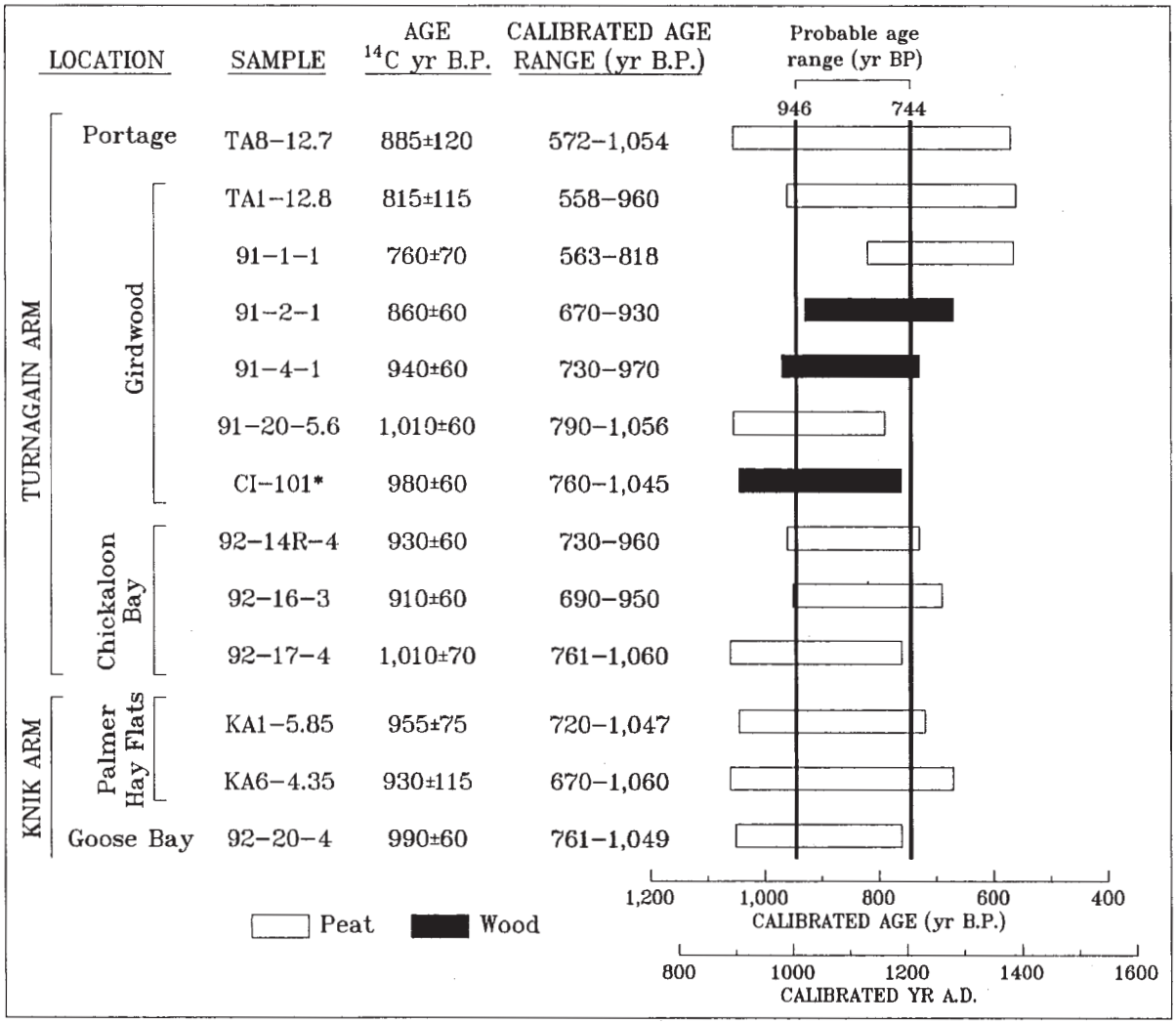

Figure 4. *Radiocarbon ages of wood and peat samples used in this study. Wood samples were collected from the outer 10-25 growth rings of rooted stumps (*CI-101 age provided by Gordon Jacoby, written commun.). Peat samples were collected from the upper 2-3 cm of buried peat. Age in ^{14}C yr B.P. is conventional radiocarbon age in years before A.D. 1950 with quoted counting error of one laboratory standard deviation. Calibrated age ranges at right are based on tree-ring data of Stuiver and Becker (1986) and incorporate an error multiplier of 2 to account for possible non-counting sources of laboratory error. Probable age range shown represents error limits of the average calibrated age of two wood samples at the Girdwood site, at 68 percent confidence (fig. 5).*

of nontectonic rise of relative sea level. As intertidal silt deposition and possibly postseismic rebound restored the tidal flat to subaerial conditions, the mud above this forest layer became increasingly rich in plant matter and a new brackish-water high marsh developed. Subsidence during the 1964 earthquake submerged this marsh in a similar fashion and resulted in burial by intertidal silt.

Age control for this penultimate earthquake comes from radiocarbon dates of outer growth rings from three rooted trees that were probably killed by salt water as a result of coseismic submergence. Mathematically combining these ages gives a calibrated age range probably within 744-946 calendar yr B.P. at 68 percent confidence. Peat samples from the top of the soil layer within which these stumps are rooted yield calibrated ages that are consistent with the wood ages but show greater variation. The wood and peat ages at Girdwood closely match ages obtained from similar buried peat layers at Portage, Chickaloon Bay, Palmer Hay Flats, and Goose Bay and from deposits formed by coseismic uplift at Copper River

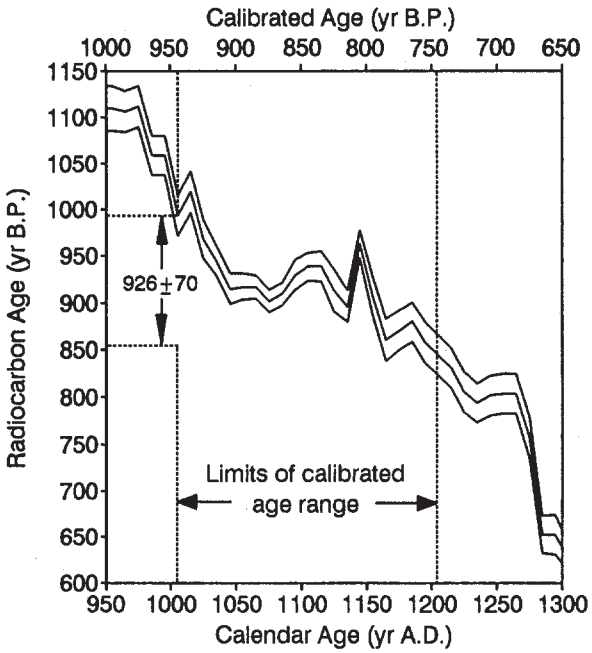

Figure 5. *Portion of tree-ring calibration curve showing translation of average radiocarbon-age range for the two wood samples to calibrated probable range shown in figure 4. Prior to calibration, the error calculated from the laboratory standard deviations is increased by an error multiplier of 2. The center line is the calibration curve and the outer lines represent uncertainty of one standard deviation in the calibration data set; this standard deviation incorporates a laboratory error multiplier of 1.6 (modified from Stuiver and Becker, 1986, fig. 1B).*

Delta. Although I presume that these vertical displacements occurred during a single great earthquake, multiple earthquakes may have affected each area separately within a period that was too brief to resolve with conventional radiocarbon dating. If the vertical displacements occurred during a single earthquake, its magnitude was probably 7.8 or larger.

ACKNOWLEDGMENTS

The U.S. Geological Survey, Department of the Interior, supported this study under National Earthquake Hazards Reduction Program award 14-08-0001-G1949 to the Alaska Division of Geological & Geophysical Surveys. The views and conclusions contained in this document are those of the author and should not be interpreted as necessarily representing official policies, either expressed or implied, of the U.S. Government.

I thank Richard Reger for his assistance in the field and for his knowledgeable insights. Beta Analytic, Inc. and Geochron Laboratories Division, Krueger Enterprises, Inc. performed all radiocarbon-age determinations. Reger, Brian Atwater, and George Plafker reviewed the manuscript and provided many valuable suggestions for improvement.

REFERENCES CITED

Allen, C.R., 1986, Seismological and paleoseismo-logical techniques of research in active tectonics, *in* Studies in geophysics: Active tectonics: Washington, D.C., National Academy Press, p. 148-154.

Atwater, B.F., 1987, Evidence for great Holocene earthquakes along the outer coast of Washington State: Science, v. 236, p. 942-944.

Atwater, B.F., and Yamaguchi, D.K., 1991, Sudden, probably coseismic submergence of Holocene trees and grass in coastal Washington State: Geology, v. 19, no. 7, p. 706-709.

Atwater, B.F., Stuiver, Minze, and Yamaguchi, D.K., 1991, Radiocarbon test of earthquake magnitude at the Cascadia subduction zone: Nature, v. 353, p. 156-158.

Bartsch-Winkler, S.R., and Garrow, H.C., 1982, Depositional system approaching maturity at Portage Flats, *in* Coonrad, W.L., ed., The U.S. Geological Survey in Alaska: Accomplishments during 1980: U.S. Geological Survey Circular 844, p. 115-117.

Bartsch-Winkler, Susan, and Schmoll, H.R., 1987, Earthquake-caused sedimentary couplets in the upper Cook Inlet region, *in* Hamilton, T.D., and Galloway, J.P., eds., Geologic Studies in Alaska by the U.S. Geological Survey during 1986: U.S. Geological Survey Circular 998, p. 92-95.

Bartsch-Winkler, Susan, and Schmoll, H.R., 1992, Utility of radiocarbon-dated stratigraphy in determining late Holocene earthquake recurrence intervals, upper Cook Inlet region, Alaska: Geological Society of America Bulletin, v. 104, no. 6, p. 684-694.

Brown, L.D., Reilinger, R.E., Holdahl, S.R., and Balazs, E.I., 1977, Postseismic crustal uplift near Anchorage, Alaska: Journal of Geophysical Research, v. 82, no. 23, p. 3369-3378.

Combellick, R.A., 1986, Chronology of late-Holocene earthquakes in southcentral Alaska: Evidence from buried organic soils in upper Turnagain Arm [abs.]: Geological Society of America Abstracts with Programs, v. 18, no. 6, p. 569.

_____1991, Paleoseismicity of the Cook Inlet region, Alaska: Evidence from peat stratigraphy

in Turnagain and Knik Arms: Alaska Division of Geological & Geophysical Surveys Professional Report 112, 52 p.

Davies, J.N., 1984, Alaska's earthquakes: The Northern Engineer, v. 16, no. 4, p. 8-13.

DeMets, C., Gordon, R.G., Argus, D.F., and Stein, S., 1990, Current plate motions: Geophysical Journal International, v. 101, no. 2, p. 425-478.

Karlstrom, T.N.V., 1964, Quaternary geology of the Kenai lowland and glacial history of the Cook Inlet region, Alaska: U.S. Geological Survey Professional Paper 443, 69 p.

Lajoie, K.R., 1986, Coastal tectonics, *in* Wallace, R.E., ed., Studies in geophysics: Active tectonics: Washington, D.C., National Academy Press, p. 95-124.

McCulloch, D.S., and Bonilla, M.G., 1970, Effects of the earthquake of March 27, 1964, on the Alaska Railroad: U.S. Geological Survey Professional Paper 545-D, 161 p.

Nelson, A.R., 1992, Discordant ^{14}C ages from buried tidal-marsh soils in the Cascadia subduction zone, southern Oregon coast: Quaternary Research, v. 38, no. 1, p. 74-90.

Nelson, A.R., and Personius, S.F., in press, The potential for great earthquakes in Oregon and Washington: An overview of recent coastal geologic studies and their bearing on segmentation of Holocene ruptures, central Cascadia subduction zone, *in* Rogers, A.M., Kockelman, W.J., Priest, G., and Walsh, T.J., eds., Assessing and reducing earthquake hazards in the Pacific Northwest: U.S. Geological Survey Professional Paper 1560.

Obermeier, S.F., Gohn, G.S., Weems, R.E., Gelinas, R.L., and Rubin, Meyer, 1985, Geologic evidence for recurrent moderate to large earthquakes near Charleston, South Carolina: Science, v. 227, p. 408-411.

Ovenshine, A.T., Lawson, D.E., and Bartsch-Winkler, S.R., 1976, The Placer River Silt—An intertidal deposit caused by the 1964 Alaska earthquake: Journal of Research of the U.S. Geological Survey, v. 4, no. 2, p. 151-162.

Plafker, George, 1969, Tectonics of the March 27, 1964, Alaska earthquake: U.S. Geological Survey Professional Paper 543-I, 74 p., 2 sheets, scales 1:2,000,000 and 1:500,000.

Plafker, George, and Rubin, Meyer, 1967, Vertical tectonic displacements in south-central Alaska during and prior to the great 1964 earthquake: Journal of Geosciences, Osaka City University, v. 10, p. 53-66.

_____1978, Uplift history and earthquake recurrence as deduced from marine terraces on Middleton Island, Alaska, *in* Proceedings of Conference VI, Methodology for Identifying Seismic Gaps and Soon-to-break Gaps, National Earthquake Hazards Reduction Program, 25-27 May, 1978: U.S. Geological Survey Open File Report 78-943, p. 687-721.

Plafker, George, Lajoie, K.R., and Rubin, Meyer, 1992, Determining recurrence intervals of great subduction zone earthquakes in southern Alaska by radiocarbon dating, *in* Taylor, R.E., Long, Austin, and Kra, R.S., eds., Radiocarbon after four decades: An interdisciplinary perspective: New York, Springer-Verlag, p. 436-452.

Scott, E.M., Aitchison, T.C., Harkness, D.D., Cook, G.T., and Baxter, M.S., 1990, An overview of all three stages of the international radiocarbon intercomparison: Radiocarbon, v. 32, no. 3, p. 309-319.

Stuiver, M., and Becker, B., 1986, High-precision decadal calibration of the radiocarbon time scale, AD 1950-2500 BC: Radiocarbon, v. 28, p. 863-910.

Stuiver, M., and Pearson, G.W., 1986, High-precision calibration of radiocarbon time scale, AD 1950-500 BC: Radiocarbon, v. 28, p. 805-838.

Stuiver, Minze, and Quay, P.D., 1980, Changes in atmospheric carbon-14 attributed to a variable sun: Science, v. 207, p. 11-19.

Stuiver, M., and Reimer, P.J., 1986, A computer program for radiocarbon age calibration: Radiocarbon, v. 28, p. 1022-1030.

Sykes, L.R., Kisslinger, J.B., House, Leigh, Davies, J.N., and Jacob, K.H., 1980, Rupture zones of great earthquakes in the Alaska-Aleutian Arc, 1784 to 1980: Science, v. 210, no. 19, p. 1343-1345.

West, D.O., and McCrumb, D.R., 1988, Coastal uplift in Oregon and Washington and the nature of Cascadia subduction-zone tectonics: Geology, v. 16, no. 2, p. 169-172.

GEOLOGY, ALTERATION, AND MINERALIZATION OF THE VINASALE MOUNTAIN GOLD DEPOSIT, WEST-CENTRAL ALASKA

by
Jack J. DiMarchi[1]

INTRODUCTION

Vinasale Mountain is located 26 km south of McGrath, Alaska (fig. 1), on lands selected by Doyon, Limited, an Alaska Native corporation. The prospect has been the site of ongoing exploration since 1990 when Central Alaska Gold Company discovered intrusive-hosted gold mineralization. Integrated exploration programs in 1990 and 1991 generated important geologic data. Exploration work included more than 17,000 ft (5,182 m) of diamond drilling, 18.1 line-miles (29 km) each of grid-based very low frequency-electromagnetic (VLF-EM), induced-polarization (IP), resistivity, and magnetic geophysical surveys; extensive grid-based geochemical sampling and geologic mapping; petrographic and metallurgical studies; and K/Ar and fission track age dating (DiMarchi and others, 1990, 1991). This paper incorporates select elements of these data to briefly describe the general geology of the prospect, its igneous host-rock petrochemistry, and associated hydrothermal alteration and mineralization, and suggests several genetic implications of the data.

REGIONAL GEOLOGY

Vinasale Mountain is one of several widely scattered plutonic and volcano-plutonic complexes with ages of 58 to 79 m.y., that represent the last of three pre-middle Tertiary plutonic episodes in western Alaska (Silberman and others, 1979; Wilson, 1977). In addition to the gold deposit described in this paper, several other notable gold deposits and smaller mineral occurrences are associated with these alkalic igneous complexes. These deposits include the Nixon Fork gold and copper skarn deposit, the Donlin Creek intrusive-hosted gold-bearing veins, and the precious metal-bearing veins and intrusive-hosted disseminated gold in the Chicken Mountain and Black Creek stocks at Flat. Several gold placer districts that developed around these centers include Crooked Creek, Iditarod, Flat, Moore Creek, Innoko, and McGrath. More than 2.2 million oz of gold have been produced from the Iditarod, Innoko, and McGrath placer districts (Nokleberg and others, 1987).

PROSPECT GEOLOGY

Prior geologic mapping at Vinasale Mountain is limited to reconnaissance mapping by Bundtzen (1986). Because of limited outcrops, we drew the interpretive geologic map (fig. 2) largely from integrating lithologic

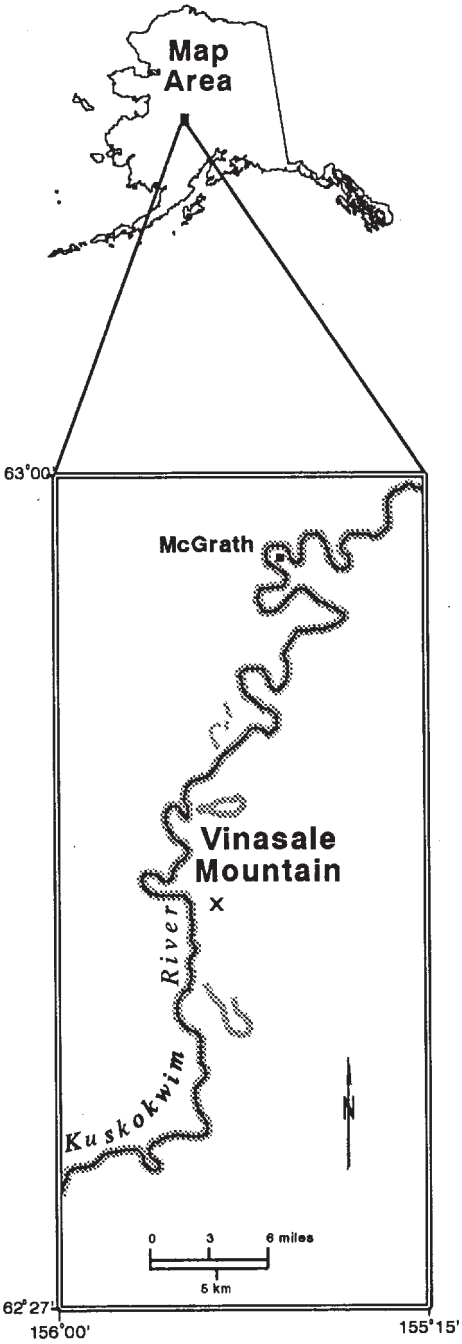

Figure 1. *Location map of Vinasale Mountain, Alaska.*

[1]Central Alaska Gold Company, 3538 International Way, Fairbanks, Alaska 99701. Present address: ASA Inc., 2700 S. Cushman Street, Fairbanks, Alaska 99701.

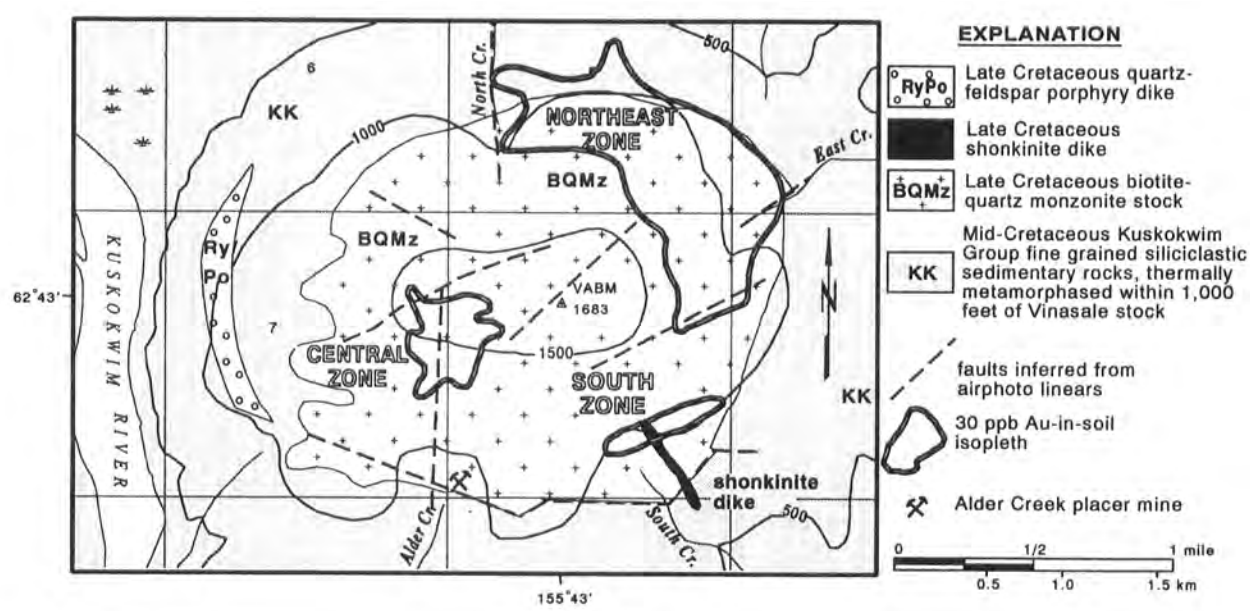

Figure 2. *Interpretive geologic map of Vinasale Mountain showing gold-in-soil geochemistry.*

and alteration information from rock fragments seen in more than 600 soil pits, from structural information interpreted from aerial photos and geophysical surveys, and from a relatively minor amount of outcrop mapping. Altered and/or mineralized rocks do not crop out on the prospect. Bundtzen (1986) reports that hand mining in Alder Creek, on the south flank of Vinasale Mountain, produced 103 oz of gold between 1929 and 1935.

Vinasale Mountain is underlain by a Late Cretaceous intrusive complex intruding fine-grained marine clastic rocks of the early Late Cretaceous Kuskokwim Group (Cady and others, 1955). We recognize four intrusive units: (1) porphyritic quartz monzonite, (2) rhyolite porphyry, (3) monzonite intrusion breccia, and (4) shonkinite.

The most voluminous phase that comprises the main stock is porphyritic quartz monzonite. This phase contains 30 percent subequant poikilitic K-feldspar phenocrysts up to 2 cm across with fine biotite inclusions, 15 percent quartz as sub-equant crystals and aggregates up to 3 mm across, 40 percent euhedral sodic-plagioclase as laths up to 5 mm long, 10 percent biotite as euhedral books up to 6 mm across, and accessory augite, ilmenite, sphene and green tourmaline. The stock has a K/Ar age date of 69 ± 2 Ma (Solie and others, 1991).

Rhyolite porphyry dikes intrude argillite near the western margin of the stock; the porphyries consist of resorbed quartz and feldspar phenocrysts with trace biotite in a light-gray aphanitic groundmass. Millimeter-scale inclusions of argillite are common in the porphyry.

The third most voluminous intrusive unit, and perhaps most important from an economic standpoint, is monzonitic breccia that is characterized by subrounded clasts of porphyritic to fine-grained equigranular monzonite and minor vein quartz in a monzonite or quartz-dolomite matrix (fig. 3). Breccia has been only observed in drill core. Primary igneous breccia textures are variably disguised by hydrothermal alteration and brecciation, and as a result it is unclear whether it is predominantly intrusive or hydrothermal in origin. The breccia occurs as a swarm of subhorizontal, cylindrical bodies that are spatially associated with a large zone of alteration and important gold mineralization.

Lastly, a single black shonkinite dike containing 10 percent medium-grained plagioclase, augite, biotite, and magnetite phenocrysts in a fine-grained groundmass of 40 percent plagioclase, 25 percent magnetite, and 25 percent biotite, intrudes the stock in the southeastern part of the prospect.

Whole-rock major-oxide data for the Vinasale intrusive rocks are presented in table 1. Plots of major-oxide data show that the main stock is weakly alkaline (alkali-calcic), and that the dikes range from ultra-alkaline to subalkaline (calc-alkalic) (fig. 4). The main stock ranges from weakly metaluminous to weakly peraluminous, the shonkinite plots in the metaluminous field, the rhyolite porphyry plots as peraluminous (fig. 5). The intrusives exhibit a range of oxidation states from weakly oxidized to weakly reduced, and are gold favorable to gold unfavorable, as defined by the methods of Leveille and others (1988).

Kuskokwim Group marine clastic rocks surround the stock along the lower flanks of the mountain. Lithologies present include fine-grained black argillite and laminated

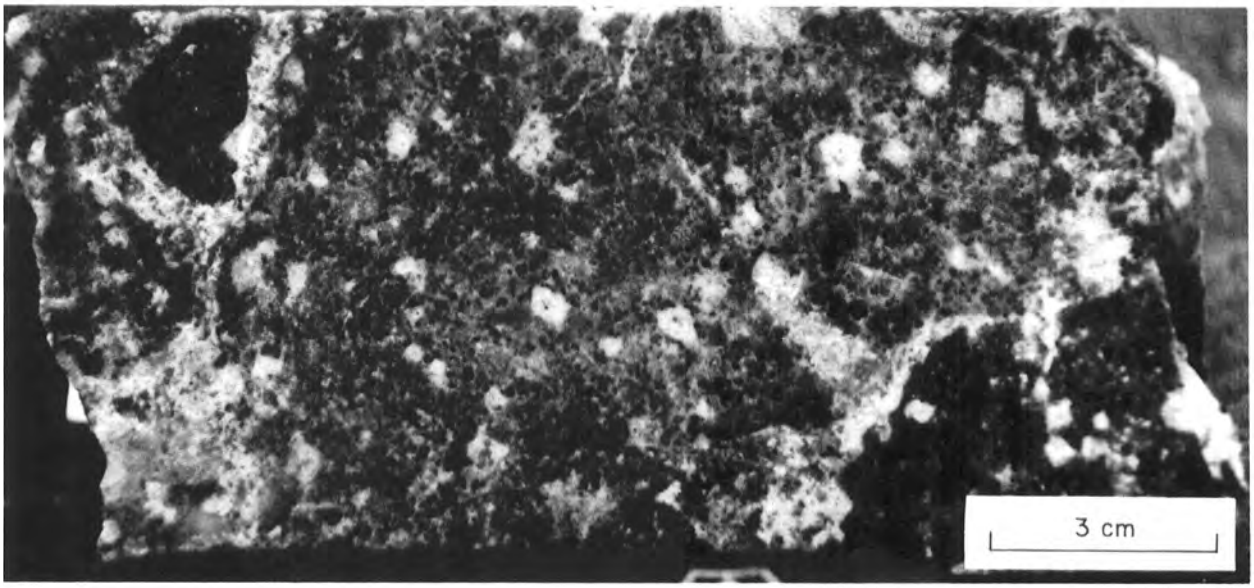

Figure 3. *Monzonitic breccia with quartz-dolomite matrix, Central Zone.*

to thin-bedded graywacke. Both are thermally metamorphosed to a maroon dense hornfels for a distance of up to several hundred meters away from the stock. We found no contact metamorphic minerals such as andalusite.

SURFACE GEOCHEMISTRY

Large areas of coincident multi-element (Au, As, Sb, Bi, Pb, Mo, and others) anomalies dominate the surface geochemistry of Vinasale Mountain, based on 626 grid-based soil samples. The contoured gold-in-soil values (fig. 2) define three anomalous zones.

(1) The Central Zone, located 762 m west of the mountain summit, is approximately 457 m by 610 m in plan, as defined by the 30 ppb Au isopleth. Soil samples in the zone reach maximum values of 2,470 ppb Au and surface rock samples contain up to 1,960 ppb Au (0.057 opt Au). Drilling shows that the source of the soil anomalies is a zone of pervasive quartz-sericite-dolomite alteration and sulfide mineralization that extends from the surface to a depth of at least 216 m.

(2) The Northeast Zone, situated approximately 914 m northeast of the mountain summit, is approximately 1,219 m by 610 m in plan, as defined by the 30 ppb Au isopleth. Soil samples in the zone reach a maximum of 185 ppb Au and surface rock samples contain up to 16,150 ppb Au (0.472 opt Au). Drilling has shown that the lode source of this extremely large surface anomaly is scattered gold mineralization associated with narrow zones of sericite alteration and quartz veinlets in, and associated with, steeply dipping, fracture zones.

Table 1. *Whole-rock major-oxide data from Vinasale intrusive rocks*

SAMPID	Al_2O_3	BaO	CaO	FeO	TFe	K_2O	MgO	MnO	Na_2O	P_2O_5	SiO_2	TiO_2	LOI	Total
QMZ901	16.46	0.22	3.20	2.23	3.98	3.72	1.52	0.07	3.61	0.37	66.41	0.47	0.75	100.53
QMZ902	16.44	0.20	3.10	2.17	3.89	3.49	1.53	0.07	3.72	0.38	66.37	0.47	0.92	100.34
QMZ903	15.98	0.20	2.85	3.11	4.01	3.79	1.53	0.09	3.70	0.36	64.14	0.44	2.87	99.62
QMZ904	16.42	0.19	3.55	2.72	3.58	3.46	1.55	0.08	3.82	0.34	65.59	0.47	1.36	100.11
QMZ911*	16.0	na	3.48	2.40	3.57	3.81	1.40	0.08	3.66	0.22	66.50	0.44	0.93	99.83
QMZ912*	16.0	na	3.66	2.40	3.42	3.87	1.44	0.09	3.64	0.22	66.20	0.44	0.70	99.42
SHN913	15.84	0.24	7.14	4.55	9.11	2.85	6.09	0.15	3.48	0.91	45.89	1.59	5.27	98.06
RHY914	14.60	0.15	1.67	0.85	2.65	4.04	0.58	0.05	3.03	0.29	70.47	0.24	1.64	99.32

QMZ-quartz monzonite stock, SHN-shonkinite dike, RHY-rhyolite dike analyses reported in weight percent.
TFe = Total iron reported as Fe_2O_3, na = not analyzed. * = analyzed by XRAL, all others by Chemex.

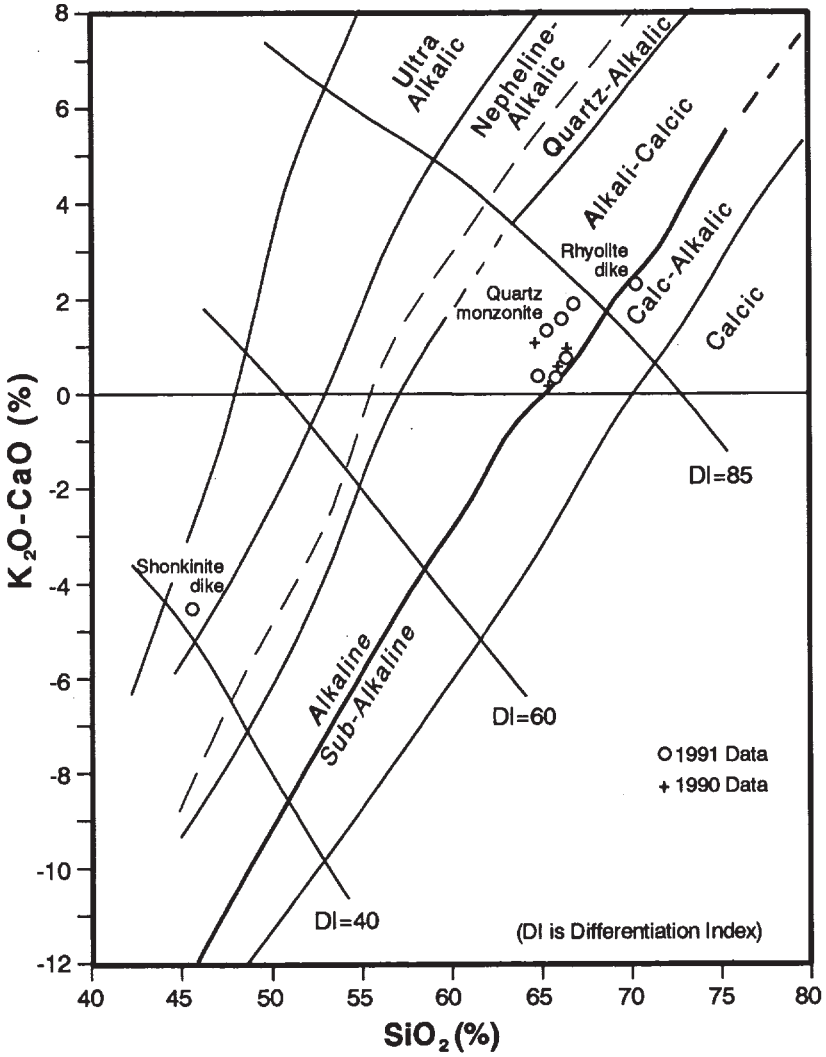

Figure 4. *K_2O-CaO vs SiO_2 variation diagram depicting alkalinity of the Vinasale Mountain intrusive phases. Diagram from Keith, 1984.*

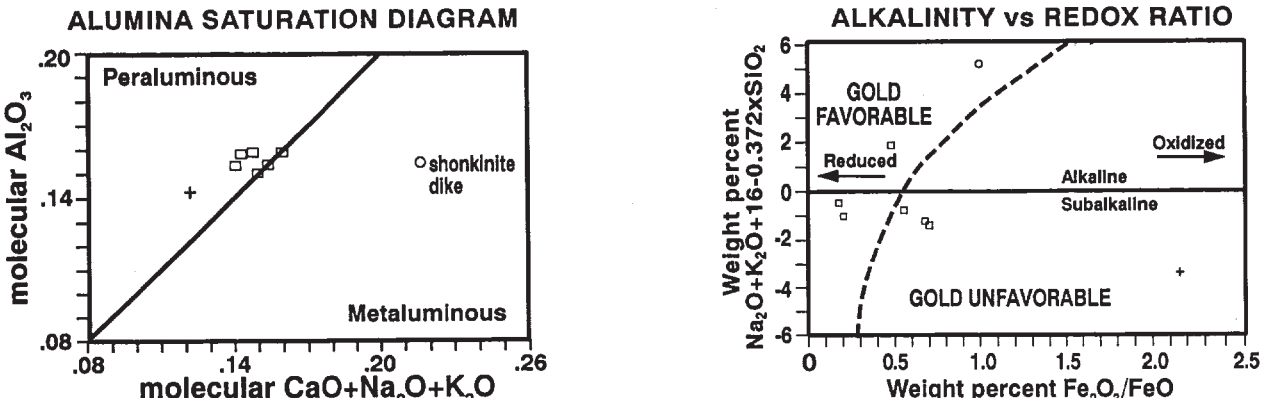

Figure 5. *Alumina saturation and gold favorability of the Vinasale Mountain intrusive phases.*

(3) The South Zone, situated 975 m southeast of the mountain summit, is approximately 610 m by 61 m in plan and includes soils with up to 335 ppb Au. A single drill hole in this zone intersected very weak gold mineralization associated with fracture-controlled veinlets similar in style to those in the Northeast Zone.

Gold-anomalous surface rock samples are restricted to the confines of these three anomalous zones and to the streams that drain them. Thirty-five of the 134 rock samples collected to date contain greater than 1,000 ppb Au (0.029 opt Au), with a maximum value of 15,980 ppb Au (0.47 opt Au).

The contoured arsenic-in-soil values (fig. 6) define a single, large, horseshoe-shaped anomaly that encompasses the three auriferous zones, and demonstrates geochemical continuity between them. The geometry of the arsenic anomaly corroborates geophysical evidence, discussed later, that suggests northeast-trending fracture zones connect the Northeast Zone with the South and Central zones.

ALTERATION AND MINERALIZATION

Understanding of the hydrothermal alteration is derived primarily from visual examination of drill core and from reflected and transmitted light study of thin sections. In this section I describe the alteration and mineralization in the two largest and strongest gold-mineralized areas at Vinasale Mountain.

Central Zone

The Central Zone is defined at the surface by a 457 m by 610 m area of anomalous gold in soils and to a depth of 216 m by the presence of pervasive alteration

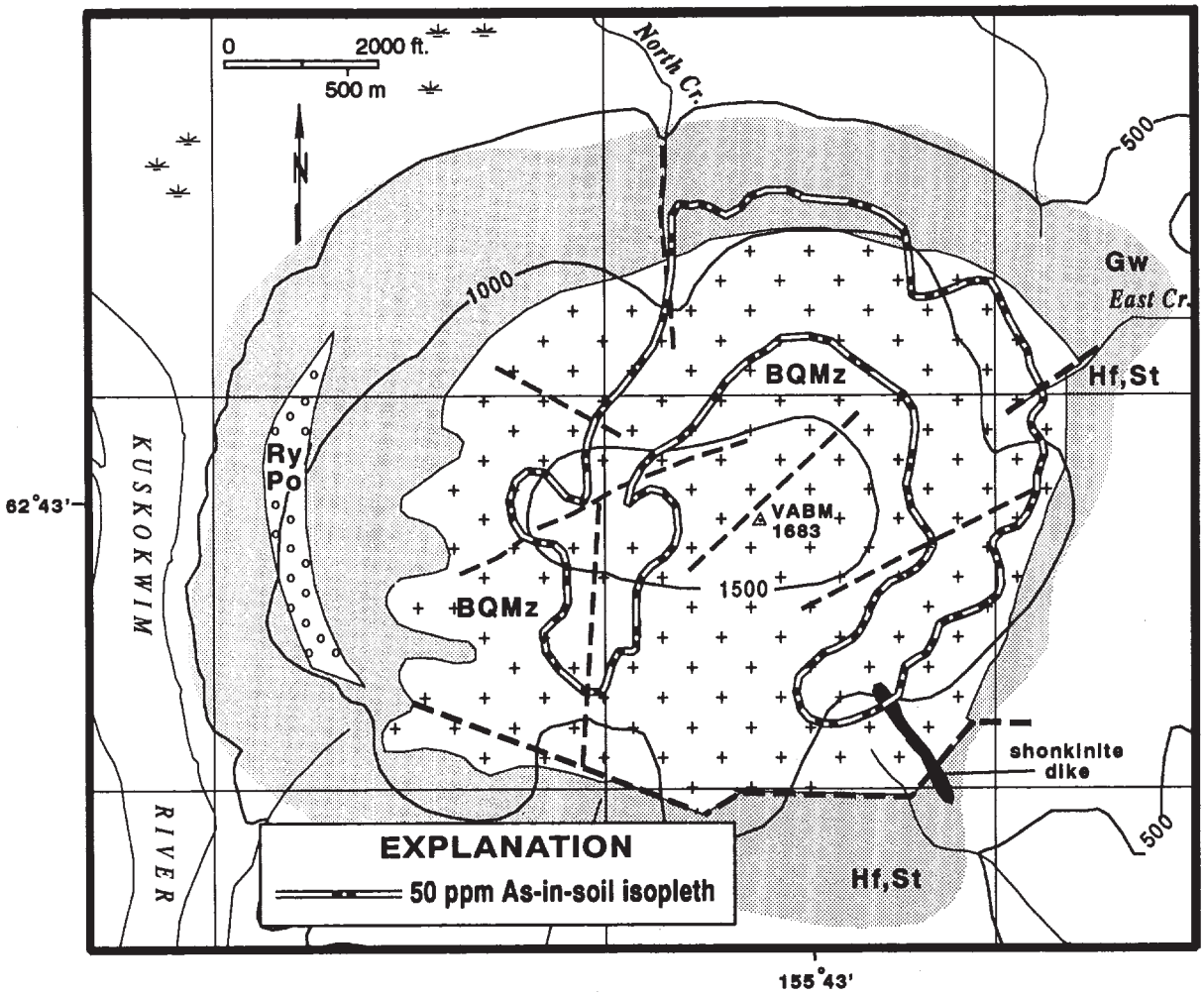

Figure 6. *Contoured arsenic-in-soil geochemistry.*

and mineralization, as indicated by data from 15 drill holes. Geometric interpretation of lithologic data and geochemical analyses indicates that (1) a broad zone of pervasive alteration envelopes the gold and sulfide mineralization, (2) mineralization occurs in multiple, subhorizontal bodies with a somewhat flattened cylindrical geometry, and (3) alteration and mineralization are crudely centered on a swarm of intrusive/hydrothermal breccias. Mineralogical and textural data, as well as K/Ar and fission-track dates, suggest a genetic link between the quartz monzonite stock and gold mineralization. The Central Zone is the largest body of potentially economic gold mineralization that has been identified at this time at Vinasale Mountain.

Alteration

We recognize three types of hydrothermal alteration in the Central Zone (1) silicification, (2) sericite alteration, and (3) propylitic alteration. In general, hydrothermal alteration in the Central Zone is centered on the intrusion breccias and extends outward for several hundred meters into the porphyritic quartz monzonite. Propylitic alteration is present as a large halo around sericitic and silicic alteration. For example, the drill holes which intersect breccia contain the strongest and most widespread silicification and sericitic alteration. Conversely, those holes drilled peripheral to the breccias (an average distance of 76 m away from the breccias) contain distinctly weaker and less widespread sericitic and silicic alteration, but contain widespread propylitic alteration.

Silicification occurs as veins, segregations, and silica flooding. Veins contain transparent, open-space-growth comb quartz, dolomite, coarse-grained sulfides, and microscopic apatite. These veins are up to 4 cm wide, and include both through-going and wispy varieties; the latter being characterized by the presence of diffuse vein terminations along strike. Quartz segregations, consisting of gray comb quartz, dolomite, and sulfides, are up to 3.8 cm wide, and have irregular shapes. Weak to moderate silica flooding accompanied by disseminated sulfides occurs in drill intercepts up to 30.5 m thick, and forms narrow envelopes around veins; this relationship suggests that veining and silica flooding are at least in part synchronous. Areas of silica flooding are commonly central to, and gradational outward into, areas of sericite alteration. Sulfide minerals associated with silicification include major pyrite, arsenopyrite, and subordinate boulangerite, stibnite, sphalerite, and galena. Both pre- and post-sulfide quartz veining occur in the Central Zone as well, as evidenced by clasts of gray vein quartz up to 2.5 cm in diameter in the breccia (which record a period of pre-sulfide veining), and a set of late, planar, gray, sulfide-barren, fine-grained quartz veinlets which cross-cut all other types of hydrothermal alteration.

Sericite alteration in the Central Zone is characterized by the progressive replacement of biotite and plagioclase by sericite and dolomite, and of K-feldspar by sericite, quartz, and dolomite. Weak sericite alteration is characterized by pale green-colored sericite which incompletely replaces interstitial chlorite, and by the chloritization of biotite inclusions in poikilitic K-feldspar phenocrysts; it is usually accompanied by up to 2 percent clotty pyrite and fine-grained acicular arsenopyrite. Moderate sericite alteration is characterized by increasing replacement of the monzonite groundmass by sericite and dolomite and by the partial replacement of K-feldspar phenocrysts by both sericite and dolomite. Chlorite inclusions in K-feldspar phenocrysts are replaced by pyrite. Intense sericite alteration is marked by the presence of corroded K-feldspar, the total replacement of the groundmass by sericite, and a decrease in dolomite, pyrite, and arsenopyrite content. Sericite alteration is very widespread in the Central Zone, occurring in every drill hole and mapped over a 457 m by 610 m area on the surface. Strong sericite alteration is usually peripheral to silica flooding or veining, and grades outward through progressively weaker sericite alteration, eventually giving way to propylitic alteration. Propylitic alteration forms a broader halo around zones of sericitic and silicic alteration It is characterized by the replacement of biotite by chlorite and calcite, and the replacement of plagioclase by epidote, calcite and chlorite. Pervasive propylitic alteration extends outward from sericite alteration for a distance of at least 100 m.

Alteration boundaries are generally intergradational over intervals up to 6 m, however, locally the boundaries are sharp, occurring over intervals less than 2.5 cm. Those sharp boundaries are distinctly more abundant in the breccias and in the selvages of quartz-dolomite veins within the enveloping quartz monzonite. This systematic difference in alteration boundary morphologies is interpreted to result from higher fluid flow rates for hydrothermal fluids in the breccias and veins.

We have obtained a K/Ar date of 68 ± 1.7 Ma from a hydrothermal sericite separate (table 2), and a fission track date of 69 ± 6.6 Ma from an apatite separate collected from the Central Zone. These dates indicate that, within analytical error, the age of hydrothermal alteration is the same as the crystallization age of the monzonite stock.

Mineralization

Sulfide mineralization in the Central Zone occurs as disseminations in areas of silica flooding or strong sericite alteration in breccias and quartz monzonite, and in quartz-dolomite veins and segregations. Pyrite and

Table 2. *Results of K-Ar analysis of sericite from altered quartz monzonite*

Sample	%K	^{40}K (ppm)	^{40}Ar rad (ppm)	^{40}Ar rad/total ^{40}Ar	^{40}Ar rad/^{40}K	Age (Ma)
290-3	8.880	10.593	.04269	.864	.004030	68.1 ± 1.7

rad = radiogenic

Constants: $\lambda_\varepsilon + \lambda'_\varepsilon = 0.581 \times 10^{-10}$ yr^{-1}, $\lambda_\beta = 4.962 \times 10^{-10}$ yr^{-1}, ^{40}K/Ktotal = 1.193×10^{-4} g/g

arsenopyrite are the dominant species and most often occur as disseminations; subordinate veinlet-hosted coarse-grained pyrite, arsenopyrite, stibnite, sphalerite and galena also occur (fig. 7). Scanning electron microscopy (SEM) performed on samples prepared from bulk sulfide flotation concentrates has also identified a lead antimony sulfide (jamesonite?, $Pb_4FeSb_6S_{14}$), a silver-bearing antimony sulfide (pyrargyrite?, Ag_3SbS_3), and native silver. In polished thin-section, inclusions of corroded and, occasionally, euhedral arsenopyrite in coarse grains of pyrite suggests there are multiple generations of arsenopyrite. This early arsenopyrite shows inner rectangular cores with lamellar structure, possibly due to zoning in arsenic, iron, or cobalt content. A second generation of arsenopyrite consists of rhomb-shaped crystals intergrown with pyrite. Two generations of stibnite have been observed, including one in quartz-dolomite-sulfide veinlets and segregations, and the second as coatings on the walls of late fractures.

Higher concentrations of gold in the Central Zone are associated with areas of intense sericite alteration and silica flooding, where fine-grained disseminated arsenopyrite is abundant. Over 90 percent of the gold reports to a sulfide concentrate, which suggests an intimate relationship between gold and the sulfide minerals. However, microscopic examination of concentrates and SEM mineralogical analyses of individual sulfide grains do not reveal either discrete grains of free gold or gold peaks in other minerals. From this we conclude that gold occurs as particles less than 1 micron in size within sulfide minerals. Because the correlation coefficient is highest between Au and As (0.81) followed by Mo (0.49), Fe (0.47), and Sb (0.43), it is likely that most of the gold is in arsenopyrite. The distribution of gold in the Central Zone bears a strong spatial association with the breccias as illustrated by the areas of 1 ppm Au or greater mineralization in figure 8. The two thickest intervals of plus 1 ppm Au are 63.1 m and 71.9 m with weighted average grades of 0.078 and 0.073 opt Au respectively. Both intervals are from a single drill hole. Selected high grade intercepts contain up to 0.81opt Au over widths of up to 17.8 cm. The Central Zone is also enriched in antimony (average 338 ppm), zinc (average 108 ppm), lead (average 75 ppm), bismuth (average 3 ppm), silver (average 0.7 ppm), and molybdenum (average 0.6 ppm). Gold:silver ratios for mineralized samples average 2:1. The highest silver values (up to 3.26 opt Ag) and lowest gold:silver ratios (as low as 0.13) occur in the eastern Central Zone and suggest the presence of lateral metal zonation. Similarly, arsenic is concentrated in the southern Central Zone where one drill hole averages 0.8 percent As.

Northeast Zone

The Northeast Zone is defined at the surface by a 1,219 by 610 m area of anomalous gold in soils. Although the Northeast Zone is the most areally extensive soil anomaly, the individual gold-in-soil values are more weakly anomalous, with a high value of 185 ppb Au, compared to a high value of 2,470 ppb Au in the Central Zone. Diamond drilling has established that the gold-in-soil anomalies collectively reflect a large number of scattered pods of alteration and mineralization associated with southeast-dipping, fracture-controlled quartz veinlets. Scattered pods of fracture-controlled veinlets and associated alteration have been identified to depths of up to 390 ft (118 m) in 23 drill holes. The style of alteration and mineralization is morphologically different from that in the Central Zone; however, other similarities suggest that the two zones result from related hydrothermal fluids.

Alteration

Hydrothermal alteration and gold mineralization in the Northeast Zone are strongly controlled by fracturing associated with three inferred, northeast-trending faults. Although hydrothermally altered drill intercepts are as thick as 30.5 m, alteration intensity is generally weak and confined to narrow envelopes around mineralized fractures; widespread pervasive alteration similar to that in the Central Zone is lacking. We recognize three types of hydrothermal alteration in the Northeast Zone including: (1) silicification, (2) sericitization, and (3) propylitization.

Silicification is manifested as veins and as weak silica flooding along veinlet margins. Two veinlet types are recognized: (1) quartz-dolomite ± sulfide veinlets up to 0.7 cm wide and, (2) sulfide-barren, open-space-growth quartz veinlets up to 1.5 cm wide.

Figure 7. *Coarse-grained stibnite in open-space-growth quartz vein cutting monzonite with disseminated pyrite and arsenopyrite, Central Zone.*

Quartz-dolomite ± sulfide veinlets constitute 60-70 percent of the total veinlet population in the Northeast Zone. Quartz, dolomite, and sulfide proportions vary within individual veins, but quartz > sulfide > dolomite veins dominate in the mineralized drill intervals seen to date. Veinlet morphologies generally consist of a comb-quartz median flanked by dolomitic vein walls. Sulfides are present as fine-grained aggregates on one or both vein selvages. Quartz-dolomite ± sulfide veinlets are generally planar and occur in zones up to 25 cm wide consisting of dense, sheeted veinlets that dip 25° to 70° in a southerly direction. Veinlets occasionally exhibit cataclastic textures consisting of milled quartz clasts in a quartz ± sulfide matrix (fig. 9). The sheeted veinlets do not display systematic crosscutting relationships, implying a rather simple veinlet paragenesis and possibly a short-lived period of alteration and mineralization. Silica flooding is not common but is weakly developed within intervals of high quartz-dolomite ± sulfide veinlet density as selvages around individual veinlets, indicating that flooding and veining are synchronous.

Open-space-growth comb quartz veinlets are very sparsely distributed throughout the Northeast Zone. They dip 20° to 40° relative to vertical core axes, and are unaccompanied by wall-rock alteration. The open-space veins are cross-cut by quartz-dolomite ± veinlets and therefore represent the earliest generation of veins.

Sericite alteration typically occurs as centimeter-scale envelopes surrounding veinlets and fractures and it grades outward to propylitic alteration. Within the sericitic envelopes, biotite and plagioclase are altered to sericite and quartz, and K-feldspar phenocrysts are weakly sericitized. In very intense sericitization, K-feldspar phenocrysts are corroded and almost completely replaced by quartz, dolomite, and sericite. In sheeted veinlet zones, the alteration envelopes coalesce into continuous intervals of moderate to intense sericite alteration, commonly containing trace to 1 percent disseminated pyrite which replaces biotite.

Propylitic alteration forms halos up to 7.5 m wide around fracture zones and is characterized by variably chloritized biotite and weakly epidotized plagioclase. Propylitization intensifies towards mineralized intervals where biotite books are totally replaced by chlorite, poikilitic biotite inclusions in K-feldspar are at least weakly chloritized, plagioclase is strongly sausseritized, and the quartz monzonite takes on a light green color.

We have obtained fission track dates of 73 ± 8 Ma and 69 ± 5.8 Ma from two apatite separates from hydrothermally altered rocks in the Northeast Zone. These dates indicate that, within analytical error, the hydrothermal

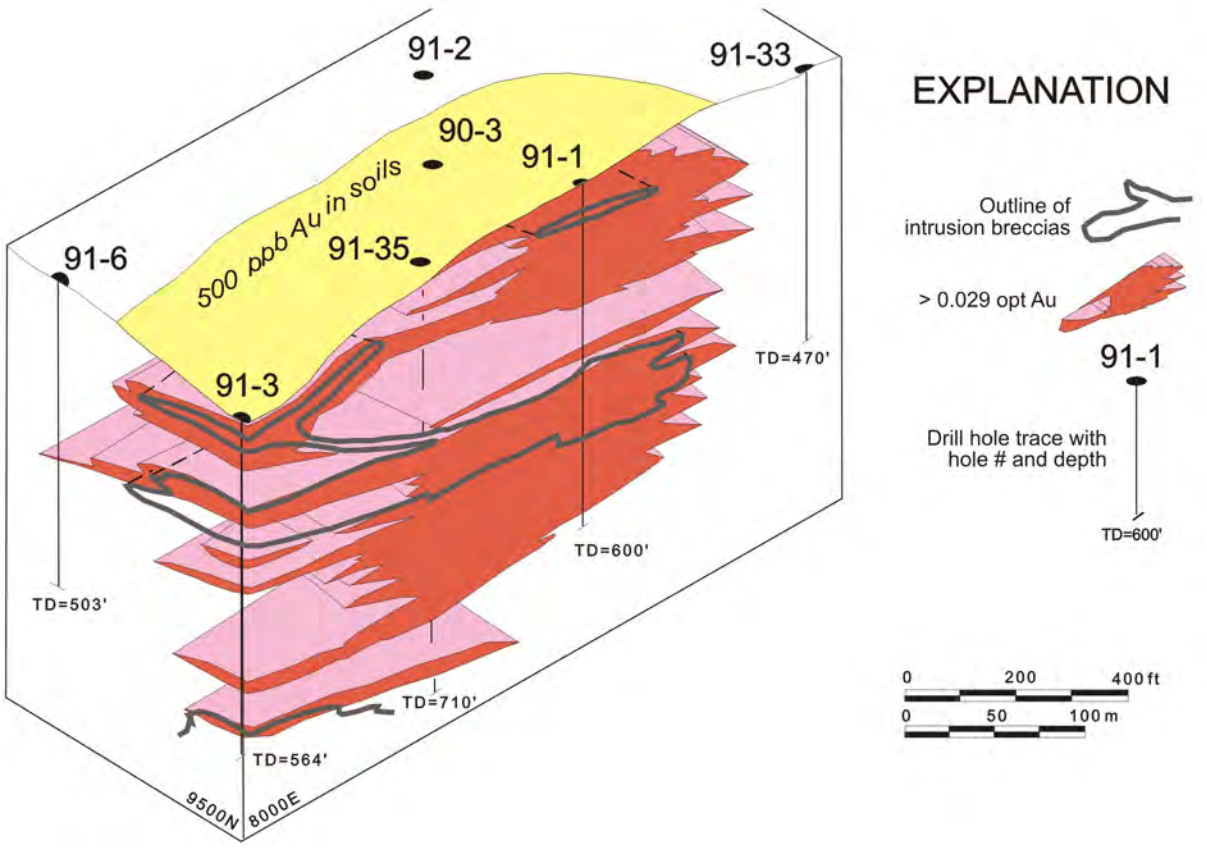

Figure 8. *Block model of the Central Zone depicting distribution of gold mineralization and the monzonite intrusion breccias.*

alteration in the Northeast Zone is the same age as that in the Central Zone.

Mineralization

Sulfide mineralization in the Northeast Zone most often occurs as fine-grained aggregates on quartz-dolomite veinlet selvages and as disseminations in silica flooded areas within pods with a high veinlet density. Pyrite is the dominant species in veinlets, whereas arsenopyrite is more common in areas of silica flooding. Trace disseminated pyrite also replaces biotite in areas of moderate to intense sericite alteration. Stibnite commonly occurs as late fracture coatings and occasionally occurs within quartz-dolomite ± sulfide veinlets. Base metal sulfides or free gold do not occur in the Northeast Zone.

Gold mineralization in the Northeast Zone is spatially associated with the pods of fracture-controlled quartz-dolomite veinlets accompanied by pyrite and arsenopyrite. Gold-bearing intercepts range in grade and thickness from 21 m of 0.083 opt Au to 2.4 m of 0.03 opt Au or less. A plot of grade x thickness vs. elevation (fig. 10) illustrates that gold has a bimodal distribution with modes at elevations of 900 ft (274 m) and 1,200 ft (366 m) above mean sea level (MSL). Significant gold values are lacking at elevations below 800 ft (244 m) and above 1,300 ft (396 m) MSL. The systematic distribution of gold indicates that the Northeast Zone is vertically zoned and that physical and/or chemical factors favored precipitation of sulfides and gold above 800 ft (244 m) and specifically at the 900 ft (274 m) and 1,200 ft (366 m) elevations. The gradual decrease of grade x thickness below 800 ft (244 m) suggests that the drill intercepts represent a cross-section through at least the lower portion (and all that remains) of the Northeast Zone. Higher grade x thicknesses correspond with higher veinlet density, and thus map areas of higher fracture density within the Northeast Zone.

Correlation of mineralized fracture sets in closely spaced drill holes indicates a southeast-dipping polarity to mineralized fractures. Furthermore, the consistency of mineralized veinlet inclinations in all of the drill holes in the Northeast and South zone implies that mineralization is controlled by a number of co-planar fracture

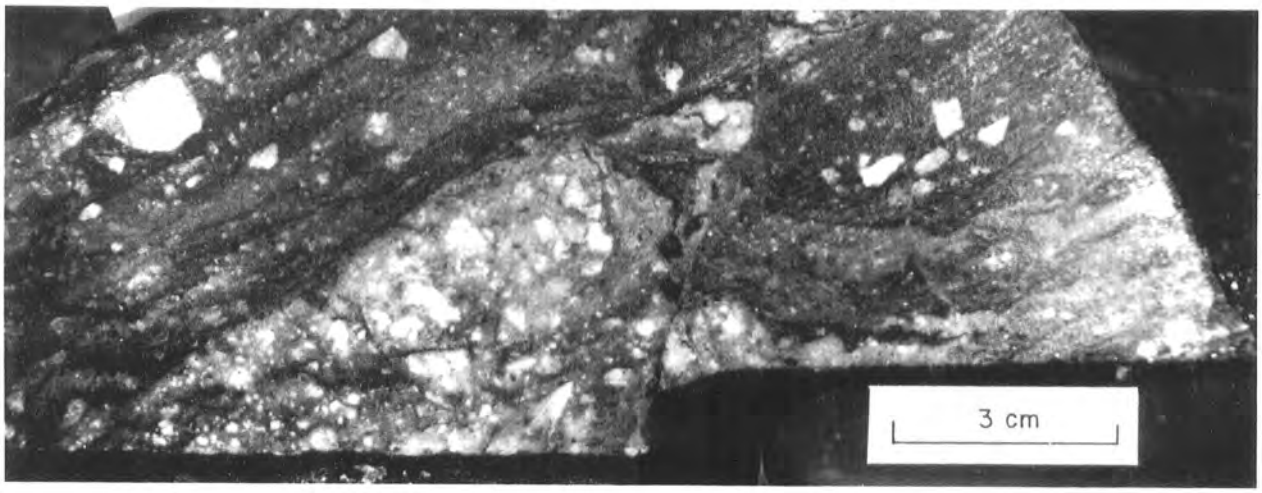

Figure 9. *Cataclastic texture in quartz-sulfide vein, Northeast Zone.*

sets. Contoured VLF geophysical data define three prominent north-northeast to northeast trends and weaker east-west trends (fig. 11). These prominent northeast trends are partially coincident with anomalous arsenic-in-soil geochemistry and are parallel to aerial-photo linears, strongly suggesting the presence of major northeast-trending fracture zones. We infer that the widespread fracturing that hosts veinlet gold and sulfide mineralization, and alteration, collectively comprises these northeast-trending fracture zones.

The Northeast and Central zones exhibit both similar and contrasting geochemical features. As in the Central Zone, there is a strong gold-arsenic association in the Northeast Zone, which suggests that arsenopyrite is again the principal gold-bearing sulfide species. Northeast Zone mineralization is comparatively less enriched in antimony (average 233 ppm), zinc (average 43 ppm), lead (average 17 ppm), bismuth (average 0.8 ppm), silver (average 0.6 ppm), and molybdenum (0.5 ppm). Barium values are slightly higher in the Northeast Zone (100 -300 ppm) than in the Central Zone (less than 100 ppm), though both are depleted relative to the host quartz monzonite (400 - 600 ppm). These variations in concentrations of both enriched and depleted elements could result from intrinsic chemical differences in the respective causative hydrothermal fluids, but is as likely a function of contrasting physical conditions between the two zones, that is, rock/fluid ratios, rock permeabilities, or the contrasting sizes of the two zones.

DISCUSSION AND CONCLUSIONS

Synthesis of the data presented here provides a geologic framework for constraining the controls and mode of emplacement of alteration and mineralization at Vinasale Mountain. The key geological components of the Central Zone are summarized below.

(1) Hydrothermal alteration and gold-sulfide mineralization are centered on the intrusion breccias. Alteration boundaries are sharper in the breccias and veins

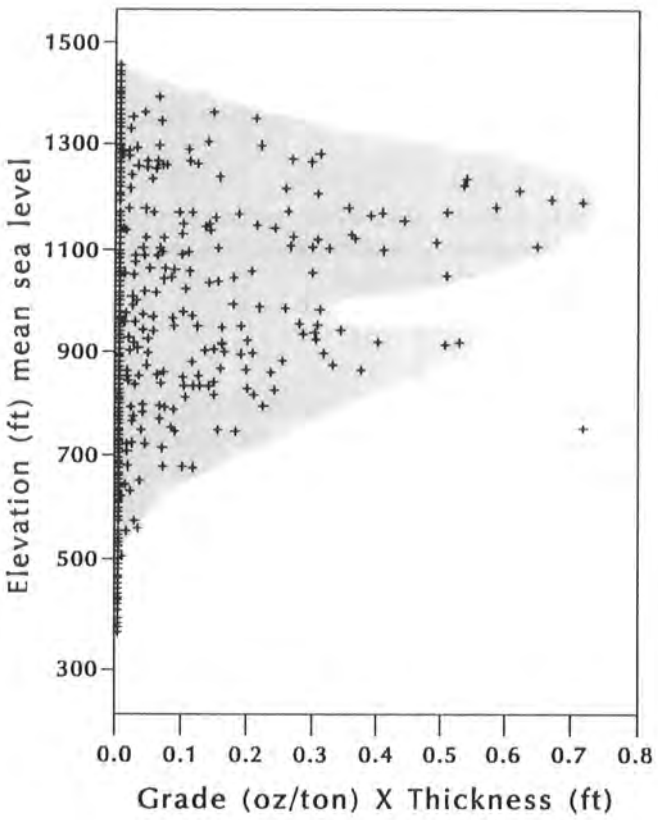

Figure 10. *Bimodal vertical distribution of gold in the Northeast Zone.*

compared to the enclosing quartz monzonite. Collectively these features strongly suggest that the breccias acted as a primary conduit for the causative hydrothermal fluids.

(2) The Central Zone is situated at the intersection of northeast- and north-trending photo linears and coincident with northeast-trending VLF anomalies. The combination of these two factors suggests structural control of the emplacement of the intrusion breccias.

(3) The K/Ar and fission track dates on the hydrothermal alteration are, within analytical error, the same age as the quartz-monzonite host rock, suggesting that the alteration and the stock are coeval. The development of igneous breccias, hydrothermal alteration, and brecciation within the monzonite stock during a relatively brief time interval (<1 million years) suggests a continuum between magmatic processes, the evolution of a silica-CO_2-rich fluid, and the onset of hydrothermal alteration, brecciation, and gold-sulfide precipitation. Vila and others (1991) recently suggested similar temporal and mineralogical interrelationships between late magmatic intrusion breccias and hydrothermal alteration at the Marte porphyry gold deposits in Chile.

Cumulatively these data suggest an empirical model for the Central Zone wherein alteration and mineralization are temporally and genetically related to the development of intrusion and hydrothermal breccias. Initially, monzonite intrusion breccia acted as the primary fluid conduit for a silica-CO_2-rich fluid resulting in the development of a hydrothermal cell centered on the intrusion breccias and extending into the enclosing quartz monzonite. Local hydrothermal brecciation occurred within the monzonite intrusion breccia. Fractures within the enclosing quartz monzonite provided second order pathways for fluid migration. The ensuing rock-fluid interaction resulted in moderate to strong hydrothermal alteration in and

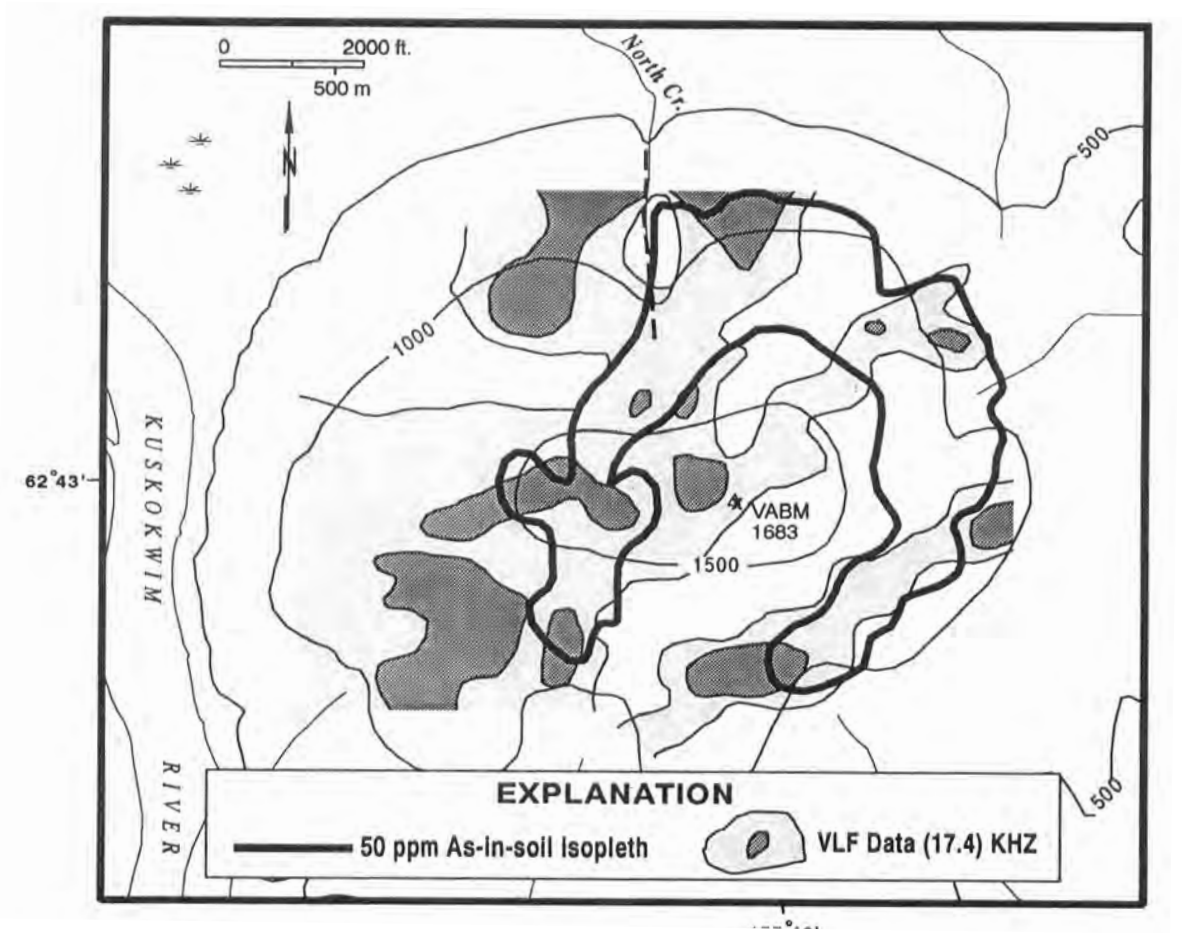

Figure 11. *Frazer filtered VLF data depicting prominent northeast-trending structural grain and arsenic-in-soil geochemistry.*

proximal to the breccias and subsidiary fractures, where fluid flow and chemical exchange rates were highest. Alteration progressively weakened with distance from the breccias where fluid flow was more restricted and chemical exchange rates were limited by the relatively buffered condition of the fluids. Gold and sulfide precipitation was coeval with hydrothermal alteration and occurred preferentially within and proximal to the intrusion breccias. Multiple generations of arsenopyrite and stibnite crystallized in response to episodic fluctuations in the hydrothermal fluid physiochemistry. The circulation in the system eventually ceased, likely in response to rapid cooling as suggested by the overlapping age determinations from the stock, hydrothermal sericite, and apatite. The last vestige of the hydrothermal system is a set of late fractures accompanied by thin stibnite fracture coatings in the absence of hydrothermal alteration.

The cumulative data from the Northeast Zone suggest that mineralization was initiated with the onset of brittle fracturing. This fracturing allowed hydrothermal fluids to migrate upward and laterally, depositing quartz, dolomite, arsenopyrite, pyrite, and gold as quartz-sulfide ± dolomite veinlets in northeast-trending fracture zones, predominantly above 800 ft (244 m) MSL. The systematic distribution of gold with respect to elevation suggests that the Northeast Zone is vertically zoned. Weak average gold grades and comparatively low concentrations of other introduced metals, the discontinuity of the mineralization, simple veinlet paragenesis, and the nearly total lack of hydrothermal veinlet breccias suggest that the Northeast Zone formed from a relatively poorly focussed, passive hydrothermal system.

Similarities between the Central and Northeast zones, including strong gold-arsenic metal assemblages, ages, and alteration types indicate that the two zones are coeval and result from related hydrothermal fluids. The differences between the two zones are primarily of size and intensity of alteration and mineralization, and appear to be the result of different structural controls. The intrusion breccias in the Central Zone provided a focussed fluid pathway whereas the fracture system in the Northeast Zone provided a larger but more diffuse fluid pathway. This difference is critical from an economic standpoint because the relatively focussed hydrothermal circulation centered on the breccias in the Central Zone resulted in a coherent zone of gold mineralization with a geologic resource of approximately 1 million oz (31,000 kg) of gold. The fracture system in the Northeast Zone, though areally extensive, is host to lower average grade and more diffuse gold mineralization that is judged to be subeconomic at this time.

ACKNOWLEDGMENTS

The author is grateful to Central Alaska Gold Company, Placer Dome U.S., and Doyon, Limited for permission to publish this paper. Thanks are especially extended to C.C. Puchner and L.C. Nicholson for their frequent discussions which helped clarify some of the ideas presented here. Warm thanks go to Rainer Newberry and Tom Bundtzen for their technical review which improved the final version of the paper. Acknowledgement is also extended to John Murphy, LaTrobe University, Victoria, Australia for the fission track dating.

REFERENCES CITED

Bundtzen, T.K., 1986, Prospect examination of a gold-tungsten placer deposit at Alder Creek Vinasale Mountain area, western Alaska: Alaska Division of Geological & Geophysical Surveys Public-data File 86-49, 10 p.

Cady, W.M., Wallace, R.E., Hoare, J.M., and Weber, E.J., 1955, The Central Kuskokwim Region, Alaska: U.S. Geological Survey Professional Paper 268, 132 p.

DiMarchi, J.J., Nicholson, L.C., Bradley, M.A., and Poage, M.A., 1991, Central Alaska Gold Company 1991 Annual Report—Vinasale Mountain Project, v. 1, unpublished report, 51 p.

DiMarchi, J.J., Weglarz, T.B., Dickey, C.F., Laux, D.P., Smith, M.T., Toro, J., Kurtz, J. P., 1990, Central Alaska Gold Company 1990 Annual Report, Alaska Field Operations—Doyon Option, v. 1, unpublished report, 192 p.

Keith, S.B., 1984, Magma series and mineral deposits, MagmaChem Exploration, Inc., company report, 60 p.

Leveille, R.A., Newberry, R.J., and Bull, K.F., 1988, An oxidation state-alkalinity diagram for discriminating some gold-favorable plutons: an empirical and phenomenalogical approach: Geological Society of America, Abstracts with Programs, v. 17, p. A142

Nokleberg, W.J., Bundtzen, T.K., Berg, H.C., Brew, D.A., Grybeck, D., Robinson, M.S., Smith, T.E., Yeend, W., 1987, Significant metalliferous lode deposits and placer districts of Alaska: U.S. Geological Survey Bulletin 1786, 104 p.

Silberman, M.L., Moll, E., Patton, W.W., Jr., Chapman, R. M., and Connor, C. L., 1979, Potassium-argon age of granitic and volcanic rocks from the Ruby, Medfra, and adjacent quadrangles, west-central Alaska, *in* Johnson, K. M., and William, J. R., eds., U.S.Geological Survey Circular 804-B, p. B63-B66.

Solie, D.N., Bundtzen, T.K., and Gilbert, W.G., 1991, K/Ar ages of igneous rocks in the McGrath Quadrangle, Alaska: Alaska Division of Geological & Geophysical Surveys Public-Data File 91-23, 8p.

Vila, T., Sillitoe, R.H., Betzhold, J., and Viteri, E., 1991, The porphyry gold deposit at Marte, northern Chile: Economic Geology, v. 86, p. 1271-1286.

Wilson, F.H., 1977, Some plutonic rocks of southwestern Alaska—A data compilation: U.S. Geological Survey Open-file Report 77-501, 8 p., 4 pls., scale 1:1,000,000.

FUMAROLIC GAS CHEMISTRY (1982) AND THERMAL SPRING WATER CHEMISTRY, CRATER PEAK (1985), MOUNT SPURR, ALASKA

by
Roman J. Motyka[1] and Christopher J. Nye[2]

INTRODUCTION

The Spurr volcanic complex (SVC) is a Quaternary sequence of calc-alkaline andesites located on the west side of Cook Inlet, 125 km west of Anchorage (fig. 1). At least five areas of surface thermal manifestations have been identified at the SVC (fig. 2): (1) diffuse fumarolic activity on the flanks of the Mount Spurr summit cone (elevation 3,000 m; 9,400 ft); (2) photographic evidence of snow melt at the Mt. Spurr summit crater; (3) the fumaroles and crater lake of Crater Peak (elevation 2,300 m; 7,200 ft), a satellite stratovolcano; (4) thermal springs near the southern base of Crater Peak; and (5) a snow cave rimmed with icicles 1.5 km northeast of the inferred caldera rim.

This paper describes the geochemistry of gases collected from Crater Peak fumaroles in 1982 and of waters collected from thermal springs 4 km south of Crater Peak, in 1985. These fluid geochemical investigations were undertaken as part of a broader program to assess the geothermal potential of the SVC. Understanding the geochemistry of thermal fluids aids in assessing the type of subsurface geothermal system and in estimating subsurface temperatures. Observations resulting from other geothermal investigations at the SVC, discussed in Turner and Wescott (1986) and in Wescott and others (1988), include controlled source audio-magnetotelluric, self-potential, and Hg and He soil-gas surveys as well as investigations of ice depth in the caldera. Petrology, geochemistry, and age of the SVC are discussed in Nye and Turner (1990). The state of Alaska has leased two tracts southeast of the thermal springs to a private company for geothermal development.

Thermal fluid geochemistry is also useful for monitoring volcanic activity and shows potential as a forecasting tool. Because of their proximity to populated areas, Mount Spurr and Crater Peak pose volcanic hazards to upper Cook Inlet. Air traffic, which was disrupted during the 1989-90 eruption of Mount Redoubt, is particularly susceptible to volcanic hazards. Our data now provide a baseline for assessing any future changes in geochemistry, such as increases in SO_2 emissions or in the ratio of $^3He/^4He$, changes which could signal the onset of increased magmatic heating or influx of new magma beneath the volcano, or both.

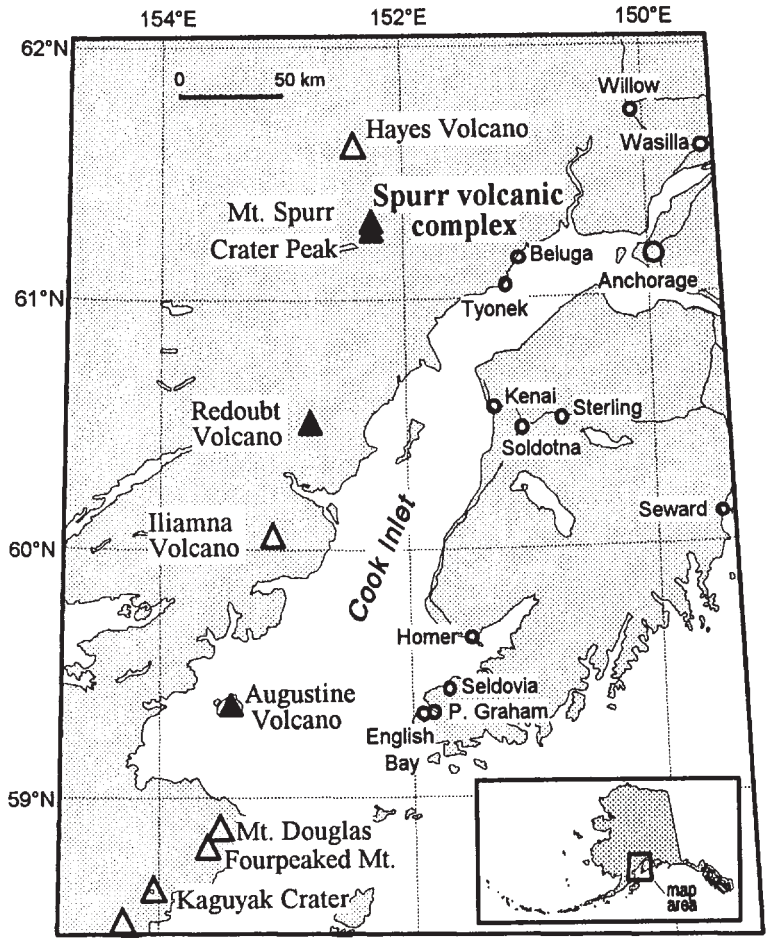

Figure 1. *Location of the Spurr volcanic complex with respect to other Cook Inlet Holocene volcanic centers. Volcanoes marked with solid triangles have had historic eruptions.*

[1]Alaska Division of Geological & Geophysical Surveys, 400 Willoughby Center, 3rd floor, Juneau, Alaska 99801.

[2]Alaska Division of Geological & Geophysical Surveys, 794 University Ave., Fairbanks, Alaska, 99709-3645, and Geophysical Institute, University of Alaska, Fairbanks, Alaska, 99775

Our analyses show that the 1982 Crater Peak fumarolic gases are dominated by wet steam and CO_2. The only sulfur gas detected was H_2S. The chemistry and estimated temperature of equilibration (200°-250°C) are consistent with a hydrothermal rather than a direct magmatic source for these fumarolic gases. The $^3He/^4He$ ratio of 6.6 found for the fumarolic gases indicates a magmatic influence on the hydrothermal system. We suggest that the fumarolic CO_2 and H_2S are probably derived in part from a magmatic source, but that they first pass through and interact with a hydrothermal layer that has developed over the magma body. Such a model is similar to models of magma-related hydrothermal systems proposed by Giggenbach (1987; 1988) and by Henley and Ellis (1983).

The thermal springs south of Crater Peak discharge Mg-rich, near-neutral HCO_3-SO_4-Cl waters. The chemistry of these waters suggests that they are derived from the margins of the hydrothermal system where steam and vapor-phase gases rich in CO_2 and H_2S are being absorbed in shallow groundwater.

GEOLOGIC SETTING

The 2,400 km Aleutian arc of active volcanism is forming in response to subduction of the Pacific plate beneath the North American plate. The SVC lies near the eastern end of this arc and is one of six volcanic centers in the Cook Inlet region that have been active in the Holocene (fig. 1). The SVC consists of a sequence of calc-alkaline andesites that were erupted over the last 250,000 years (Nye and Turner, 1990) onto rocks of the Alaska Peninsula terrane as defined by Wilson and others (1985). These Silurian to Lower Jurassic limestones, basalts and clastic rocks, along with Jurassic to Cretaceous flysch are intruded by Jurassic to Tertiary rocks of the Alaska-Aleutian Range batholith.

For most of the lifetime of the SVC, the ancestral Mount Spurr stratovolcano erupted high-silica andesitic magmas of uniform composition (Nye and Turner, 1990). Andesite production was periodically interrupted by the injection of new, mafic magma, and resultant eruptions of more mafic andesites. Near the end of the Pleistocene the ancestral Mount Spurr underwent avalanche caldera formation. Afterward a large dome (the present Mount Spurr) formed in the center of the caldera and a satellite stratocone, Crater Peak, formed in the breach 3 km south (fig. 2). Subsequently, two compositionally distinct magmas and mixtures of the two erupted from the two vents with lavas from Crater Peak more mafic than those of the Mount Spurr dome. Late Holocene activity has been restricted to Crater Peak which has erupted 35 times in the last 6,000 yr and 15 times within the last 500 yr (Riehle, 1985), most recently July 9, 1953 (Juhle and Coulter, 1955). The 1953 eruption cloud reached over 21 km in altitude and deposited 6 mm of ash on Anchorage 125 km to the east.

CRATER PEAK FUMAROLES AND THERMAL SPRINGS

The crater at Crater Peak is presently the most thermally active area in the SVC. Prior to the 1953 eruption, thermal activity at this crater was either minor or did not exist. September 1952 aerial photos show the crater was ice filled. Except for steep walls above the crater, no areas of snow-free ground were visible. We collected fumarole gas samples in August 1982 during a reconnaissance investigation of the 1953 eruption crater. The fumarole field consisted of diffuse to moderately pressurized boiling-point (94°-95°C) vents that issued from a mound of volcanic ash perched above the eastern shore of the crater lake. Warm vapor was rising visibly from the 150 m diameter milky-blue lake that had formed in the eruption crater. Steep ashy crater walls made descent down to the lake too hazardous and we could not collect lake water samples.

We revisited the crater in the summer of 1985. Fumaroles along the east rim measured 96°-98.5°C but activity was too diffuse to obtain a reliable gas sample. A fumarolic vent about 5 m in diameter had formed in the talus on the north slope of the crater lake and emitted a large but diffuse plume. Sulfur deposits were observed on the vent walls. Rockfall danger made the vent unapproachable and, in any case, gas flow appeared too diffuse for reliable gas sampling. Crater lake water temperature was estimated at 45°C.

A 1-km-long zone of warm springs was discovered in 1985 in the bottom of the valley 4 km south of Crater Peak, at an elevation of 2,000 ft (650 m) (fig. 2). We sampled 40°C water issuing from a spring in the eastern wall of the canyon. The estimated rate of flow was 20 liters per minute. Most of the warm springs are in the valley bottom and are extensively diluted with stream water. Total warm water flow for the entire valley bottom is probably about a thousand liters per minute. These springs issue from pyroclastic fan deposits which are overlain by Crater Peak volcanic flows.

METHODS

The procedures followed for collection and treatment of water samples for geochemical analyses and for field determination of pH and HCO_3 and H_2S concentrations are described in Presser and Barnes (1974) and in Giggenbach and Goguel (1989). Major, minor, and trace

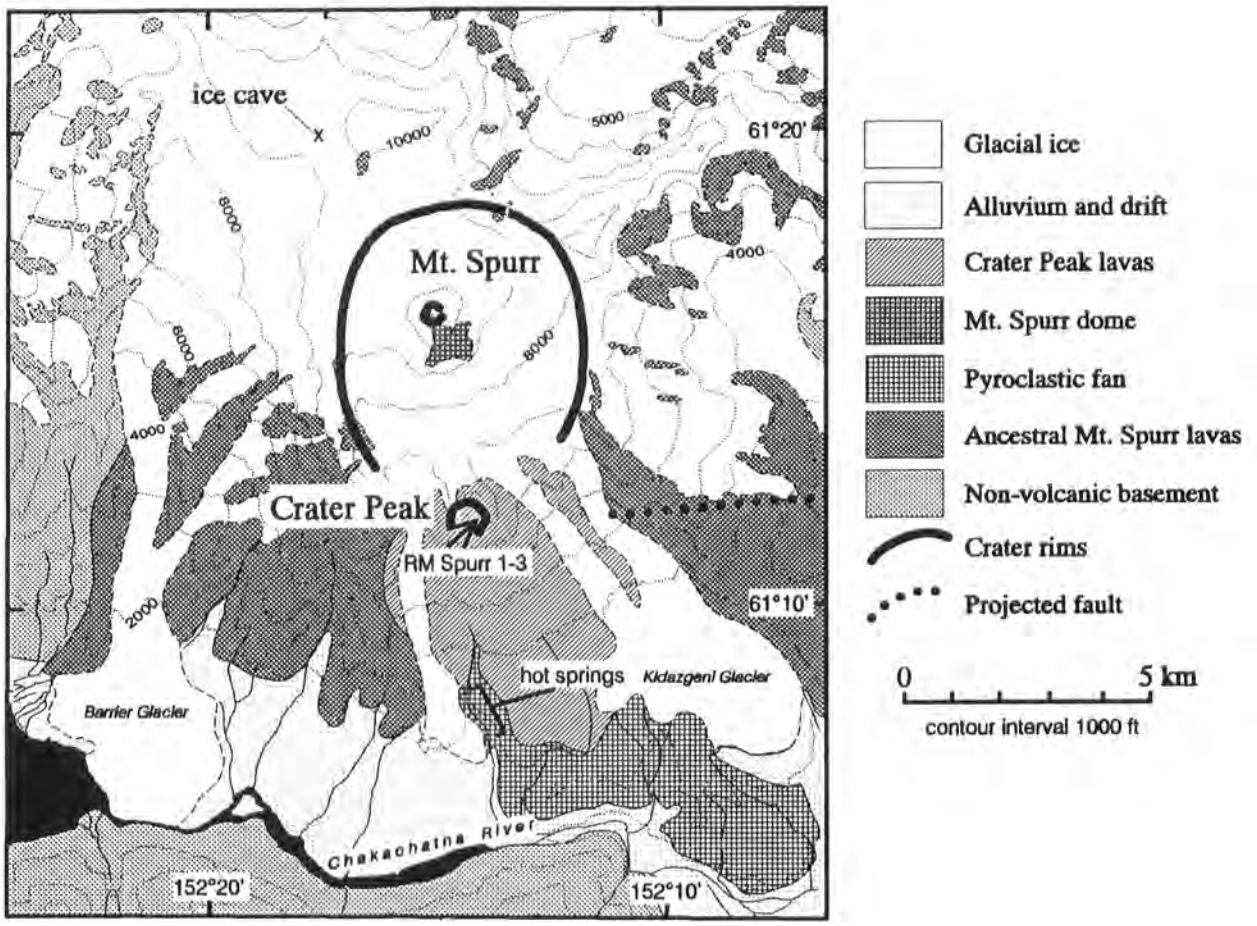

Figure 2. *Generalized geologic map of the Mount Spurr region and location of Crater Peak thermal areas, adapted from Nye and Turner, 1990.*

cation concentrations were determined by using a Model 4000 Perkin-Elmer atomic absorption spectrometer with HGA 400 graphite furnace following standard procedures outlined in Skougstad and others (1979) and in the Perkin-Elmer reference manual. Sulfates, bromide, and iodide were determined using a Dionex model 2010i ion chromatograph. Fluorides were determined by specific ion-electrode method; Cl by Mohr titration; and boron by the carminic acid method. Silica concentrations were determined by the molybdate blue method. Stable isotope compositions of water samples were analyzed at the Stable Isotope Laboratory, Southern Methodist University.

Gases were collected using a funnel placed over the fumarolic vent and connected to the collecting flask with tygon tubing. Samples RM82 Spurr 1 and RM82 Spurr 2 were collected in 50 cc evacuated flasks made from helium impermeable Corning 1720 glass. These samples were used for determining $^{3}He/^{4}He$ ratios, $\delta^{13}C\text{-}CO_2$, and gas chemistry. Sample RM82 Spurr 3 was collected in a 300 cc evacuated flask charged with 50 ml of 4 N sodium-hydroxide solution. The NaOH solution condenses and absorbs the primary fumarolic emissions (H_2O, CO_2, and sulfur gases) thus allowing accumulation of much greater quantities of gases and more accurate determination of the steam fraction.

Gas composition of sample 3 was determined following procedures discussed in Giggenbach and Goguel (1989). Head-space gases in the sodium-hydroxide charged flask (H_2, CH_4, O_2, N_2, and Ar) were analyzed on a dual-column gas chromatograph using helium- and nitrogen-carrier gases. The total moles of gas not absorbed in the sodium-hydroxide solution were determined by measuring the gas pressure and head space volume. CO_2 and total sulfur molar concentrations in the solution were determined by titration and by gravimetric means respectively, following procedures discussed in Giggenbach and Goguel (1989). Adjustments were made for head space gases dissolved in the solution using Henry's Law. Moles of each constituent collected were then determined and the mole percent of each constituent was calculated. The $^{13}C/^{12}C$ ratio in CO_2 was determined using $SrCO_3$ precipitated from the NaOH solution following methods discussed in Fahlquist and Janik (1992).

A disadvantage of NaOH gas sampling is that sulfur species (primarily H_2S and SO_2) are dissolved in the NaOH fluid and are not readily differentiated. Therefore, RM Spurr 1, a non-NaOH sample, was analyzed for both H_2S and SO_2 to determine the fraction of each species present in the fumarole emissions. Gas composition and the $^{13}C/^{12}C$ ratio in CO_2 of sample RM Spurr 1 were determined at U.S. Geological Survey, Menlo Park.

Sample RM Spurr 2 was used for determining $^3He/^4He$ ratios, He concentration, and gas composition at the Stable Isotope Laboratory, Scripps Institution of Oceanography (SIO). Methods used are described in Poreda (1983). At SIO, CO_2 and H_2S are collected by condensation in a liquid nitrogen bath. Total moles of CO_2 + H_2S are determined by measuring gas pressure and volume after noncondensible gases are pumped off and condensible gases revolatilized.

GAS CHEMISTRY

Results of geochemical and isotopic analyses of Crater Peak fumarolic gases are presented in table 1. The water-free gas composition of the three samples is similar, indicating consistency in methodology and analyses. Of the three Crater Peak analyses, we consider the analysis of the NaOH sample (RM Spurr 3) to be the best quality because of the much greater amount of total gases that can be collected using NaOH charged flasks. As oxygen in the fumarolic gases should be essentially nonexistent (Giggenbach, 1987), the slight amount of O_2 gas detected in our samples is attributable to air contamination during sampling. The N_2/Ar ratio of 75 lies between the atmospheric ratio (84) and air-saturated groundwater (34) indicating an atmospheric source of the N_2 and Ar in the fumarolic gases, probably in part from air bubbles entrained in recharge water, with oxygen removed in oxidation reactions. Sulfur dioxide was not detected in RM Spurr 1. Sulfur species collected in the NaOH flask (RM Spurr 3) were therefore assumed to be H_2S and are reported as such.

The fumarolic gases are water rich (97.9 percent steam) with the residual gases consisting almost entirely of CO_2 with minor to trace amounts of N_2, H_2S, H_2, Ar, and CH_4, a composition typical of boiling-point fumarolic vents associated with many arc volcanoes. As fumarolic activity did not exist prior to the July 1953 eruption, these fumarolic gases are likely to be related to residual 1953 magma interaction of meteoric water with hot rock heated by the magma. The water content, temperature, and residual composition point to a boiling, liquid-dominated hydrothermal source rather than a direct magmatic origin for the fumarolic gases. Meteoric water has most likely flooded and quenched the surfaces of the residual 1953 magma, creating a hydrothermal layer. While the magma probably continues to degas CO_2, sulfur, and possibly halogens into this hydrothermal system, fumarolic gas compositions are likely dominantly controlled by water-rock reactions and boiling within the liquid-dominated hydrothermal layer.

A magmatic influence on the fumarolic fluids is supported by the helium isotope ratio of R/Ra = 6.6 (table 1). This ratio is lower than values found for summit fumaroles on five other Aleutian arc volcanoes (Mounts. Okmok, Makushin, Griggs, Douglas, and Augustine) where R/Ra = 7.6-8.0, but higher than the southcentral Alaska volcano, Mount Wrangell, which has a R/Ra of 6.0 (Poreda and Craig, 1989). The higher ratios are in the range for mid-ocean-ridge basalts (R/Ra=8±1) indicating that the mantle is the dominant source of helium in Aleutian arc fluids. Poreda and Craig (1989) attributed the lower ratio at Mount Spurr to significant contribution (~20 percent) of crustal He (R/Ra<0.02) from either subducting terrigenous sediments or the overriding continental plate. Another possible source is assimilation of crust of the North American plate into the SVC magmas. Elevated Sr and Pb isotope ratios and $\delta^{18}O$ in the SVC lavas compared to other Aleutian volcanoes, and trace element systematics incompatible with fractional crystallization or bulk assimilation provide additional evidence for crustal contamination (Nye and Turner, 1990).

The Spurr $\delta^{13}C$-CO_2 values of -12 and -14 per mil are lighter than mantle-derived CO_2 (-4 to -9 per mil), but lie at the upper end of the range of values estimated for carbon dioxide derived from organic-sedimentary sources (Truesdell and Hulston, 1980). The fumarolic CO_2 may be a mixture of magmatic CO_2 or CO_2 contained in crust assimilated into the magma, or thermogenic sedimentary CO_2 or some combination of the three. The West Foreland Formation of mid-Tertiary age is exposed east of Crater Peak and probably underlies Crater Peak. The formation is nonmarine but contains abundant plant fossils and scattered coal seams (Calderwood and Fackler, 1972), which are possible sources of thermogenically generated organic-sedimentary carbon gases. The CH_4 in the fumarolic gases may also have organic-sedimentary origin.

Using empirical data, D'Amore and Panichi (1980) proposed a gas geothermometer for estimating geothermal reservoir temperatures based on the proportions of CO_2, H_2S, H_2, and CH_4 in fumarolic gases. The geothermometer is based on the assumption of gas-water-rock equilibrium in a hydrothermal system and preservation of this "deep" equilibrium composition in the emergent gases. The gas geothermometer was applied to analysis RM Spurr 3 after making a correction for air contamination based on oxygen present in the sample. For assumed CO_2 partial pressures of 1 bar, the source region

Table 1. *Analysis of gases from fumarole located on rim of Crater Peak crater, Mount Spurr, Alaska. Date sampled: August 4, 1982. Sampling temperature, 94°C*

	RM Spurr 1	RM Spurr 2	RM Spurr 3
H_2O, mole %	nd	nd	97.9
Residual gases, dry basis, mole %:			
CO_2	96.1	95.3[a]	94.7
H_2S	0.18	- -	0.77[b]
SO_2	<0.1	nd	- -[b]
H_2	nd	0.38	0.32
CH_4	0.022	0.046	0.034
N_2	2.93	3.24	4.09
O_2	0.04[c]	0.049	0.042
Ar	- -[c]	0.040	0.055
He	nd	0.0005	bd
N_2/Ar	- -	80	74
$\delta^{13}C$-CO_2, per mil[d]	-12.4	nd	-14.2
$^3He/^4He$, R/Ra[e] ratio	nd	6.6	nd

[a]$CO_2 + H_2S$.
[b]Total sulfur reported as H_2S.
[c]O_2 + Ar
[d]Value with respect to the carbonate standard "PDB." Analyses performed at U.S. Geological Survey, Menlo Park, California.
[e]Ratio of $^3He/^4He$ in sample over that in air. R. Poreda, Isotope Laboratory, Scripps Institution of Oceanography, analyst.
nd = not done; bd = below detection.

for equilibration of these gases is estimated to have a temperature of about 220°C. This geothermometer must be applied with discretion as gas-rock interactions and oxidation reactions with entrained air could have affected gas composition, particularly H_2 and H_2S, during ascent and sampling of the fluid. We note that higher values of H_2 and H_2S would increase the temperature predicted by this geothermometer. Therefore, we consider our result for this geothermometer to be a minimum temperature.

To circumvent some of the problems associated with multi-component geothermometers (such as differences in kinetic rates and secondary processes) Giggenbach and Goguel (1989) formulated gas geothermometers based on isomolar concentration with respect to argon. Argon was chosen because of its chemical inertness and the likelihood that it is introduced almost exclusively with the meteoric water component forming by far the bulk of geothermal waters. Giggenbach and Goguel (1989) found good correspondence between spring and fumarole gases and deep well temperatures for a geothermometer based on H_2/Ar. Giggenbach and Goguel (1989) also devised a geothermometer based on the ratio CO_2/Ar. Hydrogen reacts more quickly to changes in temperature and redox conditions and is thus likely to provide information on the shallower part of the system, whereas CO_2, which reacts more slowly, is likely to preserve information on the deeper part of the system. Applied to Crater Peak, these geothermometers predict "equilibrium liquid" temperatures of 229°C at shallower depths and 246°C at greater depths at Crater Peak.

WATER CHEMISTRY

The thermal water sampled near the base of Crater Peak is slightly acidic, relatively low in Cl but rich in HCO_3 and SO_4, and relatively high in Mg (table 2). The setting and chemistry of the Crater Peak thermal spring water is similar to Mother Goose Hot Springs located on the Alaska Peninsula (Motyka and others, 1981). Both sites are typified by large rates of discharge of thermal water rich in HCO_3 and SO_4 and are located at or near the base of a volcano that has active fumaroles near its summit. The HCO_3–SO_4 chemistry and presence of B in the water reflect the probable influence of volcanic gases on shallow ground waters (Giggenbach, 1987). Condensation of steam and interaction of acid gases with ground waters would produce acidic thermal water. The cation constituents and silica present in such water are largely derived through acid leaching of country rock which would in turn buffer the water to its nearly neutral but slightly acidic pH. The Cl and Br could also be derived from rock dissolution. Alternatively, these latter constituents could have originated from magmatic gases, or from mixing with minor amounts of a deeper, Cl-rich

thermal water. The anion chemistry and relatively large concentration of Mg present in the water indicates the thermal spring waters are very immature and are far from water-rock equilibrium (Giggenbach, 1988).

The stable isotope composition of the thermal water, two nearby stream waters, and snow melt from Crater Peak crater are plotted in figure 3. The meteoric water line of Craig (1961) and meteoric waters from Augustine Volcano, Cook Inlet (Kodosky and others, 1991) are also plotted for comparison. The surface streams that were sampled derive most of their water as runoff from higher elevations. Much of this runoff is probably meltwater from winter snowfall. The temperature dependency of isotopic composition in precipitation produces seasonal variations (winter precipitation is depleted in heavy isotopes with respect to summer precipitation) and altitude variations (the heavy isotope content of precipitation decreases with increasing elevation) (Panichi and Gonfianti, 1978). The isotopic composition of the thermal spring water is similar to that of Crater Peak snow melt and nearby snow melt runoff streams. This similarity indicates that the thermal springs are recharged by water that is derived from meltwater and precipitation that fell at middle to upper elevations of the SVC.

Table 3 gives the results of applying commonly used thermal water geothermometers (Fournier, 1981) and the K–Mg geothermometer proposed by Giggenbach (1988)

Table 2. *Chemical analysis of waters collected from Crater Peak hot springs, 1985.*[a] *Concentrations in mg/l unless otherwise specified*

Date sampled	8-03-85		
T, °C	40.2	$\delta^{18}O$[c]	-16.7
pH[b]	6.4	δD[c]	-138
Na	266	HCO_3[b]	622
K	75	SO_4	477
Ca	95	Cl	254
Mg	99	F	1.0
Li	0.42	Br	0.5
Sr	0.68	I	0.1
Cs	0.04	B	7.7
As	0.021	SiO_2	125
Fe	<0.1	H_2S[b]	0.1
		TDS (calc.)	1708

[a]Alaska Division of Geological & Geophysical Surveys, Fairbanks, M.A. Moorman, S.A. Liss, and R.J. Motyka, analysts.
[b]Determined in the field.
[c]Values in per mil with respect to Standard Mean Ocean Water (SMOW). Analyses performed at the Stable Isotope Laboratory, Southern Methodist University.

to the thermal water sample from the base of Crater Peak. Because of the uncertainty in mixing relationships, immaturity of the water, and the probability of disequilibrium reactions caused by acid waters, we discourage relying on these chemical geothermometers for estimating temperatures of any deep reservoir at Crater Peak. In fact, reservoir temperatures predicted by the SiO_2 and cation geothermometers span a broad range, indicating one or more of the preceding processes have affected the waters. Because K and Mg equilibrate more quickly than Na or Ca, the K–Mg geothermometer is probably the best indicator of source temperature for immature waters such as Crater Peak waters (Giggenbach, 1988). Thermal spring waters with somewhat similar chemical characteristics to those at Crater Peak have been found to be indicative of shallow vapor-dominated zones overlying boiling Cl-rich, hydrothermal reservoirs. In particular, thermal spring waters rich in HCO_3 and SO_4 were found at the Makushin geothermal area on Unalaska Island. The area was subsequently drilled and found to house a substantial hot-water reservoir (Motyka and others, 1983; Motyka and others, 1985). However, after studying the petrology and geochemistry of the Mount Spurr Volcanic Complex, Nye and Turner (1990) found no evidence for a geothermally significant large-scale, shallow magma system which could drive such a reservoir. We therefore believe these thermal spring waters are more likely associated with localized degassing of residual magma underlying Crater Peak.

DISCUSSION AND CONCLUSIONS

Figure 4 presents our model of the Crater Peak volcanic-hydrothermal system. This model is similar to models of magma-related hydrothermal systems proposed by Giggenbach (1987; 1988) and by Henley and Ellis (1983). Crater Peak lies on the extension of a regional fault that is exposed east of the eastern boundary of figure 2 and is projected as an inferred fault into the area of figure 2. To the east, this fault juxtaposes Tertiary sedimentary rocks to the south against granitic rocks to the north, and may provide a zone of weakness for upward migration of magma. It may also provide pathways for infiltration and deep penetration of meteoric waters. Following the 1953 eruption at Crater Peak, a liquid-dominated hydrothermal layer probably developed as meteoric water infiltrated the hot subsurface region overlying the residual magma (fig. 4). The magma probably continues to periodically degas steam, CO_2, SO_2, H_2S, HCl and other constituents into the hydrothermal layer, but the boiling hydrothermal layer appears to be the immediate source of the steam and gases being emitted from the crater fumaroles. Acid gases and

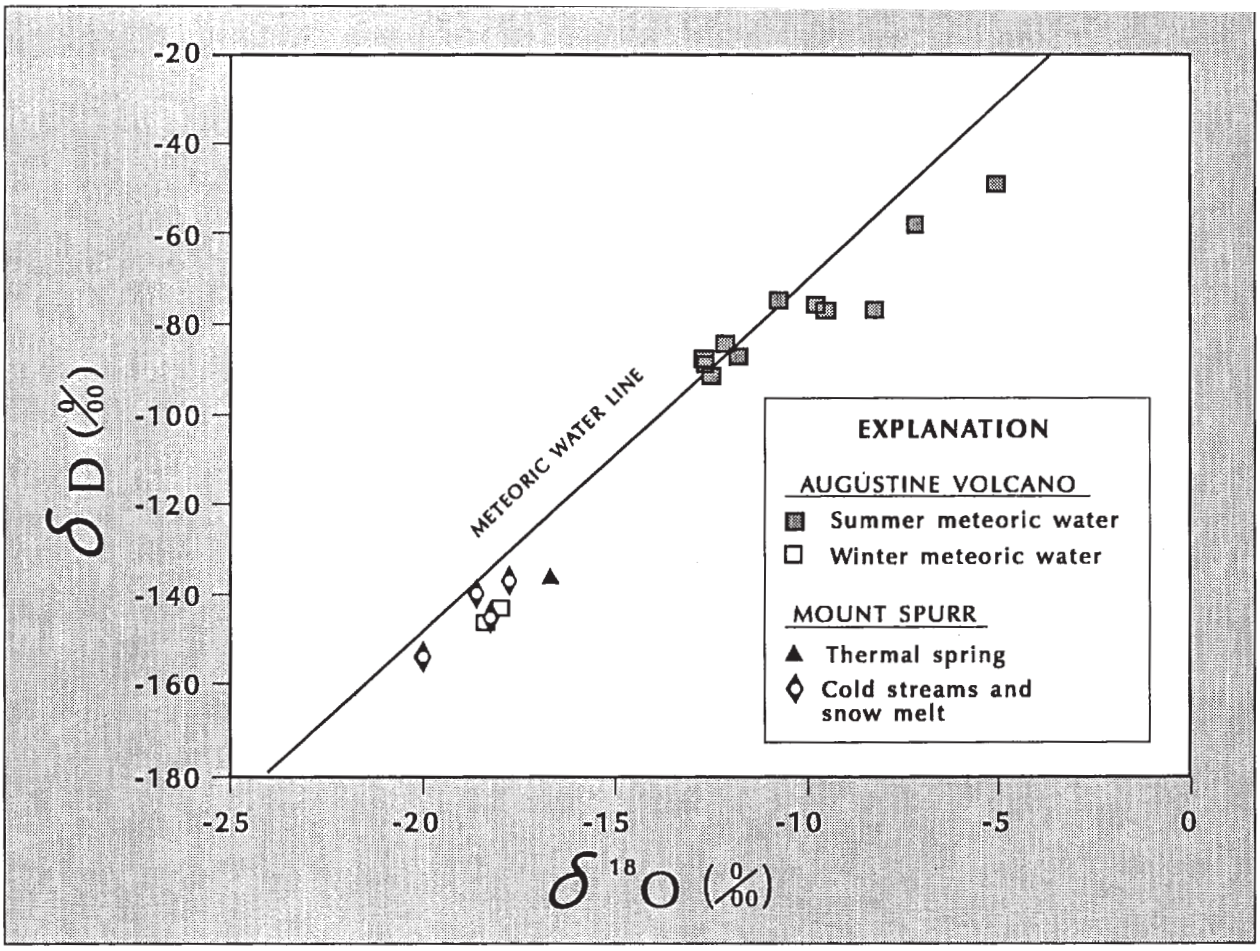

Figure 3. *Stable isotope compositions of waters from Crater Peak, Mount Spurr. Meteoric water line (Craig, 1961) and Augustine precipitation and ground water shown for comparison. Values are with respect to Standard Mean Ocean Water.*

steam escaping from this hot subsurface region form a shallow vapor-dominated zone and interact with shallow ground waters and country rocks to produce the thermal springs in the valley south of Crater Peak. These spring waters may also contain a minor component of Cl-rich thermal waters. Because of the uncertainty in mixing relationships between different waters, immaturity of the Crater Peak thermal water, and the probability of chemical disequilibrium, the thermal water geothermometers are considered to be unreliable. Gas geothermometry suggests that the equilibration temperature for fumarolic gases is at least 200°-250°C.

Crater Peak has produced approximately 35 mid- to upper Holocene tephra layers which were dispersed eastward toward population centers (Riehle, 1985). Fifteen of these eruptions took place during the last 500-600 yr giving an estimated repose time of 35-40 yr. A recent earthquake swarm, lasting from August 21 to August 28, 1991, was located at 1 - 2 km beneath Crater Peak. The swarm consisted of 28 seismic events, up to 1.2 in magnitude, and were located by the Alaska Volcano Observatory (AVO) Mount Spurr seismic network (J. Power and A. Jolly, USGS, oral commun., 1991). Measurable amounts of SO_2 (80 tonnes per day) were

Table 3. *Geothermometry of Crater Peak thermal springs*

Geothermometer	Temperature (°C)
Quartz conductive	150
Chalcedony	125
Amorphous SiO_2	29
Na-K	325
Na-K-Ca (1/3)	237
Na-K-Ca, Mg corrected	17
K-Mg	88

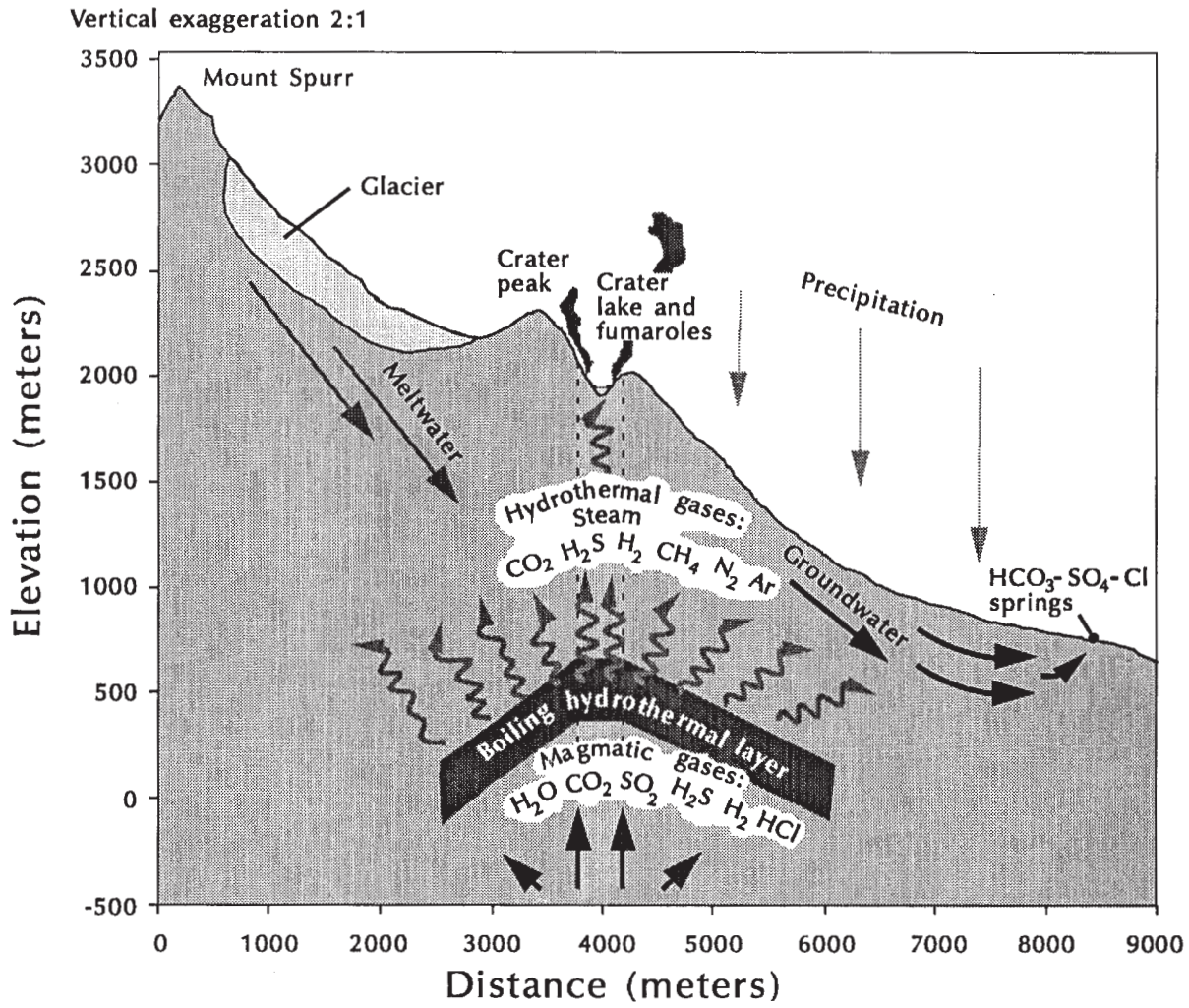

Figure 4. *Conceptual model of the Crater Peak hydrothermal system. Residual 1953 magma at unknown depth expels steam, CO_2, SO_2, HCl and other magmatic gases into overlying hydrothermal layer that was formed by post-1953 infiltration and accumulation of ground water. Steam and gases rich in CO_2 and H_2S are driven off the boiling hydrothermal layer and feed fumaroles at Crater Peak summit crater and interact with shallow groundwaters to produce HCO_3-SO_4-Cl thermal springs at lower elevations.*

detected during a September AVO correlation spectrometer (COSPEC) overflight of Crater Peak but not during August or November (M. Doukas, USGS, oral commun., 1991). These incidents could reflect transient degassing of steam and other volatiles from the residual magma, temporary boil-off of the hydrothermal layer, and production of superheated steam and SO_2. Periodic fluctuations in fumarole temperatures and gas chemistry are not uncommon at active arc volcanoes and do not necessarily signal impending eruptive activity. However, given the 35-40 yr repose time, these events could be precursors to renewed magmatic activity. Given the frequency of eruptions from Crater Peak and the potential impact explosive eruptions could have on eastern Cook Inlet, we recommend close interdisciplinary monitoring of Mount Spurr. Our 1982 data now provide a baseline for assessing any future changes in gas geochemistry, particularly SO_2 emissions, $^3He/^4He$, and $\delta^{13}C$-CO_2 that could signal the onset of increased magmatic heating, or influx of new magma beneath the volcano, or both.

ACKNOWLEDGMENTS

This work was supported by the Alaska Department of Natural Resources, Division of Geological & Geophysical Surveys and by Grant No. DE-FG07-84ID12471 from the U.S. Department of Energy. We wish to acknowledge Bill Evans and Cathy Janik, U.S. Geological Survey, and John Whelan and Robert Poreda, Scripps Institution of Oceanography, for their help in analyzing the gas samples

and Mary Moorman and Shirley Liss, DGGS, who helped analyze the water samples. We wish to thank Shirley Liss, DGGS, and Terry Keith, U.S. Geological Survey, for reviewing this manuscript.

NOTE ADDED IN PROOF: On June 27, 1992, Crater Peak explosively erupted for a period of four hours, sending a plume of ash and steam into the stratosphere. Crater Peak explosively erupted again on August 18 and September 17, 1992. As of this writing (December 4, 1992), earthquake swarms continue to be periodically produced at depths of 1 to 2 km below Crater Peak but there have been no additional eruptions. The authors.

REFERENCES CITED

Calderwood, K.W, and Fackler, W.C., 1972, Proposed stratigraphic nomenclature for Kenai Group, Cook Inlet Basin, Alaska: American Association of Petroleum Geologists Bulletin, v. 56, p. 739-754.

Craig, H. A., 1961, Isotopic variations in meteoric waters: Science, v. 133, p. 1702.

D'Amore, Franco, and Panichi, C.R., 1980, Evaluation of deep temperatures of hydrothermal systems by a new gas geothermometer: Geochimica et Cosmochimica Acta, v. 44, p. 549-556.

Fahlquist, Lynne, and Janik, C.J., 1992, Procedures for collecting and analyzing gas samples from geothermal systems: U.S. Geological Survey, Open-File Report, in review.

Fournier, R.O., 1981, Application of water chemistry to geothermal exploration and reservoir engineering, *in* Ryback, L., and Muffler, L.P.J., eds., Geothermal systems: Principles and case histories: New York, Wiley and Sons, p. 109-144.

Giggenbach, W.F., 1987, Redox processes governing the chemistry of fumarolic gas discharges from White Island, New Zealand: Applied Geochemistry, v. 2, p. 143-161.

_____1988, Geothermal solute equilibria. Derivation of Na-K-Mg-Ca-geoindicators: Geochimica et Cosmochimica Acta, v. 52, p. 2749-2765.

Giggenbach, W.F., and Goguel, R.L., 1989, Collection and analysis of geothermal and volcanic water and gas discharges: Chemistry Division, Department of Scientific and Industrial Research, New Zealand, Report CD 2401, 81 p.

Henley, R.W., and Ellis, A.J., 1983, Geothermal systems, ancient and modern: Earth Science Reviews, v. 19, p. 1-50.

Juhle, R.W, and Coulter, H.W., 1955, The Mount Spurr eruption, July 9, 1953: Transactions, American Geophysical Union, v. 36, p. 199-202.

Kodosky, L.G., Motyka, R.J., and Symonds, R.B., 1991, Fumarolic emissions from Mount St. Augustine, Alaska: 1979-1984 degassing trends, volatile sources and their possible role in eruptive style: Bulletin of Volcanology, v. 53, p. 381-394.

Motyka, R.J., Moorman, M.A., and Liss, S.A., 1981, Assessment of thermal spring sites, Aleutian Arc, Atka Island to Becharof Lake—Preliminary results and evaluation: Alaska Division of Geological & Geophysical Surveys, Open-File Report AOF-144, 173 p.

Motyka, R.J., Moorman, M.A., and Poreda, R.J., 1983, Progress report—thermal fluid investigations of the Makushin geothermal area: Alaska Division of Geological & Geophysical Surveys Report of Investigations 83-15, 48 p.

Motyka, R.J., Queen, L.D., Janik, C.J., Sheppard, D.S., Poreda, R.J., and Liss, S.A., 1985, Fluid geochemistry and fluid-mineral equilibria in test wells and thermal gradient holes at the Makushin Geothermal Area, Unalaska Island, Alaska: Alaska Division of Geological & Geophysical Surveys, Report of Investigations 88-14, 90 p.

Nye, C.J., and Turner, D.L., 1990, Petrology, geochemistry, and age of the Spurr volcanic complex, eastern Aleutian arc: Bulletin of Volcanology, v. 52, p. 205-226.

Panichi, C.R., and Gonfiantini, R., 1978, Environmental isotopes in geothermal studies: Geothermics, v. 6, p. 143-161.

Poreda, R.J., 1983, Helium, neon, water and carbon in volcanic rocks and gases: University of California, San Diego, Ph.D. thesis, 215 p.

Poreda, R.J., and Craig, H.A., 1989, Helium isotope ratios in circum-Pacific volcanic arcs: Nature, v. 338, p. 473-477.

Presser, T.S., and Barnes, Ivan, 1974, Special techniques for determining chemical properties of geothermal waters: U.S. Geological Survey Water-Resources Investigation Report 22-74, 11 p.

Riehle, J.R., 1985, A reconnaissance of the major Holocene tephra deposits in the upper Cook Inlet region, Alaska: Journal of Volcanology and Geothermal Research, v. 26, p. 37-74.

Skougstad, M.W., Fishman, M.J., Friedman, M.J., Erdmann, D.E., and Duncan, S.S. (eds.), 1979, Methods for determination of inorganic substances in water

and fluvial sediments: U.S. Geological Survey Techniques of Water - Resources Investigations, book 5, chapter A1, 626 p.

Truesdell, A.H., and Hulston, J.R., 1980, Isotopic evidence on environments of geothermal systems: *in* Handbook of Environmental Isotope Geochemistry: Elsevier, p. 179-219.

Turner, D.L., and Wescott, E.M., 1986, Geothermal energy investigations at Mount Spurr, Alaska: University of Alaska, Geophysical Institute Report UAG R-308, 12 p., 4 pl.

Wescott, E.M., Turner, D.L., Nye, C.J., Motyka, R.J., Moore, Pat, 1988, Exploration for geothermal energy resources at Mount Spurr, Alaska: Geothermal Resource Council Transactions, v. 12, p. 203-210.

Wilson, F.H., Dettterman, R.L., and Case, J.E., 1985, The Alaska Peninsula terrane; a definition: U.S. Geological Survey, Open-File Report 85-450, 17 p.

ORGANIC-RICH SHALE AND BENTONITE IN THE ARCTIC CREEK UNIT, ARCTIC NATIONAL WILDLIFE REFUGE: IMPLICATIONS FOR STRATIGRAPHIC AND STRUCTURAL INTERPRETATIONS

by
C.G. Mull[1] and John Decker[2]

INTRODUCTION

The Arctic Creek unit (Molenaar and others, 1987, p. 521; Decker and others, 1987; Robinson and others, 1989) or Arctic Creek facies (Bader and Bird, 1986; Bird and Molenaar, 1987, p. 55) crops out widely in the Kekiktuk River, Arctic Creek, and Hulahula River area southeast of the Sadlerochit Mountains in the northern part of the Arctic National Wildlife Refuge (ANWR) (fig. 1). For convenience of discussion, this area is here referred to as the Arctic Creek area. The Arctic Creek unit is poorly exposed in low-relief hills and has only scattered resistant outcrops, but has commonly been described as consisting of bentonitic shale and interbedded siltstone and sandstone turbidites, and has been thought to be thick and complexly deformed. Molenaar and others (1987) have estimated that east of the Hulahula River its thickness is about 1,100 m. Most authors have noted the apparent sharp contrast between the stratigraphic sequence in the Arctic Creek area and the apparently coeval stratigraphic sequence exposed in adjacent areas in the northeastern Brooks Range and have suggested major thrust fault juxtaposition of facies in the area.

The Arctic Creek unit is largely undated; the only significant paleontological control consists of ammonites of Albian age collected from sandstone near the headwaters of Arctic Creek (Detterman and others, 1975). As a result, the Arctic Creek unit has had a variety of age designations, based upon the ammonite and inferred lithologic correlations with better exposed and better dated

[1]Alaska Division of Geological & Geophysical Surveys, 794 University Avenue, Suite 200, Fairbanks, Alaska 99709-3645.
[2]ARCO Alaska, Inc., Box 100360, Anchorage, Alaska 99510.

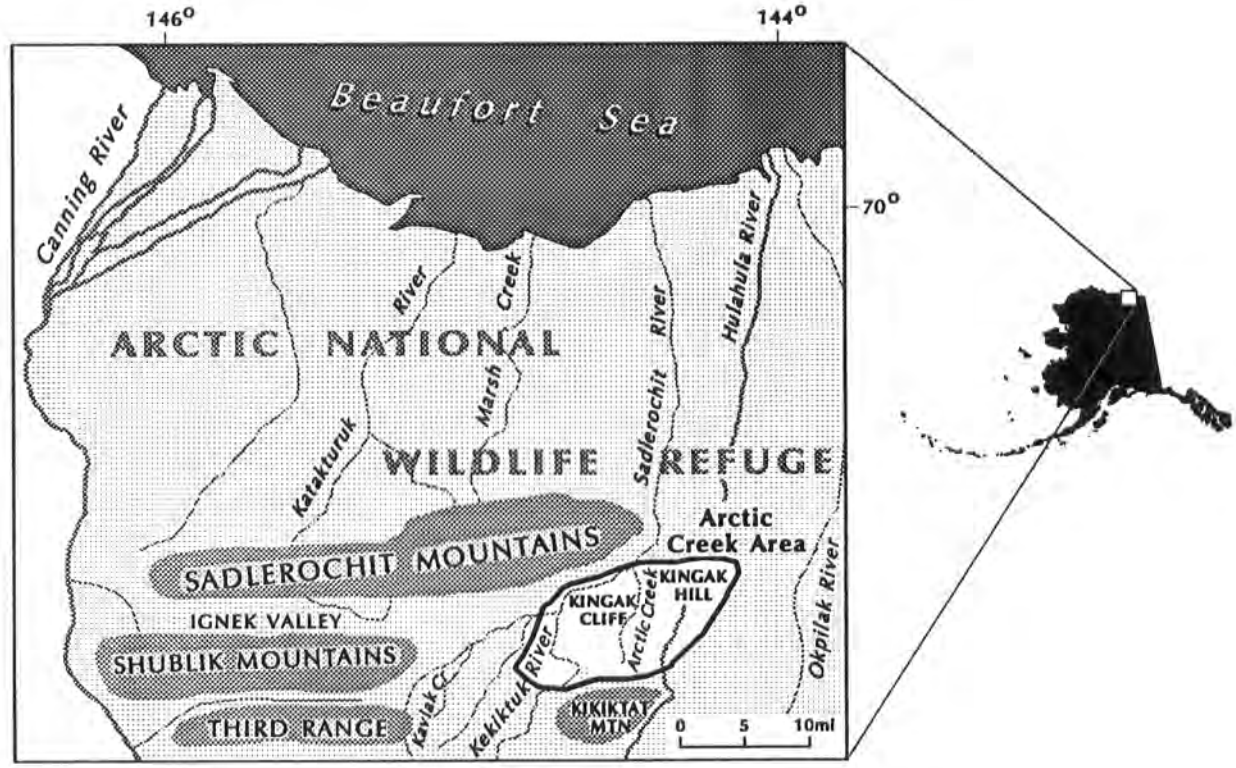

Figure 1. *Index map showing location of Arctic Creek area and Ignek Valley in northern part of Arctic National Wildlife Range, northeastern Brooks Range.*

strata in adjacent areas. Ages inferred include Campanian and Maastrichtian (Molenaar, 1983), Albian and younger (Bader and Bird, 1986), Albian (Decker and others, 1987), Albian and/or Cenomanian (Bird and Molenaar, 1987); Molenaar and others, 1987), and Jurassic(?) to Maestrichtian (Robinson and others, 1989).

Prior to naming the Arctic Creek unit by Molenaar and others (1987), various stratigraphic names had been applied to the rocks in the Arctic Creek area. Reiser and others (1971) mapped the rocks as Kingak Shale (Jurassic) and Nanushuk Group (Albian), but Detterman and others (1975, p. 29) referred the turbidites to the Tuktu Formation (Albian) of the Nanushuk Group. Molenaar (1983) described strata in the Arctic Creek area as consisting of thin Albian turbidites and "shale of the Colville Group" of Campanian or Maastrichtian age.[3] Mull (1987) followed the nomenclature of Molenaar and considered the section to be Albian turbidites overlain by the Upper Cretaceous Colville Group

The Arctic Creek area is characterized by poor exposures, limited paleontologic control, and complex structure, which make it difficult to differentiate between mappable units in the Arctic Creek unit. However, reconnaissance field studies in the Arctic Creek area in 1991 and 1992 examined the regional stratigraphic sequence and sampled a section of organic-rich shale and interbedded bentonite that had been described by Mull (1987). These studies suggest a possible alternative interpretation of the stratigraphy of the Arctic Creek unit. This preliminary report discusses details of the new lithologic and stratigraphic observations, the age of the rocks and implications concerning a possible stratigraphic sequence within the Arctic Creek unit, and the ramifications of a revised structural interpretation of the area. Additional field studies are needed to further refine our knowledge of the stratigraphic sequence in the Arctic Creek area.

NEW FIELD OBSERVATIONS

Field studies in 1991 and 1992 in the Arctic Creek area examined a 5-m-thick section of black organic-rich shale with bentonite and sampled for organic geochemical and paleontological analyses. The exposed shale and bentonite section contains more than 25 bentonite seams ranging from 0.25 to 6 cm thick. The section is exposed in a small stream cut (locality A) at the base of the west end of a prominent ridge named Kingak Cliff (figs. 2 and 3), on the south side of the Sadlerochit River (Leffingwell, 1919).[4] The exposure is at the base of a poorly exposed shale section estimated to be 100-150 m thick and apparently overlies a resistant 10-15-m-thick, dark gray, sandstone turbidite bed that dips 30° south and forms a prominent dipslope on the south side of the Kingak Cliff ridge. The section of black shale and bentonite is apparently overlain to the south by a thick section (>1,000 m) of poorly exposed thin-bedded siltstone and fine-grained sandstone turbidites with interbedded gray bentonitic shales.

POSSIBLE STRATIGRAPHIC SEQUENCE IN THE ARCTIC CREEK AREA

Summary

In the Arctic Creek area, recognition of the section containing abundant thin bentonite seams interbedded with organic-rich shale may result in a more precise understanding of the stratigraphic sequence in the area. The apparent stratigraphic sequence consists of two intervals of sandstone turbidites with interbedded bentonitic shales, separated by a section of organic-rich shale and bentonite. The lower interval seems to be relatively thin and contains at least one resistant sandstone bed. It is overlain by the organic rich shale and bentonite, and a long section of probably more than 1,000 m of thin-bedded turbidites (figs. 3 and 4A). The sequence of organic-rich shale and bentonite overlain by thin bedded turbidites is similar to the stratigraphic sequence of Hue Shale and Canning Formation (Molenaar and others, 1987) exposed to the west in the Ignek Valley area and elsewhere in the Sadlerochit Mountains area. This similarity in stratigraphic sequence suggests that the Hue Shale and Canning Formation may have correlative rocks in the Arctic Creek area. The resistant sandstone horizon that apparently underlies the bentonite and organic-rich shale in the Arctic Creek area may be a locally distinctive, mappable unit that is not present in the Ignek Valley and Sadlerochit Mountains area. However, west of the Canning River, Keller and others (1961) and Reifenstuhl (1991) have mapped rocks that may be correlative with the lower interval. Although poor exposures, limited

[3]However, as noted above, in naming the Arctic Creek unit, Molenaar and others (1987) later revised the age of the unit and considered it to be Albian and Cenomanian.

[4]The shale and bentonite exposure is at 69°32.4' N., 144°39.5' W., SW. 1/4 sec. 12, T. 2 N., R. 30 E. As noted by Molenaar and others (1987), the top of Kingak Cliff, which is presumably the upper part of the type locality of the Kingak Shale (Jurassic and Lower Cretaceous) (Leffingwell, 1919), is composed of the resistant sandstone unit that is here considered to be part of the Arctic Creek unit. In addition, it should also be noted that the location of Kingak Cliff as described by Leffingwell (1919, p. 119) does not coincide with the map location shown (plate II), that is plotted about 10 km to the east.

Figure 2. *View to the east of resistant ridges of lower sandstone interval at the west end of Kingak Cliff ridge at northern edge of Arctic Creek area. Note prominent south-dipping dip slope. Bentonite exposures are in stream cut at base of dipslope at right edge of photo.*

paleontologic control, and complex structure render it difficult to differentiate mappable horizons within the Arctic Creek unit, recognizing the presence of a probable equivalent of the Hue Shale greatly facilitates regional stratigraphic studies.

Lower Sandstone Interval

Lithology

The lower part of the inferred stratigraphic sequence in the Arctic Creek area consists of dark gray resistant sandstone and interbedded bentonitic shale. Along the western end of the ridge (Kingak Cliff of Leffingwell) that extends from the Kekiktuk River to Arctic Creek (figs. 2 and 3), the resistant bed is relatively well exposed and is folded in a tight asymmetrical anticline that is probably on the hanging wall of a thrust fault, but to the east the interval is apparently repeated by thrust faulting. At the west end of the ridge, as described above, the relationship of the resistant sandstone with the overlying bentonite and organic-rich shale appears to be straightforward.

The sandstone is dark gray, fine-grained lithic wacke that characteristically forms a resistant bed that ranges from 10 to 15 m in thickness. The lower part of this bed generally appears homogeneous or parallel bedded, but the top of the bed commonly has small-scale ripple crosslamination and is interpreted to be a turbidite. The bed generally weathers to form dark-gray, rubble-covered ridges that stand out in sharp color contrast and in resistance to weathering compared with most other sandy intervals in the Arctic Creek area.

About 3 km southwest of the Kingak Cliff ridge, similar resistant sandstone beds can be traced east-west for several kilometers (fig. 3). These beds are also dark-gray, fine-grained, lithic sandstones that appear to be parallel bedded or homogeneous at the base and contain small-scale cross-bedding at the top.

This lower sandstone interval may be the basal sandstone of the "Tuktu Formation" reported to overlie beds of probable Neocomian age along Arctic Creek (Detterman and others, 1975). However, Detterman's section cannot be located with certainty because the coordinates given do not coincide with the location of the creek.

Figure 3. *Aerial photograph of part of Arctic Creek area showing resistant sandstone turbidite beds of lower turbidite interval. The bare gray hillsides underlain by bentonitic shale and thin-bedded turbidites of the upper turbidite interval. "A" on the photograph marks the location of exposure of black organic-rich shale and interbedded bentonite. Thrust faults are approximately located with teeth on upper plate. Infrared aerial photograph ALK 60, composite of negatives 2460 and 2461, August 1982, scale 1:63,360.*

Age and Correlation

The Albian ammonite *Paragastroplites spiekeri* (McLearn) has been collected at two locations in the southernmost belt of the Arctic Creek unit near the head of Arctic Creek (Detterman and others, 1975). Molenaar (1983) has shown that these Albian beds probably represent basinal turbidites correlative with the Nanushuk Group of the central Arctic Slope (Albian to Cenomanian).

Contacts

The contacts of the lower sandstone interval with underlying and overlying units are not exposed owing to the generally poor exposures in the area. However, on the north side of the Kingak Cliff ridge that extends from the Kekiktuk River to Arctic Creek, the lower sandstone interval may be in thrust contact with underlying thin-bedded turbidite sandstones that are thought to represent the upper part of the Arctic Creek succession. Farther down the slope to the north, a sample from a brown silty shale and mudstone yielded a microfauna of possible Neocomian age (Mull, 1987, table 2) and is probably part of the pebble shale unit; a stratigraphically lower black clay shale yielded a Late Jurassic (Oxfordian) microfauna characteristic of the Kingak Shale. Both Detterman and others (1975) and Molenaar (1983) illustrate similar relationships in which Albian sandstone conformably overlies the pebble shale unit. The base of the overlying Arctic Creek unit is probably in fault contact with the Neocomian to Jurassic section, but alternatively could overlie a nondepositional hiatus or a very condensed section.

Although not exposed in the Arctic Creek area, the contact of the lower sandstone interval with the apparently overlying organic-rich black shale and bentonite thought to represent the Hue Shale can be interpreted to be conformable and may not represent a significant break in deposition. Alternatively, the contact could be a thrust fault in which the black shale and bentonite section is thrust over younger beds.

Distribution

In the Arctic Creek area, the lower sandstone interval crops out discontinuously along the Kingak Cliff ridge from near the Kekiktuk River for about 14 km northeasterly across Arctic Creek (fig. 3) to Kingak Hill, which is on the west side of the Hulahula River (fig. 1), an area of over 200 km^2. Along the northern base of another northeast- trending ridge, about 3 km south of the above locality, a second trend containing one or more resistant sandstone beds can also be traced on aerial photos from near the Kekiktuk River about 9 km northeast to the west side of the Arctic Creek valley. The resistant beds along this trend dip from about 30° to 60° S and are interpreted to be the lower sandstone interval overlain by a thick section of thinly interbedded, silty sandstone and shale that forms broad bare hilltops and slopes. The lower sandstone interval and overlying rocks are also visible in the valley of Kaviak Creek, about 10 km west of the Kekiktuk River. A third belt of exposures at the head of Arctic Creek consists of discontinuous outcrops, which on aerial photographs appear to form a broad asymmetrical syncline (fig. 3), and overlies hard ferruginous shales, which elsewhere in the northeastern Brooks Range are probably pre-Albian.

The three possible separate belts of what is interpreted as the lower sandstone interval probably represent thrust fault repetition of the interval and the overlying rocks. Other discontinuous exposures of resistant beds visible on aerial photographs may represent additional thrust slivers of this sandstone interval but have not been investigated in the field.

Mull (1987) illustrates a similar relationship with Albian turbidites overlying the pebble shale unit and Kingak Shale between the Canning River and Kavik River. These exposures suggest that isolated thrust remnants of sections similar to those in the Arctic Creek area are present north of the Brooks Range mountain front west of Canning River.

Hue Shale

Lithology

Although they are generally very poorly exposed in the Arctic Creek area, the rocks here referred as to the Hue Shale appear to consist dominantly of sooty black organic-rich shale with numerous bentonite seams. One three-m-thick interval exposed by trenching contained more than 25 separate bentonite seams that range from 0.5 to 6 cm thick. This interval appears to overlie the dipslope formed by the lower sandstone interval described above; although outcrops are not continuous, it is interpreted to be in a continuous stratigraphic succession. Smooth slopes south of the bentonite and shale exposure also appear to be underlain by an interval of deeply weathered bentonitic shale, and this section is succeeded upward by slopes containing abundant thin-bedded siltstone, sandstone, and shale.

The thickness of the Hue Shale in the Arctic Creek area is unknown owing to the poor exposures. However, based upon the width of the apparent subcrop belt south of Kingak Cliff, it is probably not more than 150 m thick. Molenaar and others (1987) report that the Hue Shale is

not more than 300 m thick in areas west of the Arctic Creek area.

The rocks in the Arctic Creek area, here referred as to the Hue Shale, appear to contain many of the distinctive characteristics of the Hue Shale, such as the organic-rich shale and bentonite as in the Ignek Valley and Canning River area 30-60 km west of the Arctic Creek area (Molenaar and others, 1987). However, the unit differs from the Hue Shale elsewhere because of the absence of silicified tuff, which is a distinctive component in many exposures in areas surrounding the Sadlerochit Mountains. Layers of prismatic calcite or *Inoceramus* prisms are also a conspicuous constituent in the lower part of the Hue Shale of the Ignek Valley area and elsewhere (Molenaar and others, 1987). However, layers of prismatic calcite have not been reported in the Arctic Creek area although detrital prismatic calcite is reported to be common in some of the sandstone beds. Thin-bedded silicified pyroclastic beds that are common in the Hue Shale elsewhere in the northeastern Brooks Range typically weather to form conspicuous red-orange weathering slopes covered with a rubble lag of the resistant silicified tuff. Absence of the tuff may have prevented previous recognition of the Hue Shale in the Arctic Creek area.

Four shale samples from the exposure of Hue Shale from the Arctic Creek area yielded from 2.8 to >4 percent total organic carbon (TOC) and one sample yielded a vitrinite reflectance value (Ro) of 2.08. Molenaar and others (1987) and Bird and Molenaar (1987) report that the lower part of the Hue Shale elsewhere commonly contains shale with greater than 4 percent TOC and is considered to be an excellent oil-prone hydrocarbon-source horizon. However, they also report vitrinite reflectance (Ro) values ranging from 1.8 to 2.0 from the Arctic Creek unit. High Ro values in the Arctic Creek area suggest that the Hue Shale in this area probably has a higher level of thermal maturity than in other areas. It is probably thermally overmature and at a maturity level commonly thought to be capable only of dry gas generation and, therefore, it is thus probably a poor hydrocarbon source horizon in the Arctic Creek area.

Contacts

In the Arctic Creek area, the contacts of the Hue Shale with the overlying and underlying units are covered. However, based upon the contact relations of the Hue Shale with the adjacent units in other parts of the Sadlerochit Mountains area, unless disrupted by faulting, the Hue Shale in the Arctic Creek area is probably conformable with the overlying thin-bedded turbidite unit and the underlying resistant sandstone.

Distribution

The Hue Shale in the Arctic Creek area is recessive and very poorly exposed. On aerial photographs a recessive interval appears in some places to lie between the resistant sandstone and the overlying light-gray-weathering beds that form the conspicuous rolling uplands in the Arctic Creek area. Based upon the wide distribution of the overlying and underlying units, the Hue Shale is probably present in many tundra-covered areas.

Age

The Hue Shale in the Arctic Creek area has not been dated by fossil control. Four samples submitted for biostratigraphic analysis were barren of both foraminifera and identifiable palynomorphs. Molenaar and others (1987) date the Hue Shale at its type locality west of the Arctic Creek area as Aptian(?) to Campanian but suggest that its top is regionally diachronous and becomes younger to the north and east. They suggest that a zone of Inoceramus prisms near the base of the Hue Shale in the Ignek Valley area is probably Cenomanian age, and, inasmuch as the organic shale and bentonite in the Arctic Creek area appear to overlie at least some beds of Albian age, we infer that it is probably no older than Cenomanian in the Arctic Creek area.

Thin-bedded Turbidite Interval

Lithology

Conspicuously bare light-gray-weathering hilltops and slopes with splotchy yellow-orange streaks characterize the rolling hills of much of the uplands in the Arctic Creek area (fig. 3). Outcrops are poor, but the hills appear to be underlain dominantly by thinly bedded calcareous siltstone, fine-grained calcareous and micaceous sandstone, and abundant bentonitic shale. Most of the beds are less than 15 cm thick, but occasional beds of apparent limited lateral extent range up to 2 m thick. Sandstone beds containing abundant fragmental calcite prisms that have been interpreted as *Inoceramus* prisms are also reported (Detterman and others, 1975, and Robinson and others, 1989). Resistant beds that can be traced for more than a few meters either in outcrop or on aerial photographs are not present.

Many of the siltstone and sandstone beds contain abundant characteristics of fine-grained turbidites (fig. 4), including flute and groove casts, graded bedding, and well-developed Bouma sequences. These are interpreted by Robinson and others (1989) as indicative of deposition

in middle fan to outer fan depositional environments. Orientation of flute and groove casts in these turbidites indicate an average east-northeast paleocurrent direction similar to that of the Canning Formation elsewhere (Molenaar, 1983).

Although many of the characteristics of these rocks, including the paleocurrent directions, are similar to those of the Canning Formation as described by Molenaar and others (1987), there are notable differences. The calcareous and micaceous siltstone and sandstone in the Arctic Creek area differ from the Canning Formation elsewhere, which is not notably calcareous or micaceous and lacks the prismatic calcite fragments reported in the Arctic Creek area. Because of the contrasting lithofacies, Decker and others (1987) suggested that deposition took place in two separate basins or in non-overlapping portions of the same basin. Further study will be necessary to clarify the relationship of the thin-bedded turbidites in the Arctic Creek area to the type Canning Formation.

Owing to poor exposures and structural complications, the thicknesss of the interval of thin-bedded turbidites in the Arctic Creek area is uncertain, but it is probably quite thick. Molenaar and others (1987) calculated a thickness of about 1,100 m for part of the Arctic Creek unit along a tributary of the Okerokovik River, 40 km east of the Hulahula River. It seems likely that the thin-bedded turbidites in the Arctic Creek area may be as much as 1,000 m thick, although part of this apparent thickness may be due to structural duplication of section.

Distribution

The thin-bedded turbidites are probably present in much of the rolling upland area between the Kekiktuk River and Arctic Creek, in the valley of Kaviak Creek, and in stream cuts in the Hulahula River valley and other valleys to the east. Because the Arctic Creek unit is thought to have been thrust northward, Molenaar and others (1987) suggested that these rocks are probably not present in the subsurface north of the outcrop belt in the Arctic Creek area.

Age

No fossils have been reported from the thin-bedded turbidites in the Arctic Creek area. The turbidite age is constrained only by its apparent stratigraphic position above the organic shale and bentonite, here thought to represent the Hue Shale. Molenaar and others (1987) show that to the west, the Canning Formation is diachronous and suggest that north of the Sadlerochit Mountains it may range to as young as Oligocene. However, in the Arctic Creek area it seems likely that the thin-bedded turbidites are probably mostly Upper Cretaceous and may range in age to as young as Maastrichtian (Molenaar, 1983).

STRUCTURAL RELATIONSHIPS IN THE ARCTIC CREEK AREA

Local Structure

Owing to the poor outcrops and imperfectly known stratigraphy in the Arctic Creek area, there is little detailed information concerning structure in the area. However, most workers have thought that the area is structurally complicated as a result of thrust faulting and intense folding. Based upon the outcrops of what is here considered to be the lower sandstone unit in three separate south dipping trends, it appears likely that the stratigraphic sequence has been imbricated by at least two south dipping thrust faults. However, as noted above, on aerial photographs , the southernmost (and presumably the uppermost) thrust sheet appears to be folded into a broad syncline (fig. 3). This relationship suggests that the inferred thrust faults may daylight near Old Woman Creek, on the north side of Kikiktat Mountain (fig. 1), which forms the south side of the outcrop belt of the Arctic Creek unit.

Regional Structural Implications

In addition to the evidence of internal structural complications, there is evidence that the entire stratigraphic succession above the Kingak Shale in the Arctic Creek area has been thrust northward. Many workers have noted the apparent pronounced contrast between the inferred stratigraphy of the Arctic Creek area with the stratigraphic sequence exposed in Ignek Valley, 30 km to the west (Decker and others, 1987; Mull, 1987; Molenaar and others, 1987; Bird and Molenaar, 1987; Robinson and others, 1989). Ignek Valley contains a distinctive sequence composed of, from the base upward, Kingak Shale, Kemik Sandstone (Hauterivian), pebble shale unit, Hue Shale, and Canning Formation (fig. 5). The distinctive characteristics of the section are the Kemik Sandstone (Hauterivian), which is a resistant quartzose sandstone and conglomerate unit about 30 m thick, and the presence of abundant silicified tuff in the Hue Shale, which weathers to form conspicuous red-orange weathering hillsides. Neither of these characteristic lithologies are present in the Arctic Creek area. In addition, the apparent absence of Albian beds in the Ignek Valley section, and the interpretation of the entire Arctic Creek unit as Albian and/or Cenomanian (Molenaar and others, 1987; Decker and others, 1987) further emphasized the difference between the stratigraphic sequences in the two areas.

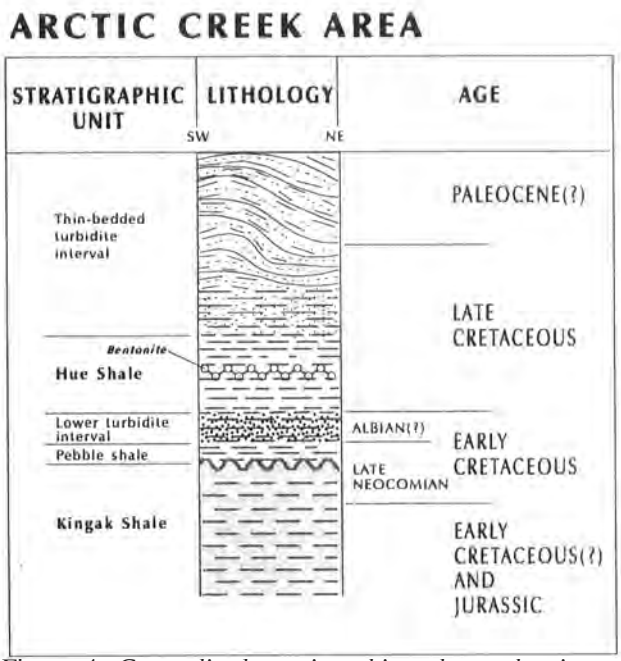

Figure 4. *Generalized stratigraphic column showing inferred stratigraphic sequence of strata exposed in Arctic Creek area.*

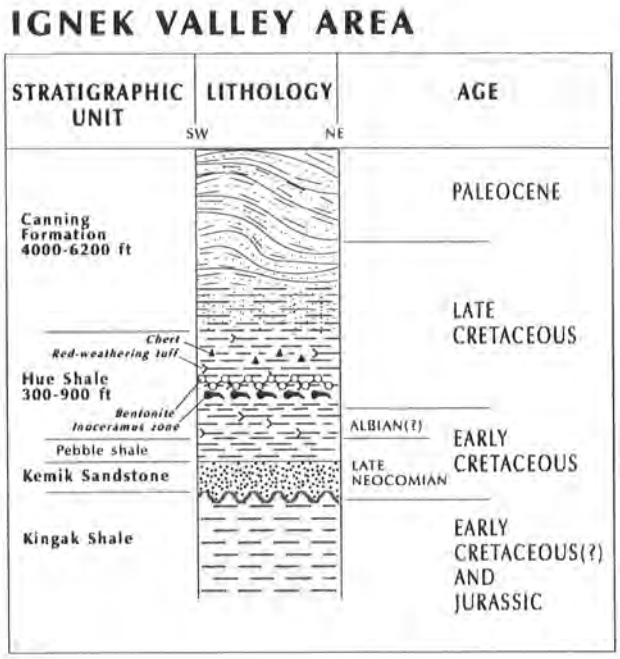

Figure 5. *Generalized stratigraphic column showing stratigraphic sequence of strata exposed in Ignek Valley area and also on north side of Sadlerochit Mountains. Modified from portion of stratigraphic column of Bird and Molenaar, 1987.*

As a consequence of focusing on the differences between the areas, most workers believe that the rocks in the Arctic Creek area have been displaced a long distance relative to the rocks of the Sadlerochit Mountains area, although no definitive distances have been cited. Mull (1987) diagrammatically illustrated the relationships at the north side of the Arctic Creek outcrop belt, and inferred a major thrust fault in the Sadlerochit River valley with at least 16 km of dislocation. Other workers have inferred greater dislocation. Based upon the assumption that the Arctic Creek unit was entirely Albian in age and noting lithologic similarities, Decker and others (1987) suggested that the Arctic Creek unit bears more resemblance to the stratigraphic sequence at Bathtub Ridge, about 90 km to the southwest, than to the stratigraphic sequence in Ignek Valley. At Bathtub Ridge, the stratigraphic sequence contains thick turbidites that overlie hard ferruginous shale that is similar to beds in the Arctic Creek area.

SUMMARY

Recent studies in the Arctic Creek area have documented the presence of a section of bentonite and organic-rich shale that resembles the rocks of the Hue Shale elsewhere in the northern part of the Arctic National Wildlife Refuge. Recognition of this section suggests that at least two distinct depositional units may be present in the Arctic Creek area. These two units consist of the interval of organic-rich black shale with interbedded bentonite seams, which is correlated with the Hue Shale, and sandstone, siltstone, and shale turbidites, some of which apparently overlie the Hue Shale and in some aspects resemble the Canning Formation. This inferred stratigraphic sequence thus bears closer similarity to the rocks in Ignek Valley and elsewhere in the Sadlerochit Mountains area than has been previously recognized. Although some aspects of the rocks in the Arctic Creek area also bear similarities to the stratigraphic sequence in the Bathtub Ridge area, future studies may result in revised structural interpretations that reduce the magnitude of the inferred dislocations of the rocks in the Arctic Creek and adjacent areas.

ACKNOWLEDGMENTS

We thank C.M. Molenaar and R.R. Reifenstuhl for helpful reviews of an earlier version of this manuscript. The senior author gratefully acknowledges helicopter support by Conoco, Inc. and Mobil Exploration and Producing, Inc. Geochemical analyses were performed by DGSI.

REFERENCES CITED

Bader, J.W., and Bird, K.J., 1986, Geologic map of the Demarcation Point, Mount Michelson, Flaxman Island, and Barter Island Quadrangles, Alaska: U.S. Geological Survey Miscellaneous Investigations Map I-1791, scale 1:250,000.

Bird, K.J., and Molenaar, C.M., 1987 Stratigraphy, Bird, K.J., and Magoon,L.B., eds., *in* Petroleum geology of the northern part of the Arctic National Wildlife Refuge, northern Alaska: U.S. Geological Survey Bulletin 1778, p. 37-60.

Decker, John, Vandergon, M.A., Camber, Wendy, Mull, C.G., Knock, D.K., and Crowder, R.K., 1987, Contrasting Cretaceous lithofacies in the Arctic National Wildlife Refuge, northeastern Alaska (abs): Alaska Geological Society seminar on Petroleum Geology of the 1002 area, ANWR Coastal Plain, Alaska, November 16-17, 1987, abstracts with program.

Detterman, R.L., Reiser, H.N., Brosgé, W.P., and Dutro, J.T., Jr., 1975, Post-Carboniferous stratigraphy, northeastern Alaska: U.S. Geological Survey Professional Paper 886, 46 pp.

Keller, A..S., Morris, R.H., and Detterman, R.L., 1961, Geology of the Shaviovik and Sagavanirktok Rivers Region, Alaska: U.S. Geological Survey Professional Paper D 303-D, 222 pp.

Leffingwell, E. de K., 1919, The Canning River region, northern Alaska: U.S. Geological Survey Professional Paper 109, 251 pp.

Molenaar, C.M., 1983, Depositional relations of Cretaceous and Tertiary rocks, northeastern Alaska: American Association of Petroleum Geologists Bulletin, v. 67, no. 7, p. 1066-1080.

Molenaar, C.M., Bird, K.J., and Kirk, A.R., 1987, Cretaceous and Tertiary stratigraphy of northeastern Alaska, *in* Tailleur, Irv, and Weimer, Paul, eds., Alaskan North Slope Geology: Society of Economic Paleontologists and Mineralogists, Pacific Section, and Alaska Geological Society, Bakersfield, Calif., p. 513-527.

Mull, C.G., 1987, Kemik Sandstone, Arctic National Wildlife Refuge, northeastern Alaska, *in* Tailleur, Irv, and Weimer, Paul, eds: Alaskan North Slope Geology: Society of Economic Paleontologists and Mineralogists, Pacific Section, and Alaska Geological Society, Bakersfield, Calif., p. 405-431.

Reiser, H.N., Brosgé, W.P., Dutro, J.T., Jr., and Detterman, R.L., 1971, Preliminary geologic map of the Demarcation Point Quadrangle, Alaska: U.S. Geological Survey Open-file Map 71-237, 2 sheets, scale 1;200,000.

Reifenstuhl, R.R., 1991, Gilead Sandstone, northeastern Brooks Range, Alaska: An Albian to Cenomanian marine clastic succession, *in* Reger, R.D., ed., Short notes on Alaskan Geology 1991, Alaska Division of Geological & Geophysical Surveys Professional Report 111, pp. 69-76.

Robinson, M.S., Decker, John, Clough, J.G., Reifenstuhl, R.R., Bakke, Arne, Dillon, J.T., Combellick, R.A., and Rawlinson, S.E., 1989, Geology of the Sadlerochit and Shublik Mountains, Arctic National Wildlife Refuge, northeastern Alaska: Alaska Division of Geological & Geophysical Surveys, Professional Report 100, 1 sheet, scale 1:63,360.

DATING HOLOCENE MORAINES OF BLACK RAPIDS GLACIER, DELTA RIVER VALLEY, CENTRAL ALASKA RANGE

by
Richard D. Reger,[1] Alfred G. Sturmann,[1] and James E. Begét[2]

INTRODUCTION

One of several glaciers located near the active McKinley strand of the Denali fault that exhibits evidence of periodic surges (Post, 1960, 1969), Black Rapids Glacier first attracted national attention by its spectacularly rapid advance of about 4.8 km in 3 months during the winter of 1936-37 (Hance, 1937; Geist and Péwé, 1957; Giddings, 1988). This surge began during October or November 1936 and was essentially completed by the following September (Moffit, 1942).

During the 1936-37 surge, the steep terminal wall of broken ice blocks and slabs slid over an unvegetated moraine of a previous Holocene advance. This older, debris-covered ablation moraine was present in 1910 when a U.S. Geological Survey field party visited the area, and Moffit (1942, 1954) speculated that three pre-1937 end moraines were the products of prehistoric surges. The purpose of our paper is to present evidence that constrains the timing of three pre-1937 advances and indicates that at least one advance was a surge.

SETTING

Black Rapids Glacier is a 40-km-long valley glacier that flows from snowfields high along the crest of the central Alaska Range eastward down the linear trough of Denali fault (Denton, 1975). The lower 10 km of the glacier diverts from this fault trough (Stout and others, 1973) and flows east-northeast to end at the western wall of the glacier-scoured middle Delta River valley in the southeastern corner of the Mt. Hayes C-4 Quadrangle. The terminal moraine of the 1937 surge is as close as l.5 km west of Richardson Highway near Mile 226 (fig. 1). Historic Black Rapids Roadhouse is 5.8 km northeast of the 1937 terminus and east of Delta River and Richardson Highway. Falls Creek and Gunnysack Creek are significant local tributaries to the Delta River and enter the terminal area from the east.

Valley-floor elevations in the terminal zone range between 645 and 675 m (2,125 and 2,200 ft), about 150 to 200 m below the highest local limits of white spruce trees. Nearby ice-carved peaks reach elevations as high as 3,455 m (11,400 ft).

Extensive pre-1937 terminal positions of Black Rapids Glacier are delineated by three Holocene moraines (fig. 1). The oldest moraine is densely forested with white spruce, quaking aspen, and balsam poplar and loops across drift of the Donnelly glaciation of late Wisconsinan age (Mendenhall, 1900; Péwé, 1951, 1953, 1965, 1975; Péwé and Holmes, 1964) and bedrock composed of pelitic greenschist and amphibolite (Nokleberg and others, 1990). East of Delta River this moraine arcs between the lower reaches of Gunnysack Creek and Lower Suzy Q Creek. Just inside the maximum limit of the earliest known Holocene advance and almost parallel to it, the Hidden Lake-Falls Creek diversion channel marks the former course of Delta River, which was temporarily blocked by this early advance (Péwé and Reger, 1983, 1989). Post and Mayo (1971, sheet 2) traced faint former shorelines of the resulting lake along the lower walls of Delta River valley at least 8.5 km upstream from the outermost moraine. Nested within the most extensive moraine is a second forested Holocene moraine, which forms a prominent ridge parallel to the trans-Alaska pipeline east of Richardson Highway betweeen lower Falls Creek and Suzy Q Creek (fig. 1). Much of the moraine in this area consists of well-sorted alluvial sand and stream gravel. A much younger pre-1937 end moraine extends to within 1.5 km of the limit of the maximum Holocene advance (fig. 1). None of these Holocene moraines are ice cored. Their maximum local relief is 1 to 5 m, and tills are generally coarse cobbly and bouldery gravels with sand lenses.

Most of the 1937 surge moraine and post-1937 drift liberated by thinning and retreat of lower Black Rapids Glacier during the past 55 yr is generally unvegetated, except for willow thickets and small balsam poplar trees, because of the unstable substrate resulting from the melting of the ice beneath. The first small spruce trees, which began growing about 1953, were found in 1957 on part of the 1937 terminal moraine that was not ice cored (Péwé and Reger, 1983, 1989).

[1]Alaska Division of Geological and Geophysical Surveys, 794 University Avenue, Suite 200, Fairbanks, Alaska 99709-3645.
[2]Department of Geology and Geophysics, University of Alaska, Fairbanks, Alaska 99775.

AGES OF PRE-1937 MORAINES

Several methods, including dendrochronology, lichenometry, and radiocarbon dating have been used to establish the ages of the pre-1937 end moraines of Black Rapids Glacier (Péwé, 1951, 1965; Reger, 1964; Reger and Péwé, 1969), but the results have not been consistent (Péwé and Reger, 1983). Recently recognized physiographic and stratigraphic evidence, including new radiocarbon dates and reliable tephra correlations, clarify the late Holocene history of the glacier.

Oldest Holocene Moraine

Tree-ring Evidence

Péwé (1951, 1965) counted the growth rings of sound and rotten-center spruce growing on several moraines in an attempt to date these moraines. He assumed that white spruce was locally established before the oldest recognized Holocene advance of Black Rapids Glacier because he found many fallen and decayed trees estimated to be several centuries old just outside the limit of Holocene glaciation. In the oldest solid-center spruce found on the outermost moraine east of Delta River, he counted 131 annual rings and estimated the age of the tree at 133 yr (Péwé and Reger, 1983, fig. 50 and table 4) (fig. 2). However, he also found several large spruce with decayed heartwood, which he concluded were older than 133 yr. Based on this tree-ring evidence and the weakly developed soils on the moraine, he estimated that the oldest Holocene advance of Black Rapids Glacier occurred only about 330 yr ago (Péwé and Reger, 1983, p. 85).

Lichenometric Evidence

Reger (1964) attempted to use the time-dependent increase in the diameter of the crustose lichen *Rhizocarpon geographicum* s.l. to indirectly date the moraines of Black Rapids Glacier, but his initial growth curve was calibrated using the tree-ring assessments of Péwé (1951, 1965) and is much different than the growth curve developed for this same species in the St. Elias Mountains by Denton and Karlén (1973, 1977). The Denton-Karlén curve was essentially duplicated by Ten Brink and his colleagues (unpubl. data, 1981) for the northcentral Alaska Range (Calkin, 1988), so it was one scale we considered for estimating the ages of the moraines of Black Rapids Glacier, even though it is, in part, developed from uncalibrated radiocarbon dates. Clearly, there is a problem with the initial lichen-growth curve based solely on tree-ring estimates (Péwé and Reger, 1983, fig. 52).

The oldest terminal moraine of Black Rapids Glacier is unsatisfactory for lichen dating probably because of the heavy tree cover, which severely reduces ground-level solar radiation critical for lichen growth. Dead *R. geographicum* s.l. thalli up to 80 mm diam were measured on the moraine east of Delta River and rare live thalli up to 30 mm diam were found (Reger, 1964, Reger and Péwé, 1969). Assuming that changes of growing conditions resulting from forest invasion killed the initial lichen flora, the Denton-Karlén curve for *R. geographicum* s.l. indicates that the largest dead lichens were killed after growing for at least 1,390 yr (fig. 2). If the largest live lichens indirectly measure time since the microenvironment was altered by forest growth (185 yr), the moraine is at least as old as the sum of both ages (1,575 yr).

Radiocarbon and Tephrochronological Evidence

The oldest Holocene advance of Black Rapids Glacier pushed Delta River eastward to cut the Hidden Lake-Falls Creek diversion channel (fig. 1) and to erode the distal end of the large alluvial fan of Gunnysack Creek. Organic material and volcanic ash that were found in till of this advance and in the frontal scarp of the dissected Gunnysack Creek fan provide evidence for maximum ages for the oldest advance (fig. 2).

In 1981 in the roadcut north of the bridge over lower Falls Creek, Reger found several discrete blocks and pods of undisturbed to remolded outwash material in the bouldery till of the oldest recognized Holocene advance of Black Rapids Glacier (fig. 1, locality C-F; fig. 2, locality C-J-F) (Péwé and Reger, 1983, fig. 49). These unique erratics are up to 1.9 m diam and as thick as 0.6 m. They represent remnants of the former turf- and loess-covered outwash deposits in front of Black Rapids Glacier that were overridden and transported by the early advance. Near the north end of the roadcut (Péwé and Reger, 1983, Stop 15), some of the exotic blocks are undeformed internally, except for a thin surface layer, where silty block material is mixed with the enclosing gravelly till.

Radiocarbon dates and tephrochronological evidence in one of the undeformed blocks provide a maximum age for this earliest recognized advance (fig. 1, locality C-F; fig. 2, locality C-J-F). Two thin, discontinuous layers of turf separated by 7 to 13 cm of sandy loess were dated at 3,120 ± 120 and 4,350 ± 140 radiocarbon yr, respectively (table 1, samples C and F). Sandwiched between these organic layers was a discontinuous layer of volcanic ash up to 2.5 cm thick. The major-oxide content of the glass fraction of this tephra was analyzed by electron microprobe and strongly correlates with glass fractions

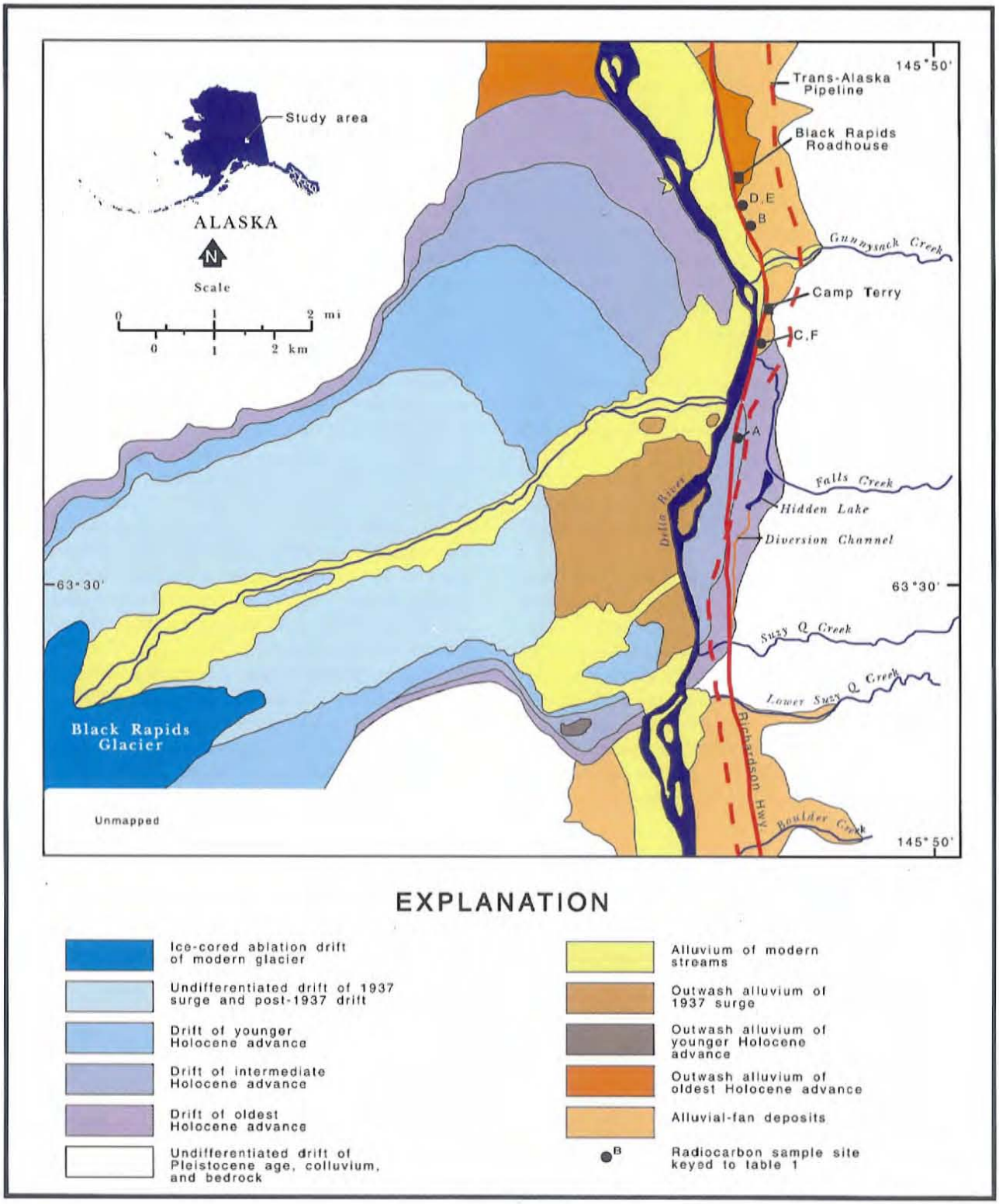

Figure 1. *Geologic map showing radiocarbon sampling sites in terminal area of Black Rapids Glacier. Drawn from infrared aerial photograph ALK 60, negative 3825, taken August 24, 1981.*

of the Jarvis Creek Ash that were collected nearby in the central Alaska Range—including the type locality of the Jarvis Creek Ash—and elsewhere in southcentral Alaska (Begét and others, 1991). Similarity coefficients for two ash samples from the Falls Creek roadcut compared to a sample from the type locality are 0.98 and 0.99 (Begét and others, 1991, table 4, samples ATC634-636).

Thus, stratigraphic evidence in the highway cut near Falls Creek demonstrates that the earliest known and most extensive Holocene advance of Black Rapids Glacier occurred after 3,120 radiocarbon yr ago (3,364 mean calendar yr ago with a 1-σ range of 3,469 to 3,209 calendar yr ago) (table 1, sample C). The difference between this younger date and the older date of 4,350 radiocarbon yr (possible mean calender ages of 4,962, 4,956, and 4,873 yr with a 1-σ range of 5,251 to 4,733 calendar yr) (table 1 sample F) indicates that Black Rapids Glacier had not advanced as far as the sample locality for at least 1,230 radiocarbon yr (1,509 to 1,598 calendar yr with a 1-s range of 1,264 to 2,042 calendar yr). During this interval the Jarvis Creek Ash was deposited locally.

Stratigraphic evidence from the Falls Creek road-cut is corroborated by evidence in the highway cut through the dissected alluvial fan of Gunnysack Creek, deposits of which underlie advance outwash and till of the earliest advance of Black Rapids Glacier west of Delta River (fig. 2). A discontinuous layer of volcanic ash up to 1.5 cm thick was collected 10 m below the top of fan gravels near the north end of the roadcut (fig. 1, locality D-E; fig. 2, locality D-J-E). Similarity coefficients of 0.99 were obtained with ash samples from the type locality of Jarvis Creek Ash and the Falls Creek roadcut, providing positive identification of Jarvis Creek Ash (Begét and others, 1991, table 4, samples ATC634-637). Small pieces of charcoal from the base of the volcanic ash provide a close maximum date for tephra deposition of 3,660 ± 275 radiocarbon yr (mean calendar age of 3,986 yr with a 1-σ range of 4,409 to 3,639 calendar yr) (table 1, sample E). Scattered charcoal fragments from 1 to 2 cm above the Jarvis Creek Ash in the roadcut date 3,360 ± 200 radiocarbon yr (mean calendar age of 3,626 yr with a 1-σ range of 3,859 to 3,379 yr) (table 1, sample D), providing a close minimum age for deposition of the tephra.

The age of small, scattered charcoal chunks from the base of loess overlying alluvial-fan deposits in the roadcut indicates that the upper half of the alluvial-fan section was deposited before 1,885 ± 220 radiocarbon yr ago (1,834 mean calendar yr ago with a 1-σ variation of 2,104 to 1,560 yr ago) (table 1, sample B). Dissection of the large fan could have occurred before or after 1,885 radiocarbon yr ago in response to the early advance of Black Rapids Glacier and displacement of Delta River. Unfortunately, the date for charcoal from the base of the loess is not directly related to fluctuations of Black Rapids Glacier. Instead, it establishes both a maximum age for the initial deposition of the 40-cm-thick loess blanket, which is still receiving silt, and a minimum age for fan deposition at the site. Clearly, however, the large fan of Gunnysack Creek was still growing 3,360 radiocarbon yr ago (3,626 mean calendar yr ago with a 1-σ range of 3,859 to 3,379 yr ago) (table 1, sample D), so the earliest known advance of Black Rapids must have occurred later.

Table 1. *Summary of radiocarbon dates associated with Holocene features in terminal area of Black Rapids Glacier, keyed to figures 1 and 2. All samples but I-12108 and I-12109 corrected for natural isotopic fractionation based on carbon-13 content. Calibration to calendar years B.P. based on changes in radiocarbon contents of dendrochronologically dated tree rings (Stuiver, 1982; Pearson and Stuiver, 1986; Pearson and others, 1986; Stuiver and Pearson, 1986; Stuiver and Reimer, 1986)*

Sample	Materials dated	Radiocarbon age (yr B.P.)[a]	Calibrated mean age and 1σ range (cal. yr B.P.)[a]	Laboratory number
A	Organic silty fine sand	1,780 ± 85	1,711; 1,605-1,824	GX-14439
B	Small charcoal chunks	1,885 ± 220	1,834; 1,560-2,104	GX-15537
C	Thin, discontinuous turf	3,120 ± 120	3,364; 3,209-3,469	I-12109
D	Small charcoal chunks	3,360 ± 200	3,626; 3,379-3,859	GX-14442
E	Small charcoal chunks	3,660 ± 275	3,986; 3,639-4,409	GX-14443
F	Thin, discontinuous turf	4,350 ± 140	4,873; 4,956; 4,962; 4,733-5,251	I-12108

[a] Referenced to A.D. 1950.

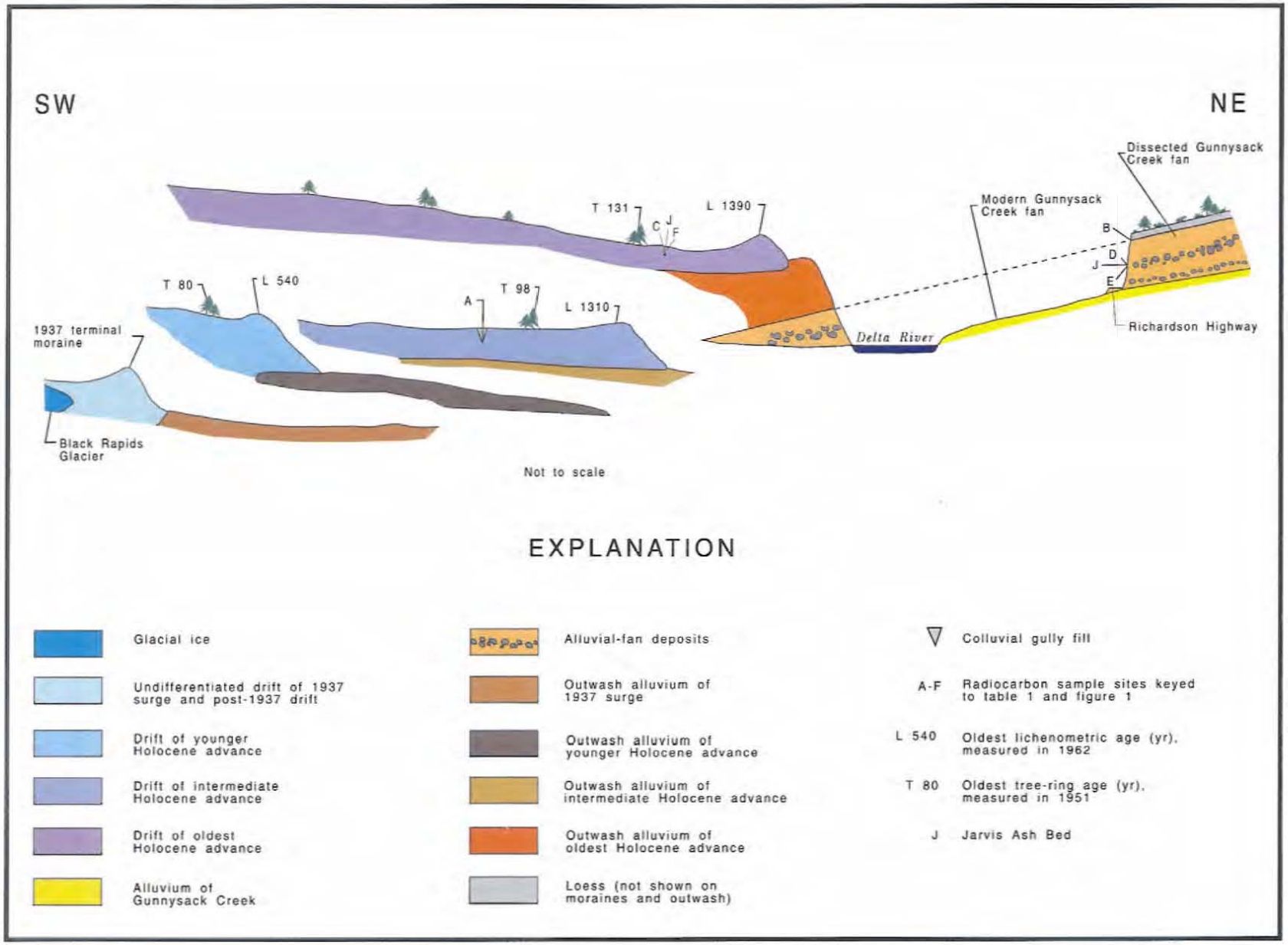

Figure 2. *Exploded composite projection showing relations of Holocene features in terminal area of Black Rapids Glacier to tree-ring, lichen, and radiocarbon ages. Vegetation shown diagrammatically.*

Intermediate Holocene Moraine

Tree-ring Evidence

In 1951 on the secondmost extensive Holocene terminal moraine, Péwé counted up to 95 growth rings in the largest, apparently most vigorous white spruce and estimated the age of the tree as 98 yr (Péwé and Reger, 1983, fig. 50 and table 4, sta. 32) (figs. 1 and 2). Assuming that spruce trees do not develop on moraines in this part of the central Alaska Range until about 20 yr after the advance that builds the moraine (Péwé and Reger, 1983, p. 83), the dendrochronological evidence indicates that the intermediate Holocene advance of Black Rapids Glacier occurred about A.D. 1833.

Lichenometric Evidence

The intermediate moraine west of Delta River is partly blanketed by eolian sand, and dead thalli of crustose lichens show the effects of sandblasting. In 1961, Reger (1964) measured apparently dead circular thalli of *R. geographicum* s.l. up to 75 mm diam and found live circular *R. geographicum* s.l. as large as 40 mm diam. Reger and Péwé (1969, p. 234) suggested that the lichen flora initially growing on this moraine may have been killed by windblown sand picked up from nearby outwash, perhaps derived from a later advance, and live thalli may represent a later (secondary) colonization. Based on the Denton-Karlén growth curve for *R. geographicum* s.l., the largest dead lichens were about 1,310 yr old when they were killed, and the largest live individuals had been growing for about 290 yr in 1961. Thus, the lichen evidence indicates that the intermediate Holocene moraine was at least 1,600 yr old (the sum of both ages) in 1961.

Radiometric Evidence

A minimum age for the intermediate Holocene moraine is established by a single radiocarbon date of 1,780 ± 85 yr (1,711 calendar yr with a 1-σ range of 1,824 to 1,605 yr) for the basal colluvial fill in a former gully eroded into the moraine (figs. 1 and 2 and table 1, sample A).

Younger Holocene Moraine

The youngest pre-1937 end moraine of Black Rapids Glacier is sparsely discontinuously vegetated and bears only a very weak soil. This moraine looked very fresh in 1910 when it was ice cored (Moffit, 1942).

Tree-ring Evidence

In 1951, Péwé counted up to 69 growth rings in healthy spruce growing on this moraine and estimated that the largest tree was 80 yr old (Péwé and Reger, 1983, fig. 50 and table 4, sta. 33), indicating that the moraine was formed a century earlier in about A.D. 1850.

Lichenometric Evidence

In 1961, among 82 of the largest circular thalli of *R. geographicum* s.l. at 11 sites on the younger end moraine, maximum diameters ranged from 11 to 48 mm and maximum diameters between stations averaged 26 mm (Reger, 1964, table 2). Assuming that the largest individual lichen (48 mm) measured on this moraine best represents the age of the moraine, according to the Denton-Karlén growth curve, it was 540 yr old when measured (fig. 2). The average maximum thalli diameter among the population studied indicates that the moraine was at least 180 yr old in 1961. Thus, the lichens indicate that Black Rapids Glacier advanced to form this end moraine at least as early as A.D. 1780 and probably before A.D. 1420.

IMPLICATIONS

Comparisons of the results of dendrochronologic, lichenometric, and radiocarbon dating of the oldest and intermediate Holocene moraines demonstrate that age estimates based on lichen sizes more accurately approximate the actual ages of the moraines than do tree-ring estimates. However, compared with the results of radiocarbon dating, both methods produce estimates that are centuries to millenia too young. Although not conclusively demonstrated by this study, the evidence presented implies that tree-ring and lichen estimates diverge more from actual ages for older features and events than for younger features and events. In this study, we found no remains of forests later overridden by one or more advances. Therefore, radiocarbon dates provide only approximate maximum and minimum ages.

We conclude that Black Rapids Glacier advanced twice between 1,711 calendar yr ago (the minimum age of the intermediate Holocene moraine) and 3,364 calendar yr ago (the age of the youngest organic material actually carried by the oldest advance) (fig. 3). We suggest that the presence of undeformed allochthonous blocks of outwash material in till of the earliest advance is evidence that the advance was a surge that picked up blocks of frozen outwash, probably in late winter based

on block thicknesses up to 0.6 m, and then deposited them before they thawed the following summer. Other nearby pods of similar material are mixed with the surrounding till, although they are still recognizable by their color and composition. This condition indicates that they thawed and were partially remolded, but not destroyed, before being deposited by the glacier. We speculate that these exotic blocks were not displaced far by the surge, perhaps as part of a frontal push moraine, like the wedge of material bulldozed by the 1937 surge as the glacier slid forward (Moffit, 1942).

The intermediate moraine appears to be, at least in part, a push moraine. The 10- to 20-m-high, sharp-crested moraine near the Richardson Highway east of Delta River is composed of alluvium that we believe may have been pushed into place by the advancing terminus. This moraine closely resembles mounds of outwash alluvium west of Delta River that were produced during the 1937 surge of Black Rapids Glacier across its own outwash fan, and it may record a prehistoric surge.

Although the younger Holocene moraine was still ice cored and looked very fresh in 1910 (Moffit, 1942), the lichen data indicate that it was built by an advance certainly before A.D. 1780 and probably before A.D. 1420 (fig. 3). We do not know if this advance was a surge.

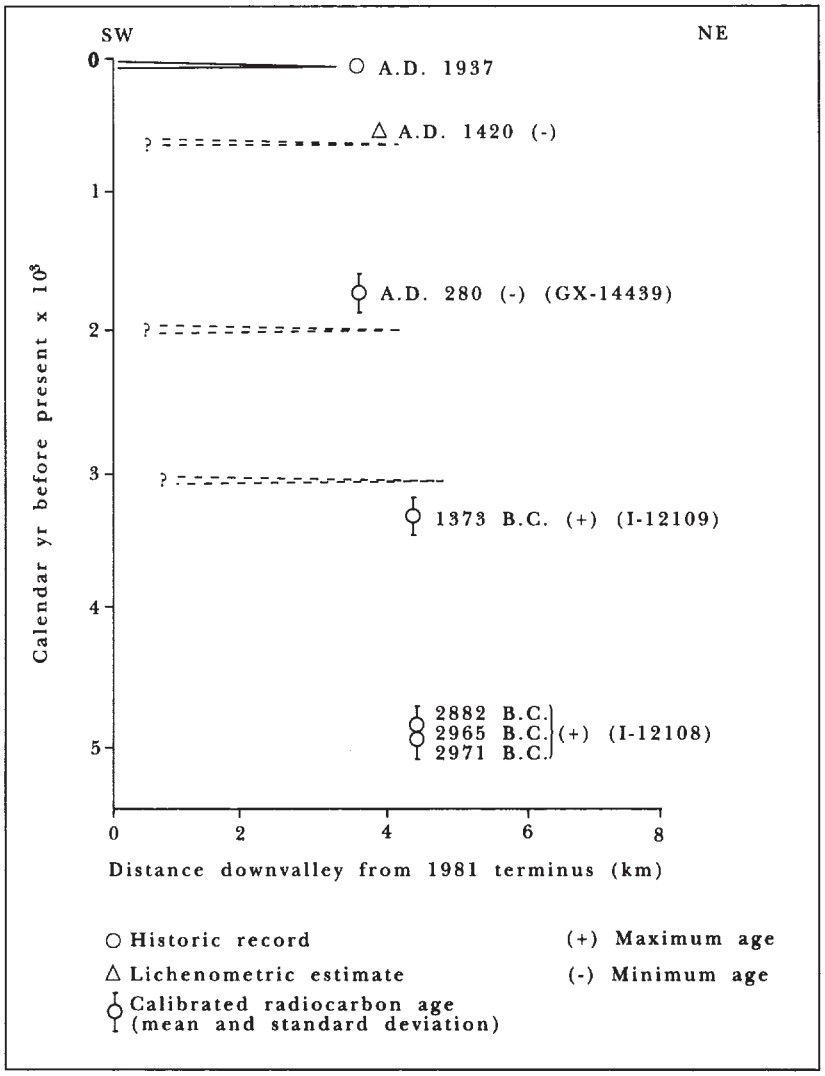

Figure 3. *Late Holocene variations of Black Rapids Glacier terminus relative to 1981 terminus. Dashed lines indicate timing of advance is approximate. Radiocarbon ages keyed to table 1.*

ACKNOWLEDGMENTS

Troy L. Péwé has maintained an active research interest in Black Rapids Glacier for the past 40 years. His work and continuing encouragement have inspired us to pursue our search for more evidence to reconcile conflicting interpretations of the history of this remarkable glacier.

The glass fraction of the Jarvis Creek Ash samples was analyzed in the electron-microprobe facility, Department of Geology, Washington State University. In addition to preparing microprobe slides, Scott Cornelius and Dianne Johnson periodically calibrated the Cameca MBX microprobe to ensure consistent, accurate results. Their cheerful cooperation is greatly appreciated. DeAnne Pinney ably assisted during preparation and analysis of the tephra samples. Christopher F. Waythomas (USGS) and Rodney A. Combellick (DGGS) provided thought-provoking, useful reviews that significantly improved this paper.

REFERENCES

Begét, J.E., Reger, R.D., Pinney, DeAnne, Gillispie, Tom, and Campbell, Kathy, 1991, Correlation of the Holocene Jarvis Creek, Tangle Lakes, Cantwell, and Hayes tephras in south-central and central Alaska: Quaternary Research, v. 35, no. 2, p. 174-189.

Calkin, P.E., 1988, Holocene glaciation of Alaska (and adjoining Yukon Territory, Canada): Quaternary Science Reviews, v. 7, no. 2, p. 159-184.

Denton, G.H., 1975, Alaska Range, *in* Field, W.O., ed., Mountain glaciers of the northern hemisphere: Hanover, U.S. Army Cold Regions Research and Engineering Laboratory, v. 2, p. 573-620.

Denton, G.H., and Karlén, Wibjorn, 1973, Lichenometry: Its application to Holocene moraine studies in southern Alaska and Swedish Lapland: Arctic and Alpine Research, v. 5, no. 4, p. 347-372.

_____1977, Holocene glacial and tree-line variations in the White River valley and Skolai Pass, Alaska and Yukon Territory: Quaternary Research, v. 7, no. 1, p. 63-111.

Geist, O.W., and Péwé, T.L., 1957, Quantitative measurements of the 1937 advance of the Black Rapids Glacier, Alaska [abs.]: Proceedings of the 5th Alaska Science Conference, Anchorage, 1954, p. 51-52.

Giddings, J.L., 1988, Thunder from below: University of Alaska 1937 Black Rapids Glacier expedition: Journal of Northern Sciences, v. 2, p. 33-40.

Hance, J.H., 1937, The recent advance of Black Rapids Glacier, Alaska: Journal of Geology, v. 45, no. 7, p. 775-783.

Mendenhall, W.C., 1900, A reconnaissance from Resurrection Bay to the Tanana River, Alaska, in 1898: U.S. Geological Survey 20th Annual Report, pt. 7, p. 265-340.

Moffit, F.H., 1942, Geology of the Gerstle River district, Alaska, with a report on the Black Rapids Glacier: U.S. Geological Survey Bulletin 926, p. 107-160.

_____1954, Geology of the eastern part of the Alaska Range and adjacent area: U.S. Geological Survey Bulletin 989-D, p. 65-218.

Nokleberg, W.J., Lange, I.M., Singer, D.A., Curtin, G.C., Tripp, R.B., Campbell, D.L., and Yeend, Warren, 1990, Metalliferous mineral resource assessment maps of the Mount Hayes Quadrangle, eastern Alaska Range, Alaska: U.S. Geological Survey Miscellaneous Field Studies Map MF-1996-A, 22 p., 4 sheets, scale 1:250,000.

Pearson, G.W., Pilcher, J.R., Baillie, M.G.L., Corbett, D.M., and Qua, F., 1986, High-precision ^{14}C measurement of Irish oaks to show the natural ^{14}C variations from AD 1840 to 5210 BC, *in* Stuiver, Minze, and Kra, Renee, eds., Proceedings of the 12th International Radiocarbon Conference, Trondheim, 1985: Radiocarbon, v. 28, no. 2B, p. 911-934.

Pearson, G.W., and Stuiver, Minze, 1986, High-precision calibration of the radiocarbon time scale, 500–2500 BC, *in* Stuiver, Minze, and Kra, Renee, eds., Proceedings of the 12th International Radiocarbon Conference, Trondheim, 1985: Radiocarbon, v. 28, no. 2B, p. 839-862.

Péwé, T.L., 1951, Recent history of Black Rapids Glacier, Alaska [abs.]: Geological Society of America Bulletin, v. 62, no. 12, p. 1558.

_____1953, Big Delta area, Alaska, *in* Péwé, T.L., and others, Multiple glaciation in Alaska: U.S. Geological Survey Circular 289, p. 8-10.

_____1965, Delta River area, Alaska Range, *in* Péwé, T.L., Ferrians, O.J., Jr., Nichols, D.R., and Karlstrom, T.N.V., Guidebook for Field Conference F, central and south-central Alaska, International Association for Quaternary Research, 7th Congress, Fairbanks, 1965: Lincoln, Nebraska Academy of Sciences, p. 55-93 (reprinted 1977, College, Alaska Division of Geological and Geophysical Surveys).

_____1975, Quaternary geology of Alaska: U.S. Geological Survey Professional Paper 835, 145 p.

Péwé, T.L., and Holmes, G.W., 1964, Geology of the Mt. Hayes (D-4) Quadrangle, Alaska: U.S. Geological Survey Miscellaneous Geologic Investigations Map I-394, 2 sheets, scale 1:63,360.

Péwé, T.L., and Reger, R.D., 1983, Delta River area, Alaska Range, *in* Péwé, T.L., and Reger, R.D., eds., Guidebook to permafrost and Quaternary geology along the Richardson and Glenn Highways between Fairbanks and Anchorage, Alaska: Alaska Division of Geological and Geophysical Surveys Guidebook 1, p. 47-135.

_____1989, Delta River area, Alaska Range, *in* Péwé, T.L., and Reger, R.D., eds., Quaternary geology and permafrost along the Richardson and Glenn Highways between Fairbanks and Anchorage, Alaska: Washington, D.C., American Geophysical Union Guidebook T102, p. 25-38.

Post, Austin, 1960, The exceptional advances of the Muldrow, Black Rapids, and Susitna Glaciers: Journal of Geophysical Research, v. 65, no. 11, p. 3703-3712.

_____1969, Distribution of surging glaciers in western North America: Journal of Glaciology, v. 8, no. 53, p. 229-240.

Post, Austin, and Mayo, L.R., 1971, Glacier dammed lakes and outburst floods in Alaska: U.S. Geological Survey Hydrologic Atlas HA-455, 10 p., 3 sheets, scale 1:2,500,000.

Reger, R.D., 1964, Recent glacial history of Gulkana

and College Glaciers, central Alaska Range, Alaska: Fairbanks, University of Alaska M.S. thesis, 75 p.

Reger, R.D., and Péwé, T.L., 1969, Lichenometric dating in the central Alaska Range, *in* Péwé, T.L., ed., The periglacial environment, past and present: Montreal, McGill-Queens University Press, p. 223-247.

Stout, J.H., Brady, J.B., Weber, F.R., and Page, R.A., 1973, Evidence for Quaternary movement on the McKinley strand of the Denali fault in the Delta River area, Alaska: Geological Society of American Bulletin, v. 84, no. 3, p. 939-948.

Stuiver, Minze, 1982, A high-precision calibration of the AD radiocarbon time scale: Radiocarbon, v. 24, no. 1, p. 1-26.

Stuiver, Minze, and Pearson, G.W., 1986, High-precision calibration of the radiocarbon time scale, AD 1950-500 BC, *in* Stuiver, Minze, and Kra, Renee, eds., Proceedings of the 12th International Radiocarbon Conference, Trondheim, 1985: Radiocarbon, v. 28, no. 2B, p. 805-838.

Stuiver, Minze, and Reimer, P.J., 1986, A computer program for radiocarbon age calibration, *in* Stuiver, Minze, and Kra, Renee, eds., Proceedings of the 12th International Radiocarbon Conference, Trondheim, 1985: Radiocarbon, v. 28, no. 2B, p. 1022-1030.

PALEOMAGNETISM OF THE FAIRBANKS BASALTS, INTERIOR ALASKA

by
J.T. Roe[1] and D.B. Stone[2]

INTRODUCTION

Fairbanks area basalts, which consist of seven isolated outcrops of olivine basalt of early Eocene age, are all located within 30 miles of Fairbanks, Alaska (fig. 1). Their composition is tholeiitic to alkalic (Furst, 1968) and includes subaerial and subaqueous flows and palagonite breccias. Four of the seven known localities were sampled as part of a paleomagnetic study of Cenozoic volcanics. The main purpose of this study is to investigate whether large-scale block rotation has occurred between the two major dextral fault systems of Alaska–the Tintina fault system to the north, and the Denali and associated faults to the south.

[1]Division of Geological & Geophysical Surveys, 794 University Avenue, Suite 200, Fairbanks, Alaska 99709-3645.
[2]Geology/Geophysics Department, University of Alaska Fairbanks, Fairbanks, Alaska 99775-0760.

Ninety-two fully oriented samples were collected and subjected to alternating field or thermal demagnetization to isolate the stable characteristic magnetization for each unit sampled. Unblocking temperatures determined by thermal demagnetization fall within a narrow range near 400°C. The medium destructive alternating field varied between sites, and ranged between 2 mT and 3 mT. The results of this study indicate that the Fairbanks basalts have undergone some 70° counterclockwise (CCW) motion relative to stable North America since mid-to early Eocene times.

TECTONIC SETTING

The Fairbanks basalts are all located within the Yukon-Tanana Upland, which is bounded on the northeast by the Tintina fault, on the southwest by the Denali fault, on the northwest by the Manley terrane, and on the

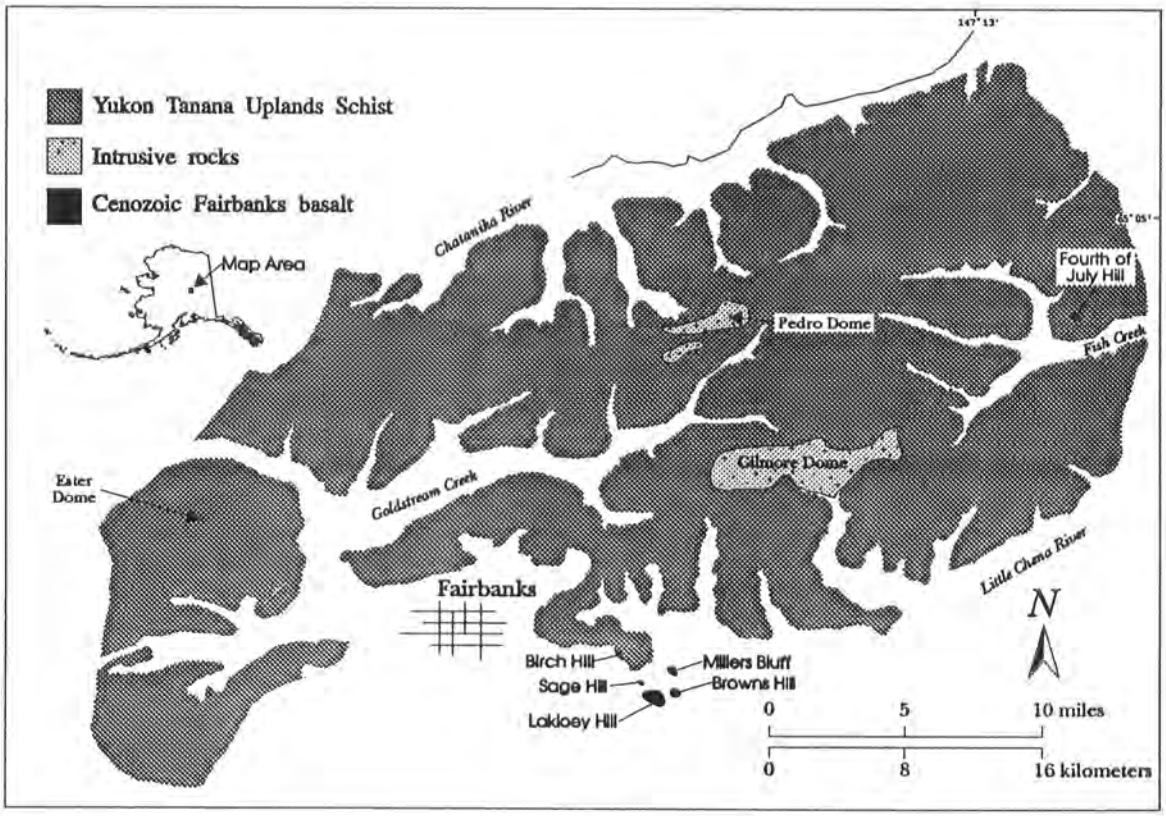

Figure 1. *Location map showing Fairbanks area basalts.*

southeast by the Stikine terrane (Jones and others, 1987; Monger and Berg, 1987). The Yukon-Tanana Upland has been subdivided into a number of terranes, the largest of which is the Yukon-Tanana terrane (Jones and others, 1987). Other subterranes within the Yukon-Tanana terrane have also been proposed, and the Fairbanks basalts are found in both the Fairbanks and Chena sub-terranes (Robinson and others, 1990).

Recent geologic mapping (Weber, 1989) aeromagnetic and gravity studies (J.W. Cady, oral commun.,1991; D.F. Barnes, oral commun., 1991; Queen, 1989) show that several northeast-southwest trending faults transect the Yukon Tanana Upland. Several of these faults appear to be seismically active today, and fault plane solutions indicate the active pattern of faulting is dominated by left-lateral strike-slip motion (Page and others, 1991).

GEOLOGY

In the Fairbanks area, the Yukon Tanana Upland consists of Precambrian to Paleozoic metamorphic rocks, Late Cretaceous intrusive bodies, and isolated mid-Tertiary basalts. Bedrock exposed in the area comprises four metamorphosed stratigraphic packages. From oldest to youngest they are the Chatanika terrane, Fairbanks schist unit, Chena River sequence, and Birch Hill sequence. The intrusive bodies in the Fairbanks area have radiometric ages of 91-93 m.y. (Blum, 1983) and are part of a regional northeasterly trend of granodiorite or quartz monzonite-granite intrusions stretching from western Alaska to Canada (Robinson and others, 1990). Robinson and others (1990) conclude that the Fairbanks basalts intrude or overlay the amphibolite facies rocks of the Birch Hill and Chena River sequences.

This study includes six outcrops of the Fairbanks Basalts. The four sampled for paleomagnetic work are Fourth of July Hill (FJY), Millers Bluff (MLB), Lakloey Hill (LAK), and Browns Hill (BRN). We describe outcrops at Sage Hill and Birch Hill, but extensive weathering prevented sampling at these locations.

Locality Descriptions

Fourth of July Hill (FJY)

Fourth of July Hill (lat 65°04' N., long 147°04' W.) is approximately 28 km northeast of Fairbanks off the Steese Highway. The outcrop is located on the southeast side of the hill. Two-hundred-twenty m above Fish Creek the basalts crop out as two benches, each of which is thought to include a separate time unit. These basalts form hexagonal columns and contain small spheroidal vesicles filled with greenish-black calcite (Furst, 1968). Hand specimens contain light green plagioclase. Composite modal analysis of two samples done by Furst (1968) show 17 percent olivine, 42 percent plagioclase, 11 percent pyroxene, 26 percent glass, and 3 percent magnetite. The hexagonal columns are roughly perpendicular to the benches. The bench surfaces were used to determine ancient horizontal.

Millers Bluff (MLB)

Millers Bluff (lat 147°28'58" N.; long 64°50'42" W.) stands on the north bank of the Chena River near its confluence with Chena Slough. The basalt outcrop forms a 10-m-high bluff that extends approximately 25 m along the bank of the river. Here the basalt occurs as near uniform columns with an estimated diameter of 80 cm (Furst, 1968). The columns are more or less vertical, which we interpret as an indication of no tectonic tilting. Magnetite content based on modal analyses of four samples varied from 2.4 to 4.9 percent (Furst, 1968).

Lakloey Hill (LAK)

Lakloey Hill (lat 64°49'30" N., long 147°30'30" W.) is 7 miles east of Fairbanks, along Badger Road. The basalt exposure is on southeast side of Lakloey Hill. Quarrying of the hillside left a 32-m vertical exposure. The flanks of the outcrop expose the contact of the basal part of the flows with the erosional surface of the schists of the Paleozoic Birch Hill Sequence. Abundant fossil wood occurs thoughout the outcrop in nearly horizontal orientations indicating little, if any, tectonic tilting has occurred. Modal analysis provided no measurable magnetite.

Browns Hill (BRN)

Browns Hill (lat 64°49' 50" N., long 147°28' 30" W.) is approximately 2 km northeast of Lakloey Hill. As a result of quarrying, the detailed description of Browns Hill outcrop constantly changes. At the time of sampling, Browns Hill was a three-tiered vertical exposure 75 m high and 150 m long. The center of the hill was composed of nearly vertical columns 20 to 35 cm in diameter. Several radial and fan arrangements of columnar jointing are present near the east end of the exposure. Along the edges of the hill, poorly developed pillows and brecciated basalt are present. The contact between the weathered top of the Birch Hill Sequence and the basalt can be seen along the edges of the hill. Direct evidence of ancient horizontal at this locality is lacking. However, the roughly vertical columns in the center of the hill have a horizontal tabular distribution (contrasted

with the fanning columns), which could indicate a lack of tilting. It should be noted that Browns Hill, Lakloey Hill, and Millers Bluff are geographically close together, and all indicate little or no tilting. Modal analyses yield 2.1 percent magnetite in Browns Hill basalt (Furst, 1968).

Birch Hill and Sage Hill

Birch Hill (lat 147°38'25" N., long 64°51'50" N.) is approximately 5 km from Fairbanks. A road cut along the south edge of Birch Hill exposes the basalt. The outcrop is composed chiefly of breciated pillows and highly fractured basaltic lenses. The current exposure is intensely weathered. The degree of brecciation combined with the effects of weathering made it impossible to find sections where there were unambiguous indicators of ancient horizontal.

Sage Hill (lat 147°38'25" N., long 64°51'50" N.) is near the easternmost end of Birch Hill and is about 35 m high. The basalt is exposed by a road cut on the south edge of the hill and by active quarrying on top. Sage Hill basalt is similar to the basalt on Birch Hill, in that its main element is pillow breccia. Like Birch Hill, sampling was impossible because of the effects of brecciation and weathering on the exposed basalt.

Model analyses of samples from Birch and Sage Hills show 10 percent olivine, 21 percent plagioclase, 69 percent glass and no measurable magnetite (Furst 1968).

Gravity and magnetic data from three (MLB, LAK, BRN) of the four localities sampled indicate that the basalt does not extend much below the surface (Queen 1989). Geophysical data also suggest that 50 to 250 feet below the surface near Millers Bluff, there appear to be basaltic hills that were later buried by alluvium.

PALEOMAGNETIC METHODS

Several collections of samples were made between 1966 and the present from Fourth of July Hill, Millers Bluff, Browns Hill, and Lakloey Hill. The most recent collection was made in conjunction with a local gravity and magnetic study (Queen 1989). All samples for paleomagnetic work were collected as 2.5 cm diameter cores drilled in the field. The cores were oriented by sighting on known geographic features or by sun compass, weather permitting, and by magnetic compass.

Selected samples were subjected to progressive alternating field (AF) demagnetization, using either 5 mT incremental steps or by doubling the applied field at each step. The initial demagnetization was done using a tumbler system in a coil controlled field free space (Collinson and others,1967) and later samples using a Schonstedt GSD-1 demagnetizer. The remainder of the samples were subjected to progressive thermal demagnetization in 50°C steps, using a Schonstedt TSD-1 demagnetizer.

Magnetizations were measured at the University of Alaska Fairbanks with a Foster spinner magnetometer (Foster 1966) or with a Schonstedt SM-1 spinner magnetometer. Initial or natural remanent magnetization (NRM) of each sample was measured after magnetic cleaning at 2.5 mT. This process removed any viscous magnetization acquired during storage or transport from the field. The remanent magnetizations were then remeasured after each progressively higher step in the applied demagnetizing field or temperature.

The resulting data were displayed for visual examination as plots of intensities of magnetization versus demagnetization level, orthogonal projections of the vectors (declination in the horizontal plane and the inclination in the vertical plane containing the vector) and as unit vectors on an equal-area stereographic projection. This visual examination allowed identification of the various components of the magnetization. Figure 2 represents intensity, orthogonal, and stereographic plots for each of the areas. Figure 3 and table 1 show within-site sample directions and site averages.

After stepwise thermal demagnetization, most of the 92 specimens measured revealed a single stable characteristic magnetization, and all had reversed polarities, as shown in figures 2 and 3. The small scatter about a straight line 9 (fig. 2) through the origin shows that demagnetization changed only the intensity of magnetization, not the direction and demonstrates the stability of the magnetization. In all localities except Fourth of July Hill a component of the present day (normal) geomagnetic field is removed by 100°C. A small distinct component of magnetization differing from that of the higher temperature stable component is present in the samples from Millers Bluff. This low temperature secondary component is removed by 400°C, perhaps indicating a local post-extrusive thermal event.

Approximate magnetic-blocking temperatures determined from the intensity- versus- demagnetization temperature curves indicate Fourth of July Hill and Millers Bluff contain magnetic material with distinct blocking temperature patterns. Fourth of July Hill samples remanence directions remain stable throughout the temperature spectra. Millers Buff remanence directions steepen from the low temperature component to the direction of the stable higher temperature carrier. Samples from the other localities exhibit blocking temperatures near 400°C with consistent stable remence directions.

Under stepwise alternating field (AF) demagnetization, all specimens yielded similar remanence directions to their companion specimens under thermal demagnetization. All AF demagnetized samples showed a very

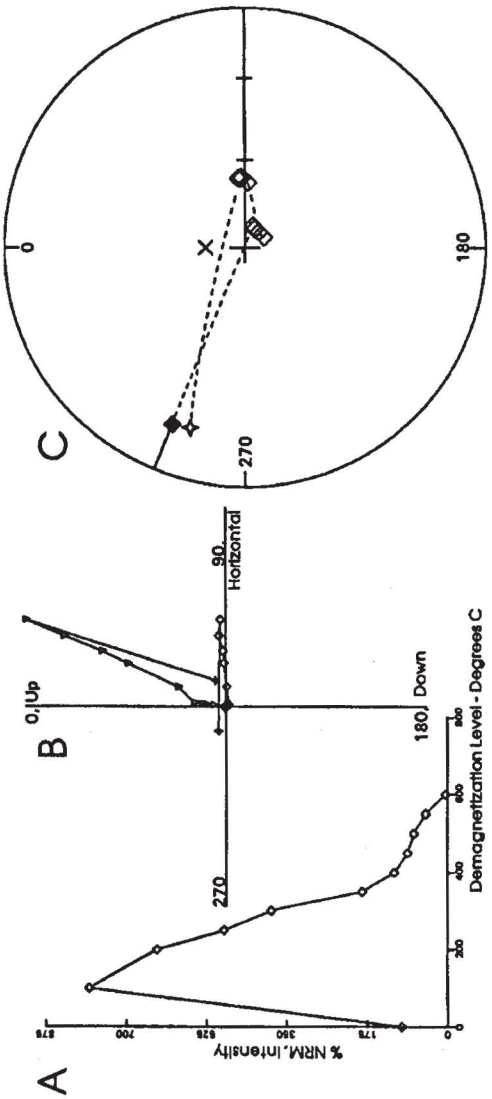

Millers Bluff, sample 8a

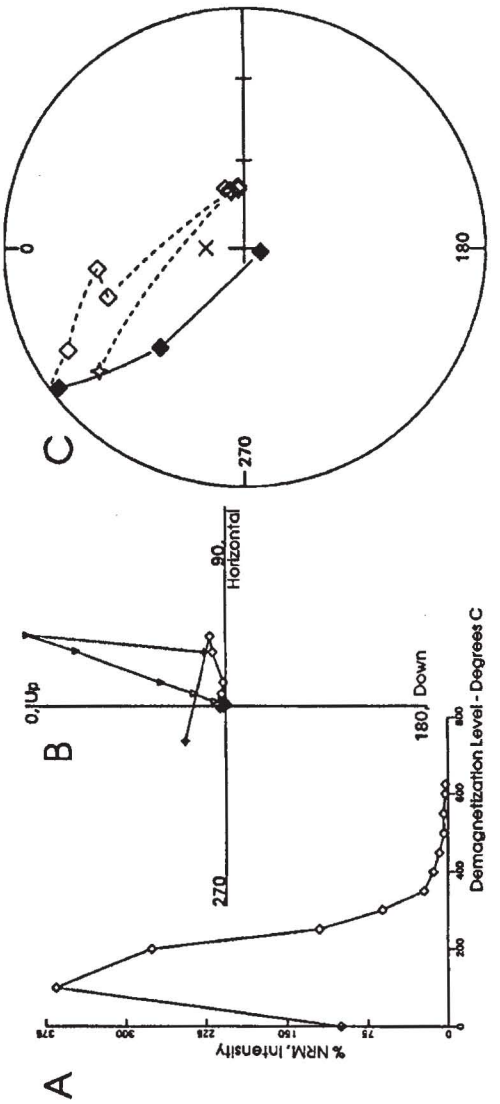

Lakloey Hill, sample 14a

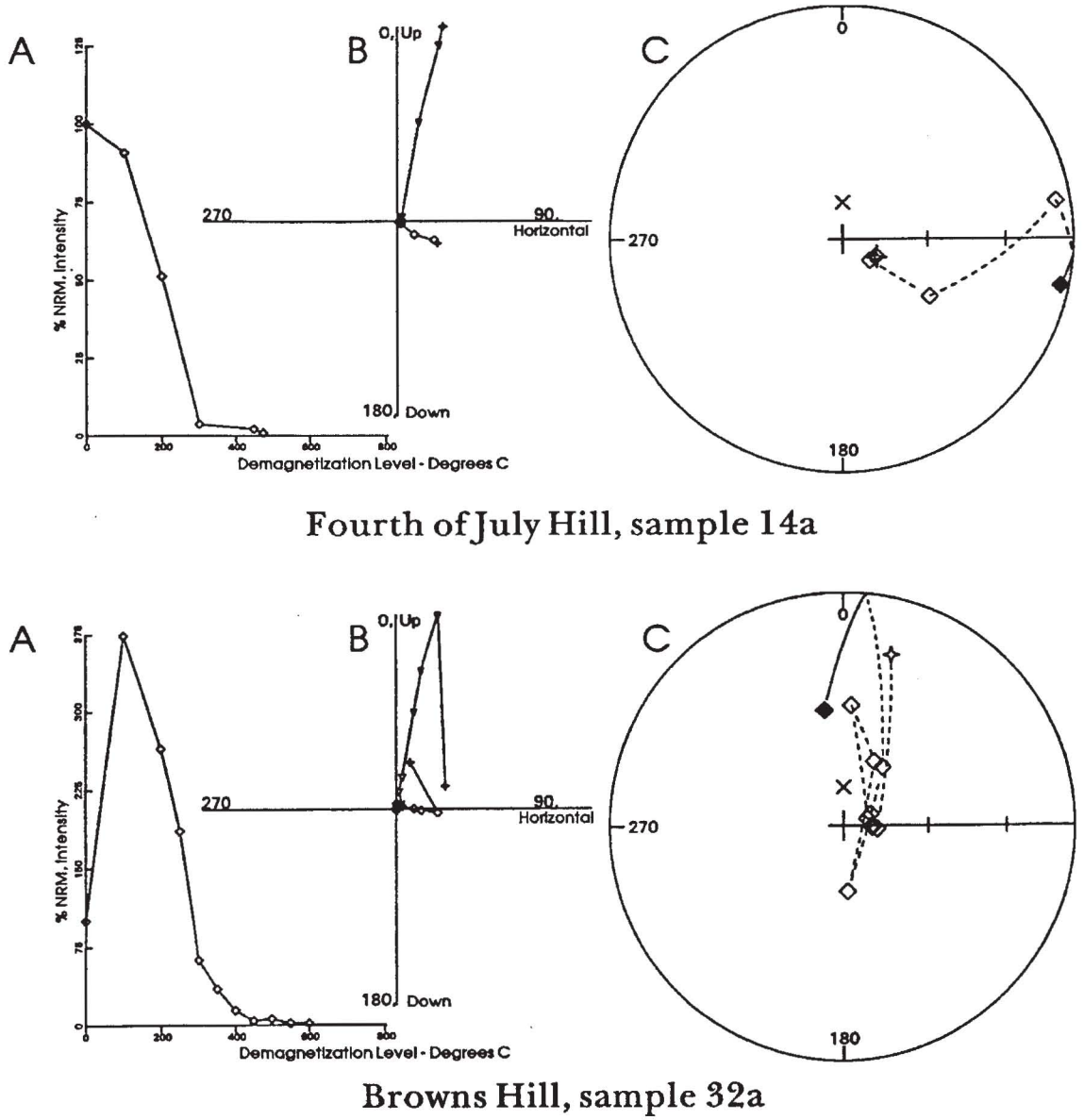

Figure 2. *Typical demagnetization plots for each of the four principal localities. In the figure for each locality, diagram* ***A*** *charts the intensity of magnetization versus demagnetization temperature; diagram* ***B*** *illustrates the declination (diamonds) plotted in a horizontal plane and the inclination (triangles) plotted in a vertical plane showing the vector direction; diagram* ***C*** *is an equal-area projection of the vector directions, with the natural remanent magnetization (NRM) shown as a star. Note: There are two components of magnetization associated with the Miller Bluff samples.*

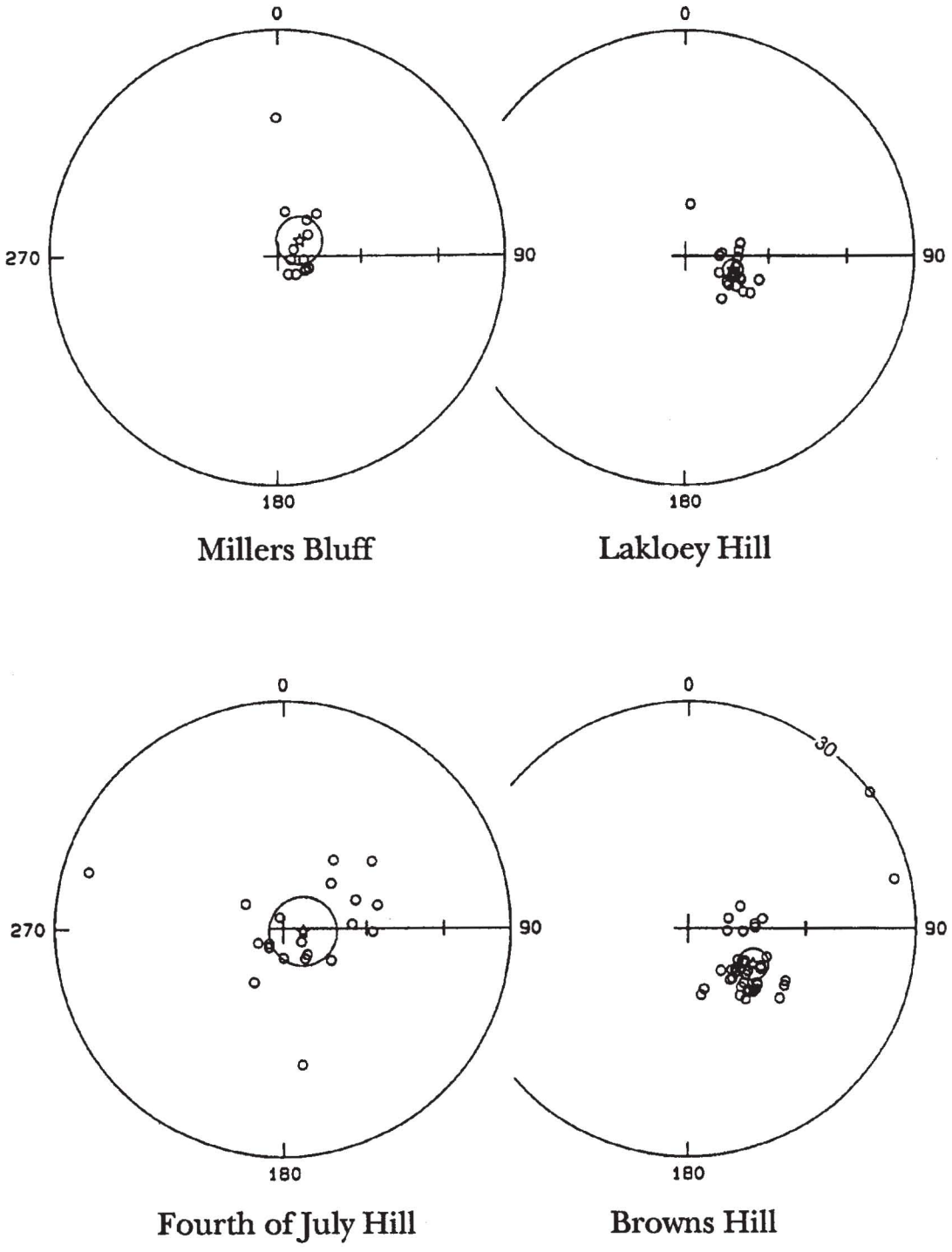

Figure 3. *Specimen and mean directions (star) for the Fairbanks basalt localities with the 95 percent confidence circle (after Fisher, 1953). Open symbols denote an upper hemisphere or reversed magnetic direction.*

small amount of scatter of magnetic directions during demagnetization.

In contrast to the relatively consistent blocking temperatures, in most localities the medium destructive alternating field varied between samples. We interpret the variations as the result of differences in the particle sizes of the magnetic carriers. Samples from Fourth of July Hill localities show consistently low coercivities of remanence, which is presumed to be the result of larger multi-domain magnetic material. We determined final mean directions from combined AF and thermal data. Table 1 lists the combined locality means. Volume susceptibility measurements including those from Queen (1989) are listed in table 1. K-Ar age data are listed in table 2.

As was mentioned above and shown in table 2, the ages of the Fairbanks basalts are early Eocene (with one radiometric age of 58 m.y., or latest Paleocene). The time span sampled at each locality is harder to determine, but based on the tabular nature of the columnar jointing, there appear to be at least three time units at Browns Hill and two at Fourth of July Hill. Lackloey Hill has both columns and pillows, and may represent at least two time units. Millers Bluff is a single time unit. If none of the four localities sampled are relatively contemporaneous, then a total of eight time units have been sampled. The overall scatter of the magnetic remanence data set is compatible with that expected for the secular variation of the geomagnetic field, so we feel secure in the assumption that sufficient time has been sampled (greater than a few thousand years) for the mean directions to be interpreted in terms of regional models.

GEOLOGIC IMPLICATIONS

Comparing the paleopole calculated from the mean magnetic vector from each locality with an early Eocene reference pole for stable North America (Coe and others, 1985) indicates that the Fairbanks basalts have rotated

Table 1. *Site mean characteristic directions, susceptibilities virtual geographic pole positions of the Fairbanks basalts*

		Stratigraphic			VGP		
Location	N[a]	D[b]	I[b]	α95[c]	Lat[d]	Long[d]	k/vol (SI units x 10^4)
Browns Hill	39	119	-71	4	-59	314	10.51
Fourth of July Hill	20	97	-83	12	-64	0	15.9
Millers Bluff	13	54	-81	8	-51	8	20.6[e]
Lakloey Hill	20	106	-72	4	-56	325	16.5[e]
Mean		101	-78	9	-60	343	15.9

[a]Number of samples.
[b]Declination (D) and inclination (I) of the magnetic vector corrected for tectonic tilt.
[c]95 is the alpha 95 of Fisher (1953).
[d]Latitude and longitude of the corresponding pole.
[e]Queen, 1989.

Table 2. *Whole rock potassium-argon ages of the Fairbanks basalts*[a]

Location (mean)	K_2O (wt %) (g)	Sample wt. (mol/g)10E-11	^{40}Ar rad	^{40}Ar rad/^{40}K 10E-3	%^{40}Ar rad	Age ± σ (m.y.)
Lakloey Hill	1.120	1.4038	8.7014	3.1357	44.40	53.18 ± 1.60
Browns Hill	1.235	1.9960	9.0870	2.9698	13.12	50.40 ± 1.51
Millers Bluff	1.685	1.3065	13.854	3.2781	26.77	55.56 ± 1.67
Fourth of July Hill	1.840	1.5862	14.156	3.0964	22.69	52.52 ± 1.52[a]

[a]Unpublished data from D.L. Turner, Geophysical Institute, Geochronology Laboratory, University of Alaska Fairbanks.
[b]Minimum age.
Constants used: $\lambda_\varepsilon + \lambda_\varepsilon' = 0.581$ x 10E-10/yr, $\lambda_\beta = 4.962$ x 10E-10/yr, ^{40}K/K total = 1.167 x 10E-4 mol/mol.

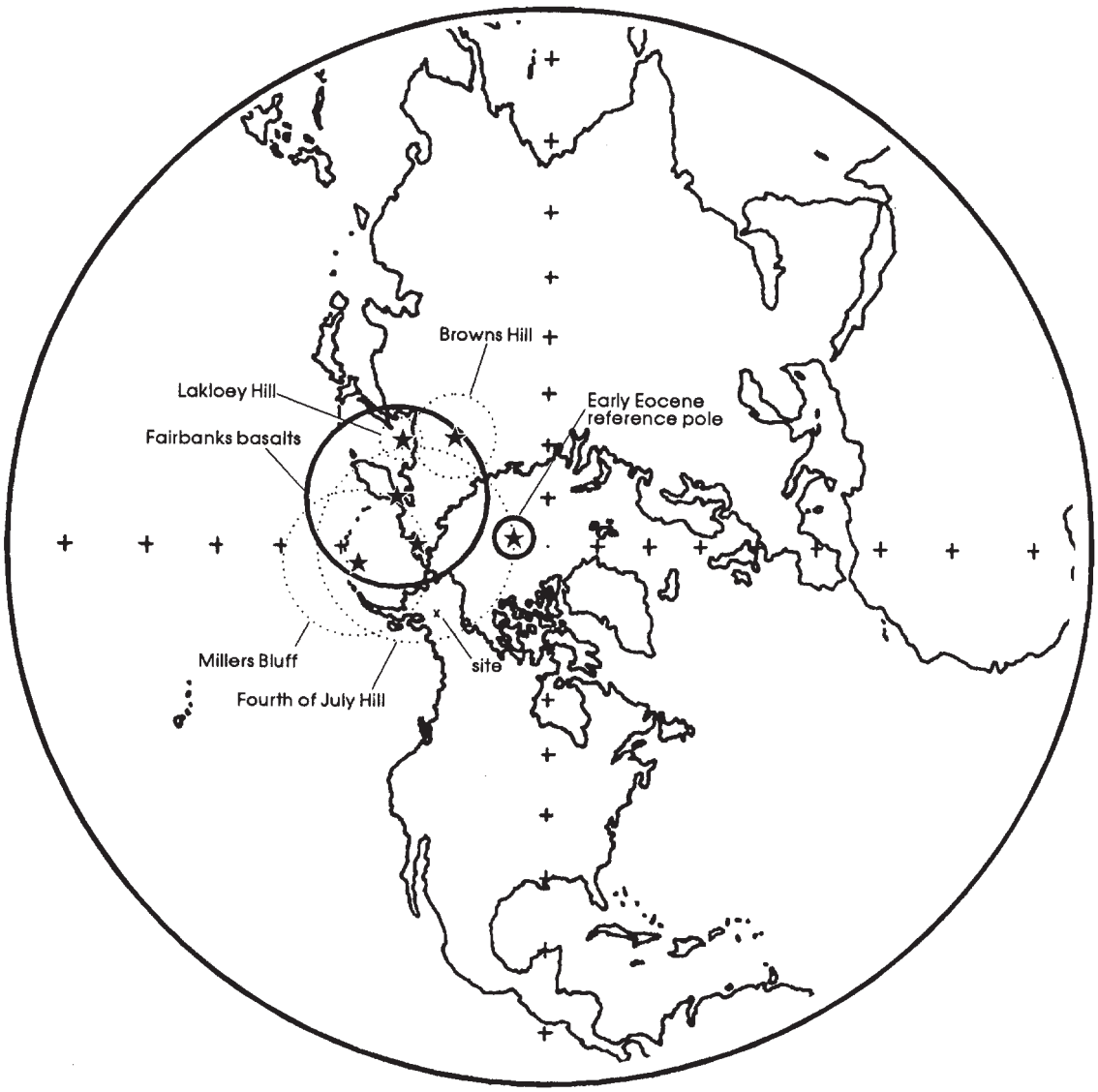

Figure 4. *Mean virtual geographic poles for each locality, and the mean of their means are shown together with the site locality and the reference pole for North America.*

71° ± 54° CCW (fig. 4). The reference pole used is located at lat 83° N., long 182° E., and is the mean pole for the time period 50-60 m.y. (Coe and others, 1985).

The rotation of the Fairbanks basalts implies that the northern section of the Yukon Tanana Upland has rotated in a similar fashion. Discussion of the Alaskan orocline, originally proposed by S.W. Carey (1958), commonly includes CCW motion of the western half of Alaska with respect to the east. The Fairbanks Basalts lie on or near the hinge area on these models where one would expect little or no rotational movement. Other models involve bending of the southern parts of Alaska, terranes south of the Denali Fault, as they are forced around the bend represented by the Tintina and Denali faults (Coe and others, 1988). The driving mechanism in is presumed to be the northward motion of the Pacific plates (Coe and others, 1988). In terms of neo-tectonics, Page and others (1991) hypothesized that observed patterns of active faults and seismicity define elongated crustal blocks within a broad dextral shear zone located between the Denali and Tintina fault systems. These active faults show evidence of left-lateral motion, which, it interpreted in terms of rotation, is clockwise movement. This rotation is opposite to that seen in the paleomagnetic data reported here, and also opposite to that reported for much of western Alaska (Coe and others, 1988). A possible explanation of this apparent contradiction in sense of rotation is that the seismicity is the result of short time scale stresses which result from the relative motion between the Denali and Tintina systems, whereas the paleomagnetic data record

the large scale motions of the terranes as they collided with ancestral Alaska.

CONCLUSION

Paleomagnetic measurements made on the basalts exposed in the Fairbanks area give an apparently reliable pole position for Early Eocene time. Although the outcrops are relatively restricted temporally, we consider that enough time is represented to average out the secular variations of the magnetic field. Thermal and alternating field demagnetization techniques remove a small component parallel to the present field, and leave a characteristic magnetization that has reversed polarity. Comparing this paleofield with a reference field for cratonic North America indicates a counter-clockwise rotation of about 70° ± 54°. This rotation is similar in both sense and magnitude to mid-Tertiary rotations seen in western Alaska (Coe and others, 1988). The Fairbanks basalts lie more or less on the hinge line for most oroclinal bending models. These new paleomagnetic data are more consistent with models involving either rotations of large individual blocks, or regional large scale rotations than with small scale neotectonic rotational models.

ACKNOWLEDGMENTS

We would like to acknowledge Jean-Paul Hulot and Valerie Huber for helping with the field and laboratory observations and Mark Robinson for his assistance with the figures. We thank Don Turner for providing the radiometric ages, and Paul Layer and Tom Smith for their thoughtful reviews of the manuscript. The work was partially supported by State of Alaska funds administered through the Geophysical Institute and by National Science Foundation grant EAR 886-18845.

REFERENCES

Blum, J. D., 1983, Peteroloy, geochemistry and isotope geochronology of the Gilmore Dome and Pedro Dome plutons, Fairbanks mining district, Alaska: Alaska Division of Geological and Geophysical Surveys, Report of Investigations 83-2, 59 p.

Carey, S.W., 1958, A tectonic approach to continental drift, *in* Symposium on Continental Drift: ed. S.W. Carey, Uiversity of Tasmania, Hobart.

Coe, R.S., Globerman, B.R., Plumley, P.W., Thrupp, G.A., 1985, Paleomagnetic results from Alaska and their tectonic implications, *in* Tectonostratigraphic Terranes of the Circum-Pacific Region: ed. D. Howell, Earth Science Series 1, Circum-Pacific Council for Energy and Mineral Resources, Houston, Texas, p. 85-108.

Coe, R.S., Globerman, B.R., Thrupp, G.A., 1988, Rotation of central and southern Alaska in the early Tertiary: Oroclinal bending or megakinking? *in* Paleomagnetic Rotations and Continental Deformation: C. Kissel, C. Laj, eds., NATO-ASI series, Kluwer Academic Publishers, v. 254, p. 327-342.

Collinson, D.W., Creer, K.M., Runcorn, S.K., 1967, Methods in palaeomagnetism: Elsevier Publishing Co., Amsterdam, p. 609.

Fisher, R.A., 1953, Dispersion on a sphere: Proceedings of the Royal Society of London, Series A., Vol. 217, p. 295-305.

Foster, J.H., 1966, A paleomagnetic spinner magnetometer using a fluxgate gradiometer: Earth and Planetary Science Letters, v. 1, p. 463-466.

Furst, G. A., 1968, Geology and petrology of the Fairbanks basalts, Fairbanks, Alaska: Master's thesis: University of Alaska Fairbanks, 53 p.

Jones, D.L., Silberling, N.J., Coney, P.J., Plafker, G., 1987, Lithotectonic terrane map of Alaska, U.S. Geological Survey Map MF-1874-A, scale 1:2,500,000.

Monger, J.W.H., Berg, H.C., 1987, Lithotectonic map of western Canada and southeastern Alaska, U.S. Geological Survey Map MF-1874-B, 1:2,500,000.

Page, R.A., Biswas, N.N., Lahr, J.C., Pulpan, Hans, 1991, Seismicity of continental Alaska, *in* Neotectonics of North America: D.B. Slemmons, E.R. Engdahl, M.D. Zoback, D.D. Blackwell, eds., Geological Society of America, Decade Map, v. 1, p. 47-68.

Queen, R. A., 1989, Gravity and magnetic survey in the Badger Road area, Fairbanks, Alaska: Master's thesis, University of Alaska Fairbanks, 138 p.

Robinson, M.S., Smith, T.E., and Metz, P.A., 1990, Bedrock geology of the Fairbanks mining district: Alaska Division of Geological & Geophysical Surveys, Professional Report 106, scale 1:250,000.

Weber, F.R., 1989., Geology between Fairbanks and the Yukon River, east-central Alaska, in Alaska Geological and Geophysical Transect, Field Trip Guidebook T104:R.A.M. Schmidt, W.J. Nokelberg, R.A. Page, eds. p. 84-95.

THE HAYES GLACIER FAULT, SOUTHERN ALASKA RANGE: EVIDENCE FOR POST-PALEOCENE MOVEMENT

by

Diana N. Solie[1] and Paul W. Layer[2]

INTRODUCTION

Geologic mapping and $^{40}Ar/^{39}Ar$ dating of igneous rocks in the Hayes Glacier region establish the existence of a previously unrecognized fault, herein referred to as the Hayes Glacier fault (HGF). The HGF lies in the northwest part of the Tyonek Quadrangle along a lineament defined by Hayes Glacier and Hayes River. The fault may be an extension of the Mulchatna Fault (Beikman, 1980), which lies about 175 km to the southwest (fig. 1).

Porcupine Butte andesite (PBA) is an erosional remnant of a porphyritic andesite volcanic neck with columnar jointing which crops out on the north side of the HGF (fig. 2). A medium- to coarse-grained phaneritic pluton with an area of about 20 km^2 lies about 5 km south of the fault. We refer informally to this as the Bear Cub pluton (BCP). Though the two igneous bodies are now at different erosional levels, $^{40}Ar/^{39}Ar$ dating indicates that the PBA and BCP have overlapping crystallization ages of about 61 Ma. The purpose of this paper is to document one line of evidence for the HGF based on the juxtaposition of these two igneous bodies and to suggest some regional implications.

PREVIOUS WORK AND GEOLOGIC SETTING

Prior to 1:40,000 scale mapping by DGGS in 1990 (Solie and others, 1991), published maps of the area were of a reconnaissance nature at 1:250,000 scale or smaller. The andesite of Porcupine Butte (fig. 2) had been mapped as undifferentiated metasedimentary rocks (Barnes, 1966; Magoon and others, 1976; Manning and Hinderman, 1982); igneous rocks south of HGF had been shown as undifferentiated intrusives and assigned ages of Jurassic and Cretaceous (Barnes, 1966), Cretaceous and Tertiary (Manning and Hinderman, 1982) and Tertiary (Magoon and others, 1976).

The bedrock geology of the area consists predominantly of dark gray to black Jurassic to Cretaceous sedimentary rocks, generally considered to be turbidites of the Kahiltna terrane (Jones and others, 1987). The sedimentary rocks are intruded by Tertiary diorite to granite, and are overlain by intermediate to felsic volcanic rocks of probable Tertiary age (Solie and others, 1991). Basalt flows and/or sills associated with the Jurassic-Cretaceous sedimentary rocks have a complex thermal history and are probably older than the nearby intrusive rocks (Layer and Solie, 1991). The stratigraphy of the sedimentary section is complicated by complex folding and faulting. Fossils have not been found in the map area. A sequence of conglomerate, sandstone and shale north of the HGF lies in ambiguous relationship with the finer-grained siltstone and sandstone of the rest of the mapped area (fig. 2) (Solie and others, 1991).

PETROLOGY AND CHEMISTRY

PBA is a roughly circular, steep-walled and flat-topped body rising about 1,400 ft (427 m) above the surrounding lowland, to an elevation of over 2,000 ft (610 m). Black siltstone is intruded by the volcanic neck and is exposed low on the cliffs of Porcupine Butte. Prominent columnar joints are visible on exposed sides of the neck. The andesite contains phenocrysts of plagioclase, clinopyroxene, orthopyroxene, opaque oxide, and minor local quartz in a dark gray, very fine-grained to aphanitic groundmass. It appears to be homogeneous across the exposure. Based on major oxide analysis (table 1), it is a calc-alkaline andesite by the classification scheme of Irvine and Baragar (1971): it is a high-K tholeiitic orogenic andesite according to the classification of Gill (1981).

BCP crops out at elevations up to 3,790 ft (1,146 m), topographically higher than PBA. The plutonic complex includes diorite, quartz diorite, monzodiorite, quartz monzodiorite, and quartz monzonite, using the classification scheme of Streckeisen (1976). Modal analyses of four representative samples are shown in table 2, based on point counts of 500 points per thin section. The rocks are generally coarse- to medium-grained and range from seriate to slightly porphyritic (fig. 3). They contain plagioclase, orthopyroxene, clinopyroxene, biotite, and opaque oxides, with interstitial quartz and alkali feldspar. Locally, hornblende replaces biotite. Apatite is a ubiquitous accessory mineral; zircon is rare. Alteration minerals include amphibole, sericite, iron oxides, and carbonate. Analytical results from BCP are

[1] Alaska Division of Geological & Geophysical Surveys, 794 University Avenue, Suite 200, Fairbanks, Alaska 99709-3645.

[2] Geophysical Institute, University of Alaska, Fairbanks, Alaska 99775.

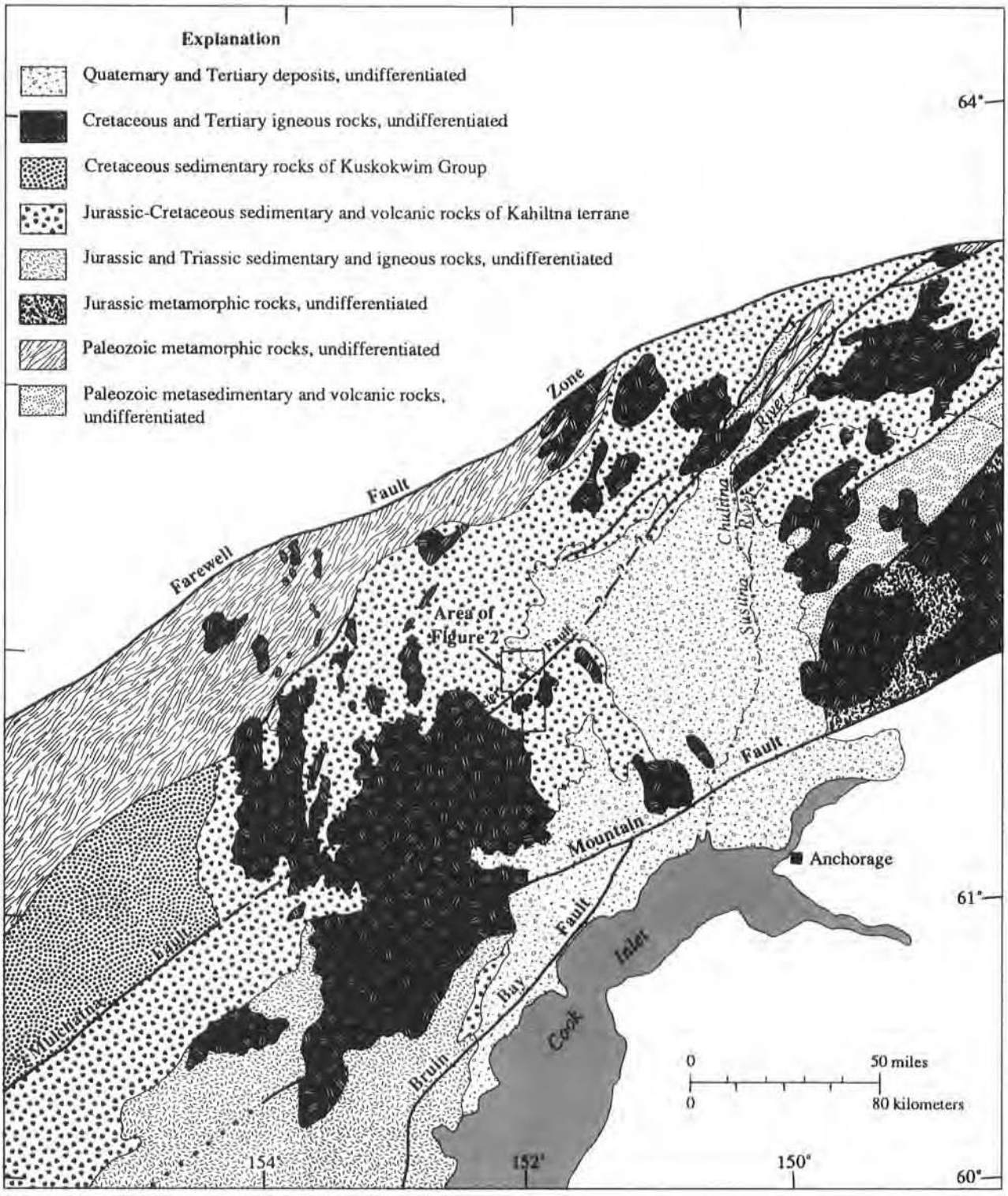

Figure 1. *Simplified geologic map of southcentral Alaska (modified from Beikman, 1980).*

shown on table 1. They cover a range of metaluminous compositions which groups closely with the composition of PBA (figs. 4 and 5).

Average electron microprobe analyses of representative clino-pyroxenes and orthopyroxenes from the PBA and BCP are shown in table 3. The data from PBA are from several phenocrysts in sample 90DNS31; the data from BCP are from one pair of adjacent pyroxenes in each of two samples. The clinopyroxene composi-tions of PBA plot in the field that does not distinguish tectonic settings on the discriminant diagrams of Nisbet and Pearce (1977).

AGE CONTROL

$^{40}Ar/^{39}Ar$ step-heating of a whole rock sample from PBA and of a biotite separate from BCP were carried out to determine precisely the ages of these two units. Analyses were performed at the University of Alaska Fairbanks (UAF) Geochronology Laboratory.

Analytical Procedures

The $^{40}Ar/^{39}Ar$ capability at UAF is relatively recent and the general operating procedures for the laboratory have not been discussed elsewhere. The following is a summary of the procedures employed at UAF.

Samples for dating are weighed and packaged in aluminum foil tubes approximately 4 mm in diameter and 20 mm long. Six packages of standard mineral mmhb-1 with an age of 513.9 Ma (Samson and Alexander, 1987; Lanphere and others, 1990) are similarly packaged. These packages are then placed in an aluminum can which is 18 mm in diameter and 40 mm long. Generally, two levels of packages can be placed in a single can. A level will consist of three standard tubes and seven or eight sample tubes. The can is irradiated at McMaster Nuclear Reactor in Hamilton, Ontario, in position 5C in the core of the reactor. This position is near the center of the core

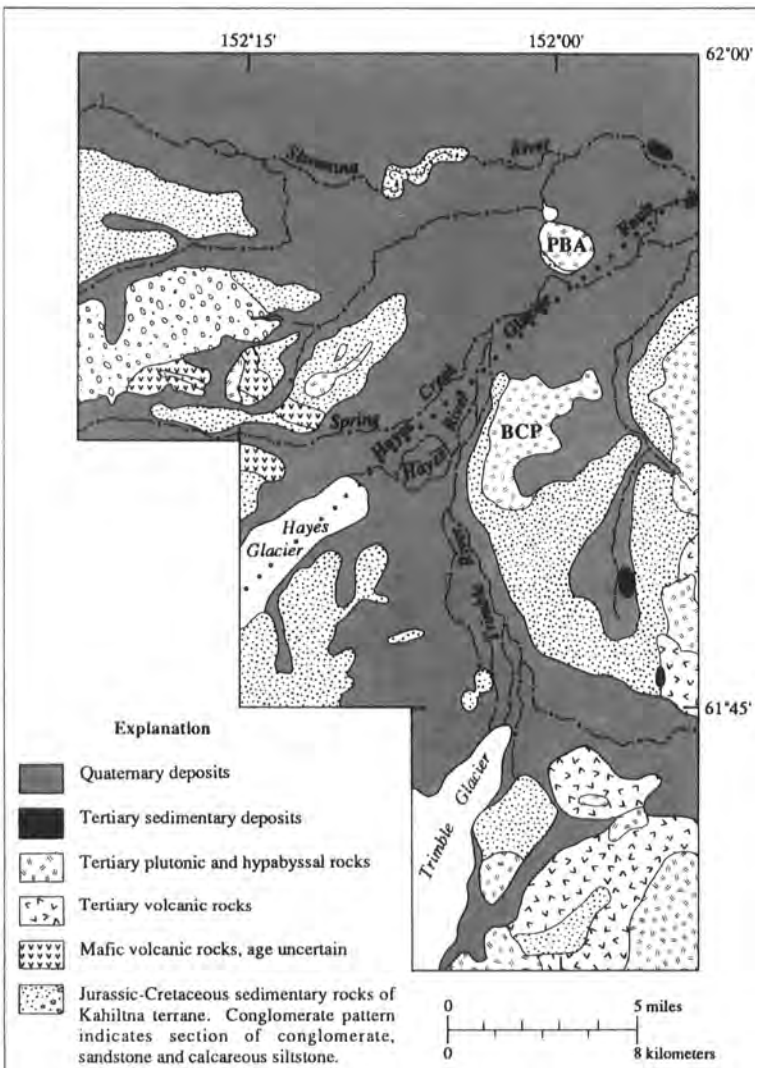

Figure 2. *Generalized geologic map of Hayes Glacier fault area (modified from Solie and others, 1991). PBA = Porcupine Butte andesite, BCP = Bear Cub pluton.*

where flux gradients are minimal. The sample can is held at the reactor for approximately two weeks to allow for decay of short-lived radionuclides.

Upon return from the reactor, the foil packages containing the irradiated samples are removed from the can and loaded directly into a multiple-sample holder where individual packages can be dropped into the furnace. In general, samples are run between 45 and 90 days after irradiation. Running samples this close to the irradiation day allows precise measurement of the ^{37}Ar signal (half-life of ^{37}Ar is 35.1 days).

The samples are step-heated in a Modifications Ltd. low-blank furnace connected on-line to the mass spectrometer. Temperature control is accurate to ±1°C, and a maximum temperature in excess of 1,600°C is achievable. The extracted argon is purified in a two-stage process. The first stage exposes the sample to a liquid nitrogen cold finger and a Ti furnace at 700°C for 20 minutes. The argon is then drawn onto activated

Table 1. *Major-oxide geochemical analyses and CIPW norms of Bear Cub pluton (BCP) and Porcupine Butte andesite (PBA) samples*[a]

Major-oxide and trace element analyses (weight percent)

Sample	90Ha112	90DNS07	90DNS08	90MR114C	90DNS31
Unit	BCP	BCP	BCP	BCP	PBA
SiO_2	62.04	56.76	56.27	59.09	60.78
Al_2O_3	16.45	17.91	17.52	17.83	17.79
CaO	4.53	6.65	6.85	5.19	5.08
MgO	2.64	3.04	4.04	2.26	1.88
Na_2O	3.61	3.87	3.61	3.92	4.15
K_2O	4.24	2.65	2.74	4.03	3.50
Fe_2O_3	2.09	na	na	na	na
FeO	3.25	na	na	na	na
FeO*	na	7.35	7.36	6.23	5.46
MnO	0.09	0.12	0.13	0.11	0.11
TiO_2	0.84	1.27	1.14	1.04	0.96
P_2O_5	0.21	0.39	0.34	0.29	0.29
Total	100.00	100.00	100.00	100.00	100.00
Cr	68	32	64	21	13
Rb	157	86	92	119	98
Sr	491	572	566	478	508
Y	<10	26	24	28	27
Zr	294	171	210	321	227
Nb	17	16.8	12.6	16.3	17.2
Ba	1,160	1,003	992	1,446	1,181
Ga	na	21	20	19	20
Cu	na	21	27	13	11
Zn	na	93	92	77	79
V	na	144	168	114	77
Sc	na	23	23	17	17
Ni	na	10	15	10	9

CIPW norms (weight percent)

quartz	11.43	5.71	4.39	6.42	9.63
corundum	0.00	0.00	0.00	0.00	0.00
orthoclase	25.08	15.62	16.15	23.76	20.64
albite	30.58	32.65	30.46	33.09	35.04
anorthite	16.12	23.60	23.45	19.11	19.53
diopside	4.00	5.53	6.68	3.84	3.05
hypersthene	7.66	9.58	12.11	7.65	6.54
magnetite	3.03	4.01	3.82	3.51	3.08
ilmenite	1.60	2.41	2.16	1.97	1.83
apatite	0.49	0.89	0.79	0.67	0.67
Total	100.00	100.00	100.00	100.00	100.00
D.I.	67.09	53.98	51.00	63.26	65.30

[a]Sample 90Ha112 analyzed by X-ray Assay Laboratories, Ontario, Canada. All others analyzed by D. Johnson, Washington State University, Pullman, Washington.
FeO* = total iron as FeO.
na = not analyzed.
D.I. = Differentiation Index (normative quartz + orthoclase + albite).

Table 2. *Modal analyses of Bear Cub pluton and Porcupine Butte andesite samples*

Sample	90Ha112	90DNS07	90DNS08	90MR114C	90DNS31
	BCP	BCP	BCP	BCP	PBA
Rock type	Quartz monzonite	Monzo-diorite	Quartz diorite	Quartz monzodiorite	Porphyritic andesite
Quartz	11	3	6	6	-
Plagioclase	36	65	61	46	28
Alkali feldspar	33	15	7	21	-
Clinopyroxene	5	7	12	4	8
Orthopyroxene	4	3	4	1	3
Biotite	6	2	5	6	<1
Opaque oxides	1	1	2	2	2
Apatite	<1	<1	<1	1	-
Zircon	-	-	-	<1	-
Secondary minerals	4	4	3	13	<1
Matrix	-	-	-	-	59
Total	100	100	100	100	100

- = not observed.

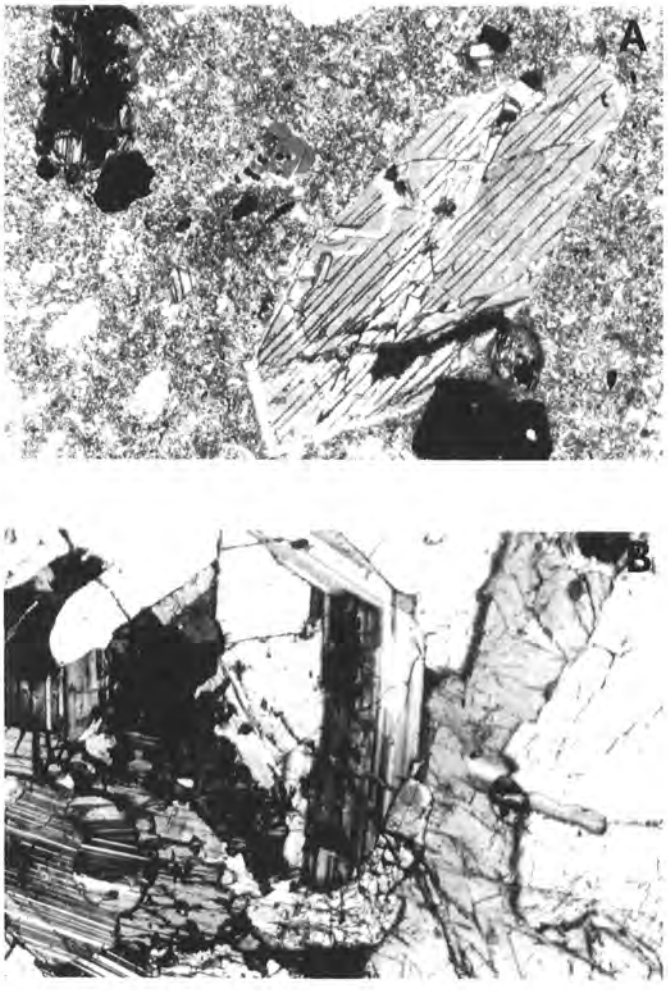

charcoal for 20 minutes. The argon is then released from the charcoal and further purified using a SAES ST101 getter for 10 minutes. The purified argon isotopes are then measured using a Nuclide 6-60-SGA 15 cm mass spectrometer. Sensitivity of the instrument is 6.5 x 10^{-15} mol/mV and system noise is generally around 0.02 mV.

System blanks are generally better than 1 x 10^{-14} mol for ^{40}Ar. Data for the samples and standards are corrected for the system blank. Estimating the system blank has traditionally been a problem. Our procedure is to measure the blank at the lowest-fraction temperature step (500-600°C) before introduction of the sample. This blank is then subtracted from all fractions in the sample. Blank step-heating experiments have shown that the system blank does not vary significantly with temperature up to about 1,600°C.

The irradiation parameter, J, for a particular level in a sample can is determined by taking the weighted average of the three standards for

Figure 3. *Photomicrographs of thin sections showing textural differences between (A) andesite (90DNS31) from Porcupine Butte and (B) biotite monzodiorite (90DNS7) from Bear Cub pluton. Field of view for each is 2 mm across length of photo.*

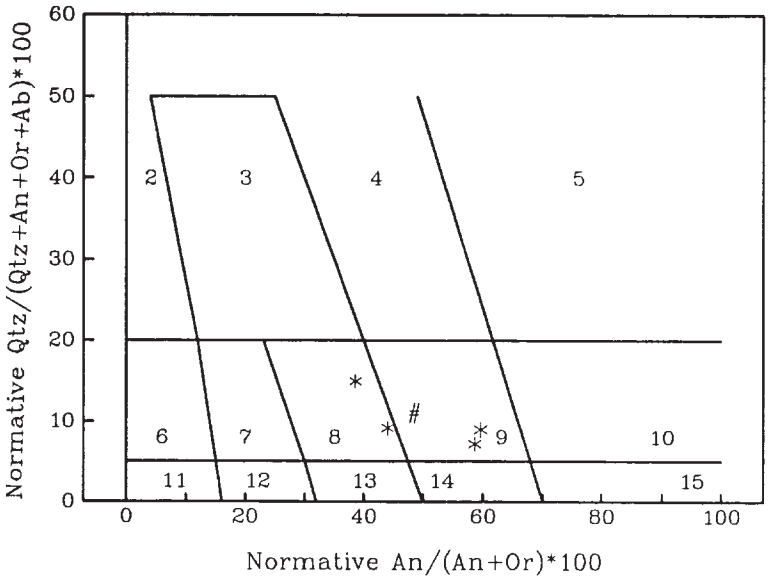

Figure 4. *Streckeisen-LeMaitre (1979) compositional diagram showing normative mineral compositions of samples from Bear Cub pluton (*) and Porcupine Butte andesite (#). Rock names are 2 - alkali-feldspar granite; 3 - granite;4 - granodiorite; 5 - tonalite; 6 - alkali-feldspar quartz syenite; 7 - quartz syenite; 8 - quartz monzonite; 9 - quartz monzodiorite; 10 - quarz diorite; 11 - alkali-feldspar syenite; 12 - syenite; 13 - monzonite; 14 - monzodiorite; 15 - diorite and gabbro. Qtz = quartz, An = anorthite, Or = orthoclase, Ab = albite.*

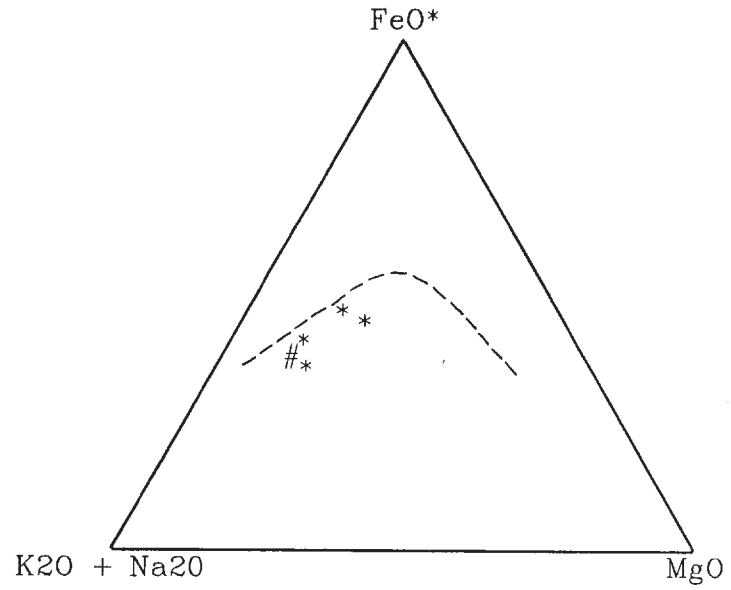

Figure 5. *Alkali-iron-magnesium (AFM) diagram showing compositions of samples from Bear Cub pluton (*) and Porcupine Butte andesite (#). Line distinguishing tholeiitic from calc-alkaline trends is from Irvine and Baragar (1971).*

that level. Ages are calculated using the 1977 decay constants (Steiger and Jäger, 1977) and are reported at the 1 sigma level.

RESULTS

Twelve temperature fractions were extracted from the biotite sample (90DNS7) from BCP and ten from the whole rock sample (90DNS31) of PBA (table 4). Age spectra from both samples show a slight amount of excess argon, seen in the stairstep down nature of the age spectra (fig. 6). Isotopic correlation diagrams define isochrons for both samples with ages of 60.78 ± 0.42 Ma (initial $^{40}Ar/^{36}Ar$ = 297.1 ± 2.2) for PBA and 60.82 ± 0.43 Ma (initial $^{40}Ar/^{36}Ar$ = 299.9 ± 3.0) for BCP. The ages of the two samples are identical within experimental error, indicating that the whole rock sample of PBA and the biotite sample of BCP closed to the diffusion of argon at 60.8 Ma. The slight amount of excess argon (initial $^{40}Ar/^{36}Ar$ greater than 295.5) most probably was incorporated in the samples during the time when the minerals closed.

DISCUSSION AND CONCLUSION

The most striking difference between PBA and BCP is textural (figs. 3a and 3b) rather than compositional (figs. 4 and 5) and suggests a difference in the depth of emplacement. The volcanic texture, cylindrical form, and columnar jointing of PBA indicate that its emplacement depth was within 1 km of the surface, just below a volcanic edifice. BCP, on the other hand, is phaneritic and coarser-grained. According to the emplacement classifica-tion of Buddington (1959), BCP is epizonal (depth of up to about 6 km), based on the low metamorphic grade of host rock, the lack of extensive contact metamorphism, discordant contact with host rock, and lack of planar foliation in the plutonic rock. Although the depth of crystallization of BCP cannot be precisely determined, it certainly was emplaced no

Table 3. *Average pyroxene compositions from Porcupine Butte andesite and Bear Cub pluton*

Sample	90DNS31	90DNS31	90DNS7	90DNS7	90DNS8	90DNS8
Mineral	CPX	OPX	CPX	OPX	CPX	OPX
Unit	PBA	PBA	BCP	BCP	BCP	BCP
Number of analyses	14	14	5	6	5	3
Weight % oxides:						
SiO_2	51.607	52.197	51.598	50.752	51.826	51.758
TiO_2	0.528	0.261	0.061	0.100	0.130	0.180
AL_2O_3	1.675	0.764	0.297	0.231	0.476	0.256
FeO*	11.318	23.559	14.127	31.790	12.078	28.502
MnO	0.362	0.704	0.223	0.695	0.292	0.652
MgO	14.251	20.959	11.018	15.589	12.929	17.878
CaO	19.961	1.613	21.823	1.007	21.721	1.055
Na_2O	0.304	0.032	0.109	0.016	0.200	0.024
Total	100.215	100.196	99.333	100.231	99.886	100.360
Atoms per 6 oxygens: (calculated following Lindsley and Anderson, 1983)						
Si	1.930	1.958	1.984	1.978	1.960	1.983
Ti	0.015	0.007	0.002	0.003	0.004	0.005
Al	0.074	0.034	0.013	0.011	0.021	0.012
Fe_3+	0.059	0.037	0.023	0.028	0.066	0.014
Fe_2+	0.295	0.702	0.432	1.008	0.316	0.899
Mn	0.011	0.022	0.007	0.023	0.009	0.021
Mg	0.794	1.172	0.632	0.906	0.729	1.021
Ca	0.800	0.065	0.899	0.042	0.880	0.043
Na	0.022	0.002	0.008	0.001	0.015	0.002
Total	4.000	3.999	4.000	4.000	4.000	4.000
Wo	0.391	0.034	0.446	0.022	0.422	0.022
En	0.444	0.604	0.329	0.463	0.403	0.520
Fs	0.165	0.362	0.225	0.515	0.175	0.458

FeO* = Total iron as FeO.
Analyses performed at University of Alaska Fairbanks using Cameca SX-50 electron microprobe.

shallower than PBA, and most significantly, is now at a higher elevation. The geochronologic study of these two units indicates that BCP was cooling through the closure temperature of biotite (~250°C) at 60.8 Ma at the same time that PBA was emplaced. The two units were probably at different depths at this one instant of geologic time. The fact that BCP and PBA are both now at the surface, with BCP topographically higher, is evidence for post-Paleocene differential uplift (down on the north) of as much as 5 km along the Hayes River valley. The most likely explanation is dip-slip movement along the distinct topographic linear formed by the Hayes Glacier and the Hayes River. We call this fault the Hayes Glacier fault (HGF).

Another result of this study is the recognition that despite their similar compositions, current proximity, and similar dates, PBA and BCP are not necessarily comagmatic. Given its small size, proximity to the surface, and very fine-grained groundmass, PBA must have experienced a high degree of undercooling and crystallized rapidly. The $^{40}Ar/^{39}Ar$ whole rock age records the age of emplacement of this unit. However, because BCP is larger and was emplaced deeper, it must have cooled more slowly. The BCP biotite age reflects the time of this slower cooling, so that the actual time of emplacement of the BCP magma must have been earlier, although we cannot constrain the cooling rate or emplacement time of BCP. Thus, the data indicate that, despite similar dates, the units were not emplaced at exactly the same time and, therefore, did not necessarily tap the same magma source. Dating of BCP using other isotopic systems or apatite fission-track analysis may provide insight on the

Table 4. *$^{40}Ar/^{39}Ar$ analyses of biotite from Bear Cub pluton (BCP) sample 90DNS7 and whole rock sample 90DNS31 from the Porcupine Butte andesite (PBA)*

Bear Cub pluton biotite (Mass = 0.0739 g)

Temperature (°C)	Cumulative ^{39}Ar	$^{40}Ar/^{39}Ar$ measured	$^{37}Ar/^{39}Ar$ measured	$^{36}Ar/^{39}Ar$ measured	Volume ^{39}Ar x 10^{-12} mol/g	% Atmospheric ^{40}Ar	$^{37}ArCa/^{39}Ar_K$	$^{40}Ar^*/^{39}Ar_K$	Age (Ma)	+/-
300	0.0005	104.052	0.226	0.359	0.092	102.021	0.226	-2.102	-32.7	105.6
400	0.0010	77.406	0.271	0.275	0.095	104.901	0.271	-3.793	-59.4	104.0
475	0.0023	41.633	0.533	0.129	0.270	91.502	0.533	3.537	53.7	34.6
550	0.0060	20.371	0.798	0.059	0.710	84.859	0.798	3.082	46.9	13.2
625	0.0287	13.063	0.066	0.030	4.422	67.855	0.066	4.190	63.4	2.1
700	0.1077	6.785	0.021	0.009	15.360	39.614	0.021	4.080	61.8	0.6
775	0.1858	5.521	0.013	0.005	15.196	26.691	0.013	4.027	61.0	0.6
850	0.2966	4.779	0.012	0.002	21.554	15.219	0.012	4.027	61.0	0.4
925	0.4419	4.445	0.012	0.001	28.260	9.093	0.012	4.015	60.8	0.3
1000	0.5989	4.764	0.012	0.002	30.533	15.045	0.012	4.023	60.9	0.3
1200	0.9958	5.829	0.046	0.006	77.203	30.279	0.046	4.044	61.2	0.1
1600	1.0000	6.870	3.804	0.013	0.808	50.372	3.813	3.403	51.7	11.5
Integrated		5.749	0.047	0.006	194.503	29.623	0.047	4.026	61.0	0.4

Porcupine Butte andesite whole rock (Mass = 0.2549 g)

Temperature (°C)	Cumulative ^{39}Ar	$^{40}Ar/^{39}Ar$ measured	$^{37}Ar/^{39}Ar$ measured	$^{36}Ar/^{39}Ar$ measured	Volume ^{39}Ar x 10^{-12} mol/g	% Atmospheric ^{40}Ar	$^{37}ArCa/^{39}Ar_K$	$^{40}Ar^*/^{39}Ar_K$	Age (Ma)	+/-
450	0.0301	27.803	0.338	0.080	2.586	85.423	0.338	4.050	61.3	1.1
600	0.2566	5.956	0.259	0.006	19.479	31.329	0.259	4.071	61.6	0.2
700	0.4585	4.730	0.310	0.002	17.360	14.305	0.310	4.029	61.0	0.2
800	0.6932	4.485	0.329	0.002	20.180	10.346	0.329	3.996	60.5	0.1
900	0.7749	4.671	0.532	0.002	7.025	14.807	0.532	3.956	59.9	0.4
1000	0.8187	5.061	0.606	0.004	3.762	20.794	0.607	3.988	60.4	0.7
1200	0.8611	6.265	1.085	0.008	3.653	36.553	1.086	3.960	60.0	0.7
1400	0.9831	5.546	0.759	0.005	10.485	28.160	0.760	3.966	60.1	0.3
1600	0.9951	6.503	0.609	0.008	1.038	37.704	0.610	4.035	61.1	2.6
1709	1.0000	7.996	0.348	0.015	0.417	53.975	0.348	3.668	55.6	6.5
Integrated		5.856	0.426	0.006	85.985	31.177	0.427	4.011	60.8	0.4

Weighted average of J from standards = 0.008538 +/- 0.000050.

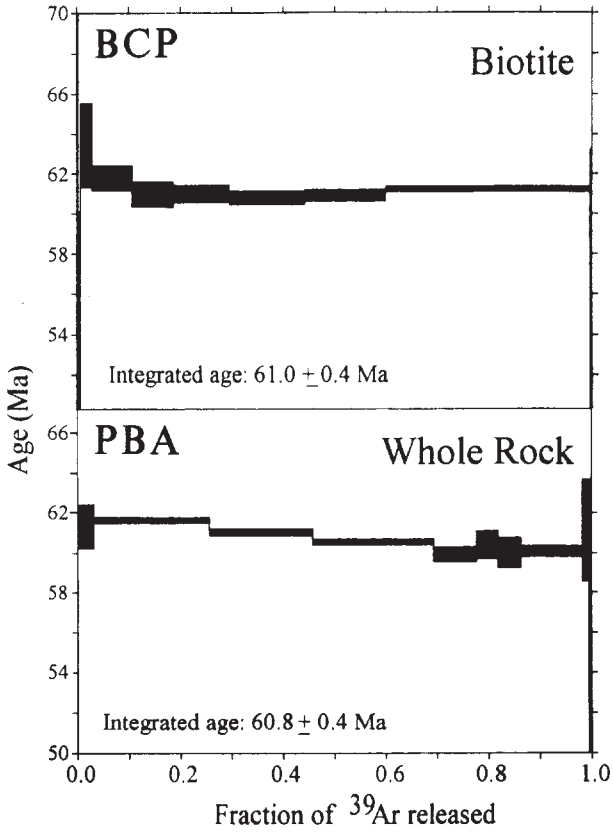

Figure 6. *$^{40}Ar/^{39}Ar$ age versus fraction of ^{39}Ar released for BCP (biotite from sample 90DNS07) and PBA (whole rock sample 90DNS31). Each box denotes apparent age of a single temperature step (see table 4). The height of each box is ±1 sigma error in age.*

cooling rate experienced by BCP and the actual time of emplacement of this unit.

Though the above evidence indicates post-Paleocene dip-slip movement on the HGF, the data do not offer constraints on the amount of strike-slip motion that may have occcurred after 61 Ma. In addition, there may have been substantial pre-Paleocene movement on the HGF, either dip-slip or strike-slip, which we have not documented. However, recognition of the existence of HGF is useful in (a) interpreting the complex Mesozoic stratigraphy of the area, and (b) possibly extending through the Alaska Range previously recognized faults on trend to the northeast and southwest.

Knowing that there has been down-on-the-north movement on the HGF, we can now interpret the enigmatic sequence of conglomerate, sandstone and shale (fig. 2) on the north side of the fault as a structurally higher and probably younger part of the Kahiltna terrane. Indeed, this interpretation invites the speculation that this section is not part of the Kahiltna terrane at all, but rather a previously undocumented group of younger rocks overlying the Kahiltna terrane.

Following a pronounced lineament to the southwest, the HGF is on trend with the Mulchatna fault (Beikman, 1980). Along much of its length, the Mulchatna fault juxtaposes Kuskokwim group and Kahiltna terrane rocks, and appears to be one of the right-lateral strike-slip faults common throughout southwestern Alaska (Wallace and others, 1989). On trend to the northeast are several northeast-southwest trending faults which could link with the HGF. On the most direct trend is the fault zone along the north side of the Chulitna River (Jones and others, 1980; Csejtey and others, 1986), which continues as a zone of discontinuous faults in the Talkeetna Quadrangle (Reed and Nelson, 1980). If the HGF links these faults, it is part of a major structural break in southern Alaska.

ACKNOWLEDGMENTS

We gratefully acknowledge the field mapping contributions of W.G. Gilbert, M.R. Robinson, E.E. Harris, J.T. Kline and S.A. Liss (all of DGGS). We thank Jeff Drake (UAF Geophysical Institute) for assistance with the $^{40}Ar/^{39}Ar$ analyses, and Ken Severin and Kerry Lear (UAF) for help with the microprobe analyses. We also thank W.G. Gilbert (DGGS) and B.L. Reed (U.S. Geological Survey) for their critical reviews of an earlier version of this paper.

REFERENCES CITED

Barnes, F.F., 1966, Geology and coal resources of the Beluga-Yentna region, Alaska: U.S. Geological Survey Bulletin 1202-C, p. C1-C54, 7 sheets.

Beikman, H.M., 1980, Geologic map of Alaska: U.S. Geological Survey Map, scale 1:2,500,000.

Buddington, A.F., 1959, Granite emplacement with special reference to North America: G.S.A. Bulletin, v. 70, p. 671-747.

Csejtey, Bela, Jr., Mullen, M.W., Cox, D.P., Gilbert, W.G., Yeend, W.E., Smith, T.E., Wahrhaftig, Clyde, Craddock, Campbell, Brewer, W.M., Sherwood, K.W., Hickman, R.G., Stricker, G.D., St. Aubin, D.R., and Goerz, D.J.III, 1986, Geology and geochronology of the Healy Quadrangle, Alaska: U.S. Geological Survey Open-File Report 86-396, 92 p., 4 sheets, 1:250,000 scale.

Gill, James, 1981, Orogenic andesites and plate tectonics: Springer-Verlag, Berlin, 390 p.

Irvine, T.N., and Baragar, R.A., 1971, A guide to the chemical classification of the common volcanic rocks: Canadian Journal of Earth Sciences, v. 8, p. 523-548.

Jones, D.L., Silberling, N.J., Coney, P.J., and Plafker, George, 1987, Lithotectonic terrane map of Alaska (west of the 141st meridian): U.S. Geological Survey Miscellaneous Field Studies Map MF-1874-A, 1 sheet, 1:2,500,000 scale.

Jones, D.L., Silberling, N.J., Csejtey, Bela, Jr., Nelson, W.H., and Blome, C.D., 1980, Age and structural significance of ophiolite and adjoining rocks in the upper Chulitna district, south-central Alaska: U.S. Geological Survey Professional Paper 1121-A, 24 p., 1 sheet, 1:63,360 scale.

Lanphere, M.A., Dalrymple, G.B., Fleck, R.J. and Pringle, M.S., 1990, Intercalibration of mineral standards for K-Ar and $^{40}Ar/^{39}Ar$ age measurements (abstract): EOS, Transactions of the American Geophysical Union, v. 71, p. 1658.

Layer, P.W., and Solie, D.N., 1991, Timing of igneous activity and basin formation, southern Alaska Range, as constrained by $^{40}Ar/^{39}Ar$ dating (abstract): EOS, Transactions, American Geophysical Union, v. 72, no. 44, p. 503.

Lindsley, D.H., and Anderson, D.J., 1983, A two-pyroxene thermometer, *in* Proceedings of the Thirteenth Lunar and Planetary Science Conference, Part 2, Journal of Geophysical Research, v. 88, Supplement, p. A887-A906.

Magoon, L.B., Adkinson, W.L., and Egbert, R.M., 1976, Map showing geology, wildcat wells, Tertiary plant fossil localities, K-Ar age dates, and petroleum operations, Cook Inlet area, Alaska: U.S. Geological Survey Miscellaneous Investigations Map I-1019, 3 sheets, scale 1:250,000.

Manning, K.H., and Hinderman, T.K., 1982, National uranium resource evaluation, Tyonek Quadrangle, Alaska: C.C. Hawley and Associates, Inc., prepared for U.S. Department of Energy, Report PGJ/F-059(82), 17 p., 14 sheets.

Nisbet, E.G., and Pearce, J.A., 1977, Clinopyroxene composition in mafic lavas from different tectonic settings: Contributions in Mineralogy and Petrology, v. 63, no. 2, p.149-160.

Reed, B.L, and Nelson, S.W., 1980, Geologic map of the Talkeetna Quadrangle, Alaska: U.S. Geological Survey Miscellaneous Investigations Map I-1174, 15 p., 1 sheet, scale 1:250,000.

Samson, S.D., and Alexander, E.C., 1987, Calibration of the interlaboratory 40Ar-39Ar dating standard, MMhb-1: Chemical Geology, v. 66, p. 27-34.

Solie, D.N., Gilbert, W.G., Harris, E.E., Kline, J.T., Liss, S.A., and Robinson, M.S., 1991, Preliminary geologic map of Tyonek D-6 and eastern Tyonek D-7 Quadrangles, Alaska: Alaska Division of Geological and Geophysical Surveys Public-Data File 91-10, 16 p., 1sheet, scale 1:40,000.

Steiger, R.H., and Jäger, E., 1977, Subcommission on geochronology: convention on the use of decay constants in geo and cosmochronology; Earth and Planetary Science Letters, v. 36, p. 359-362.

Streckeisen, A.L., 1976, To each plutonic rock its proper name; Earth Science Review, v. 12, p. 1-33.

Streckeisen, A.L., and LeMaitre, R.W., 1979, A chemical approximation to the modal QAFP classification of the igneous rocks: Neuef Jahbach Fur Mineralogie Abhandlungen, v. 136, p. 169-206.

Wallace, W.K., Hanks, C.L., and Rogers, J.F., 1989, The southern Kahiltna terrane: implications for the tectonic evolution of southwestern Alaska: G.S.A. Bulletin, v. 101, p. 1389-1407.

DETACHMENT FOLDS AND A PASSIVE-ROOF DUPLEX: EXAMPLES FROM THE NORTHEASTERN BROOKS RANGE, ALASKA

by
Wesley K. Wallace[1]

INTRODUCTION

The objective of this paper is to present observations, interpretations, and speculations about structures along the "Canning River transect," a transect across the northeastern Brooks Range of Alaska. Two structural features of this transect are of particular interest: a "passive-roof duplex" and detachment folds that change in character along the transect. These structures are illustrated using a balanced cross section first presented by J.S. Namson and myself (Namson and Wallace, 1986). The initial transect study was part of a joint project by ARCO Alaska and ARCO Research and Technical Services to characterize the regional structure of the northeastern Brooks Range. The cross section was based on a geologic map I compiled from published maps of the region (Reiser and others, 1971; Brosgé and Reiser, 1965) and mapping at a scale of 1:63,360 by myself, Namson, and others at ARCO. An initial cross section prepared by Namson and myself was balanced by Namson. Since then, studies have been conducted along the transect and in other areas with analogous characteristics by myself and my graduate students at the University of Alaska as part of a systematic study of the structural geology of the northeastern Brooks Range. This paper summarizes some of the more significant observations and interpretations about the structures of the transect, as well as suggesting aspects of the geology that may have influenced the formation of those structures. A future paper will describe the structural geology of the transect in more detail, discuss alternative structural models, and outline the methods, constraints, and assumptions used in constructing the cross section.

The Brooks Range is a northern extension of the fold-and-thrust belt that forms the eastern margin of the North American Cordilleran orogen. The northeastern Brooks Range is a topographic and structural salient of the Brooks Range (fig. 1) that formed during Cenozoic time by structural displacement in a generally northward direction. The aspects of the geology of the northeastern Brooks Range that are most relevant to this paper are summarized below. Wallace and Hanks (1990) provide a more complete overview of the structural geology of the northeastern Brooks Range.

STRUCTURAL STRATIGRAPHY

The stratigraphy of the northeastern Brooks Range is equivalent to that found in the subsurface of the Alaskan North Slope (fig. 1), and has had a major influence on the structural geometry of the region. The stratigraphic section consists of several competent structural units that are separated by incompetent units that have acted as detachment horizons (fig. 2). The lowest structural-stratigraphic unit consists dominantly of a heterogeneous assemblage of stratified sedimentary and volcanic rocks that were deformed and weakly metamorphosed in pre-Mississippian time. The sub-Mississippian rocks are inferred to have been shortened above a detachment at depth. In the north, the Mississippian Kekiktuk Conglomerate unconformably overlies the sub-Mississippian rocks and has deformed with them as part of a single structural-stratigraphic unit. At the south end of the transect, the Kekiktuk Conglomer-

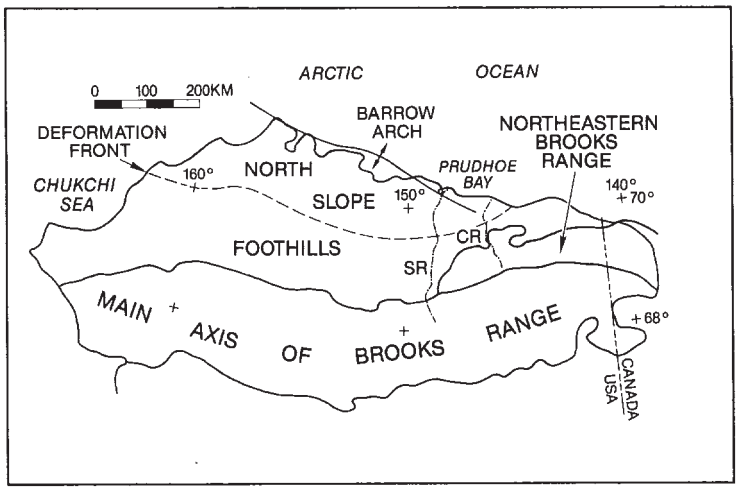

Figure 1. *Map of northern Alaska, including the northeastern Brooks Range, showing major physiographic and tectonic provinces. SR = Sagavanirktok River, CR = Canning River.*

[1]Tectonics and Sedimentation Research Group, Department of Geology and Geophysics and Geophysical Institute, University of Alaska, Fairbanks, Alaska 99775-0760.

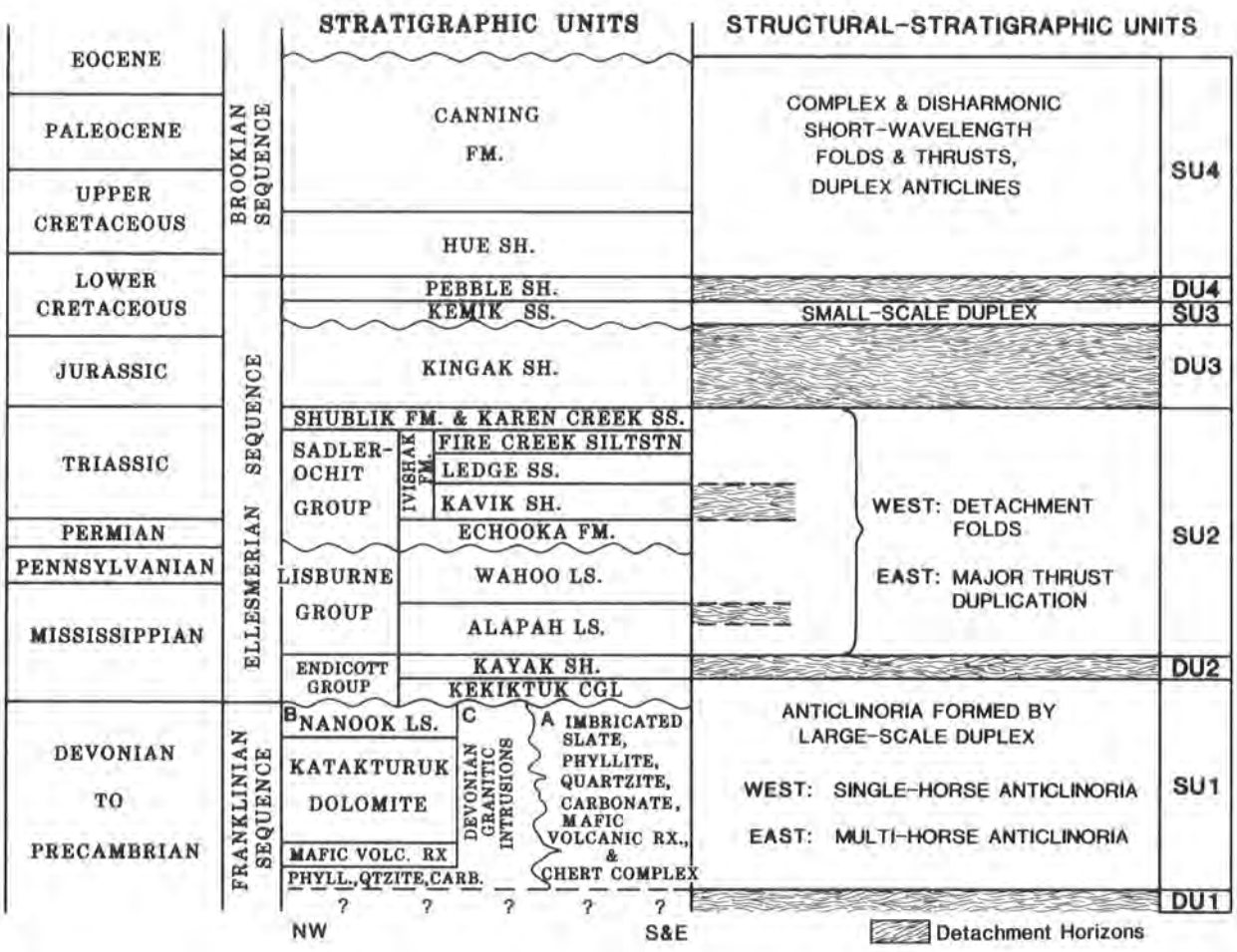

Figure 2. *Structural stratigraphy of the northeastern Brooks Range. A generalized stratigraphic column is shown to the left, and the structural-stratigraphic units and their dominant characteristics are shown to the right. Thicknesses are not to scale. Detachment horizons are shown with a wavy line pattern, which extends only partly across the column for minor detachment horizons. SU = structural unit (competent), DU = detachment unit (incompetent). The distribution of sub-units (A,B, and C) of structural unit 1 is shown in figure 2.*

ate and similar rocks as old as Middle Devonian (Anderson, 1990, 1991a and b; Anderson and Wallace, 1991) form a southward-thickening wedge of clastic rocks that acts as a separate structural-stratigraphic unit (not shown on fig. 2). The Kekiktuk Conglomerate is overlain by the Mississippian Kayak Shale, a thick, fissile shale that acts as an important detachment horizon throughout the region. The Mississippian to Pennsylvanian Lisburne Group is a thick carbonate unit that serves as the structurally dominant competent member of the overlying structural-stratigraphic unit. A sequence of dominantly terrigenous clastic Permian through Lower Cretaceous stratigraphic units overlies the Lisburne Group and has deformed with it. The Permian to Triassic Sadlerochit Group is the stratigraphically lowest part of this clastic sequence, and the part that has been most widely preserved from erosion in structural lows.

REGIONAL STRUCTURAL CHARACTER

The structure of the northeastern Brooks Range is dominated by a series of anticlinoria cored by sub-Mississippian rocks (fig. 3). These anticlinoria are interpreted to have formed above fault-bend folded (Suppe, 1983) horses in a duplex with a floor thrust at depth in the sub-Mississippian rocks and a roof thrust in the Kayak Shale (Rattey, 1985; Namson and Wallace, 1986; Wallace and Hanks, 1990). Above the roof thrust of this duplex, shortening has been accommodated mainly

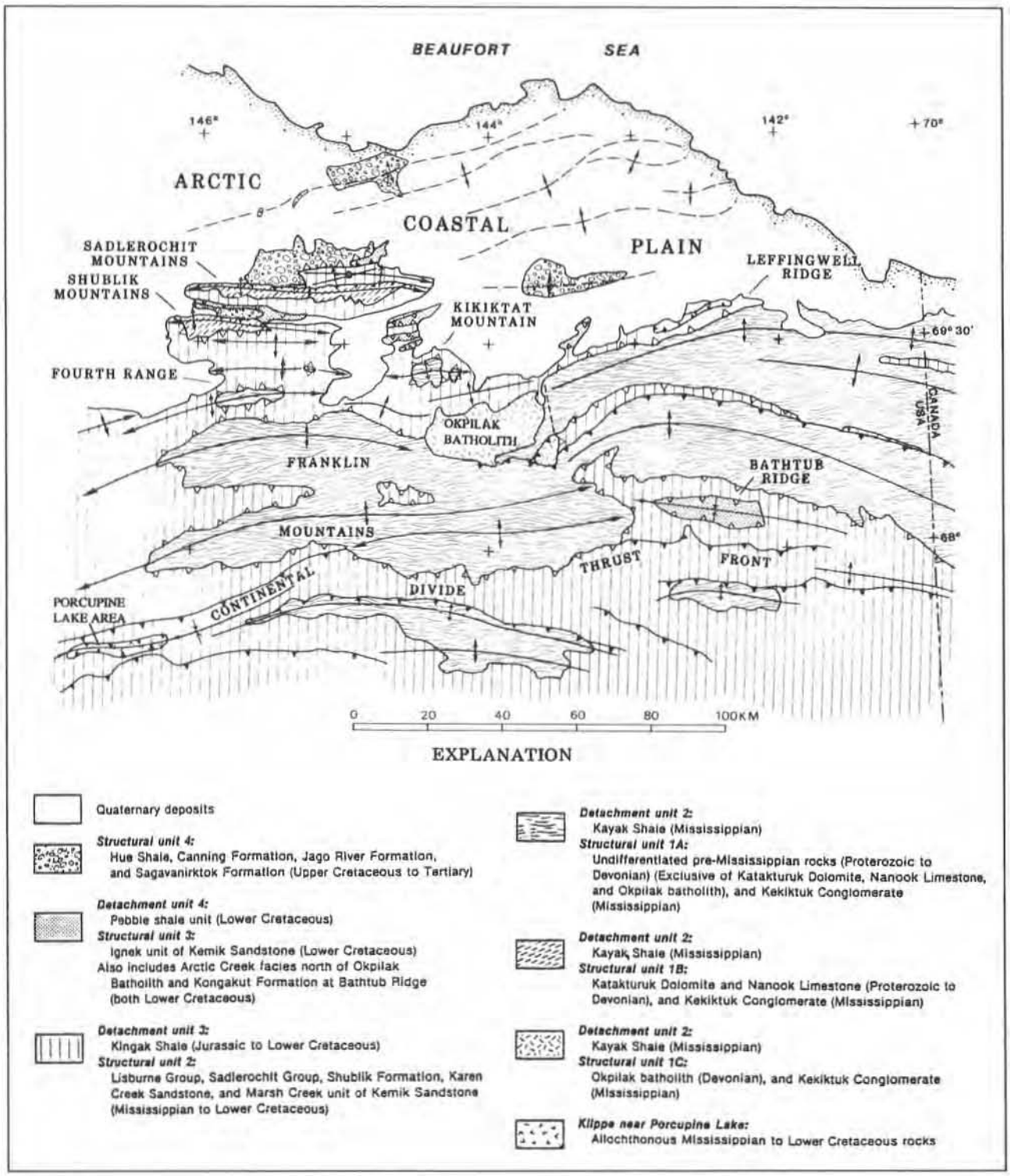

Figure 3. *Generalized tectonic map of the northeastern Brooks Range showing the distribution of the major structural-stratigraphic units and structural features of the northeastern Brooks Range. Structural-stratigraphic units are as identified in figure 2. Solid teeth on thrust faults indicate older-over-younger thrust faults that duplicate stratigraphic section; open teeth indicate detachment surfaces along which there has been slip but no disruption of the normal stratigraphic succession. Lines show trend and arrows show plunge of anticlinoria throughout the region and major synclines near the continental divide thrust front. From Wallace and Hanks, 1990.*

by detachment folds, with only local thrust faults. Three structural provinces can be identified in the northeastern Brooks Range based on variations along strike in the structural geometry above and below the detachment in the Kayak Shale (Wallace and Hanks, 1990).

This paper addresses the structure of a transect across the western structural province and extending a short distance south of the southern boundary of the province (figs. 4 and 5; Namson and Wallace, 1986). The western structural province can be divided into two structural domains, the Front Ranges and Franklin Mountains domains, based on variations in the structural geometry of Early Cretaceous and older rocks (figs. 4 and 5). These two domains are distinguished mainly by differences in the dimensions of anticlinoria cored by sub-Mississippian rocks (figs. 3 and 4). The structural geometries found throughout the rest of the northeastern Brooks Range are essentially variations on the structural geometry seen in these two domains (Wallace and Hanks, 1990). A third domain to the south, the Philip Smith Mountains domain, however, represents a significant departure from the structural geometry typical of the northeastern Brooks Range, and is more representative of structures exposed extensively in the main axis of the Brooks Range to the south and southwest (fig. 1).

Each of these three domains will be discussed in more detail below. The middle or Franklin Mountains domain will be discussed first because it is the domain in which the fault-bend fold geometry of the anticlinoria is best defined and the cover is everywhere detached along the Kayak Shale. The northern or Front Ranges domain will be discussed next because it displays smaller fault-bend folds and a northward termination of the Kayak Shale detachment. The southern or Philip Smith Mountains domain will be discussed last because anticlinoria cored by sub-Mississippian rocks are not a dominant element of its structure and the structures formed above the detachment horizon in the Kayak Shale are quite different from those in equivalent rocks to the north. One of the main objectives of this paper is to show the contrast in structural style between the northeastern Brooks Range, as exemplified by the Franklin Mountains and Front Ranges domains, and the north-central Brooks Range, as exemplified by the Philip Smith Mountains domain.

Franklin Mountains Domain

The Franklin Mountains domain is dominated by two anticlinoria cored by sub-Mississippian rocks (figs. 4 and 5, table 1). A structural form surface marked by the Mississippian Kekiktuk Conglomerate and the underlying sub-Mississippian unconformity clearly defines the geometry of these anticlinoria. Each anticlinorium is characterized by broadly curved but nearly planar dip panels that define a long, gently dipping backlimb, a flat crest, and a short, moderately dipping forelimb (fig. 5). This distinctive geometry corresponds with that of a fault-bend fold (Suppe, 1983). If the anticlinoria mark fault-bend folds, their geometry suggests that they formed by displacement over a ramp that connects a lower detachment at depth in the sub-Mississippian rocks with an upper detachment in the Kayak Shale (Wallace and Hanks, 1990). The interpretation that the pre-Mississippian rocks have deformed as coherent horses, rather than by internal thickening, is supported by the absence in most places of significant penetrative strain, small-scale folding, or small-scale imbrication along the sub-Mississippian

EXPLANATION

TK	Hue Shale and Canning Formation (Cretaceous to Lower Tertiary)
K	Kemik Sandstone and pebble shale unit (Lower Cretaceous)
KTr	Shublik Formation and Kingak Shale (Triassic to Lower Cretaceous)
TrP	Sadlerochit Group (Permian to Triassic)
lPM	Kayak Shale and Lisburne Group (Mississippian to Pennsylvanian)
pMu	Undifferentiated pre-Mississippian rocks and unconformably overlying Mississippian Kekiktuk Conglomerate
Units restricted to the north (Sadlerochit and Shublik Mountains)	
pMk	Mafic volcanic rocks, Katakturuk Dolomite, and Nanook Limestone (Proterozoic to Devonian)
Units restricted to the south (Porcupine Lake vicinity)	
KMa	Mount Annette allochthon (Mississippian to Lower Cretaceous)
Kko	Kongakut Formation (Lower Cretaceous)
MD	Kekiktuk Conglomerate, possibly transitional to Kanayut Conglomerate (Upper Devonian? to Mississippian)
Symbols	
	Older-over-younger thrust faults
	Detachment surfaces (thrust faults across which normal stratigraphic order is maintained)
	Domain boundaries

Figure 4. *Generalized geologic map of most of the western structural province of the northeastern Brooks Range. Line of cross section in figure 5 is shown; segments are labelled with letters A to J from north to south.*

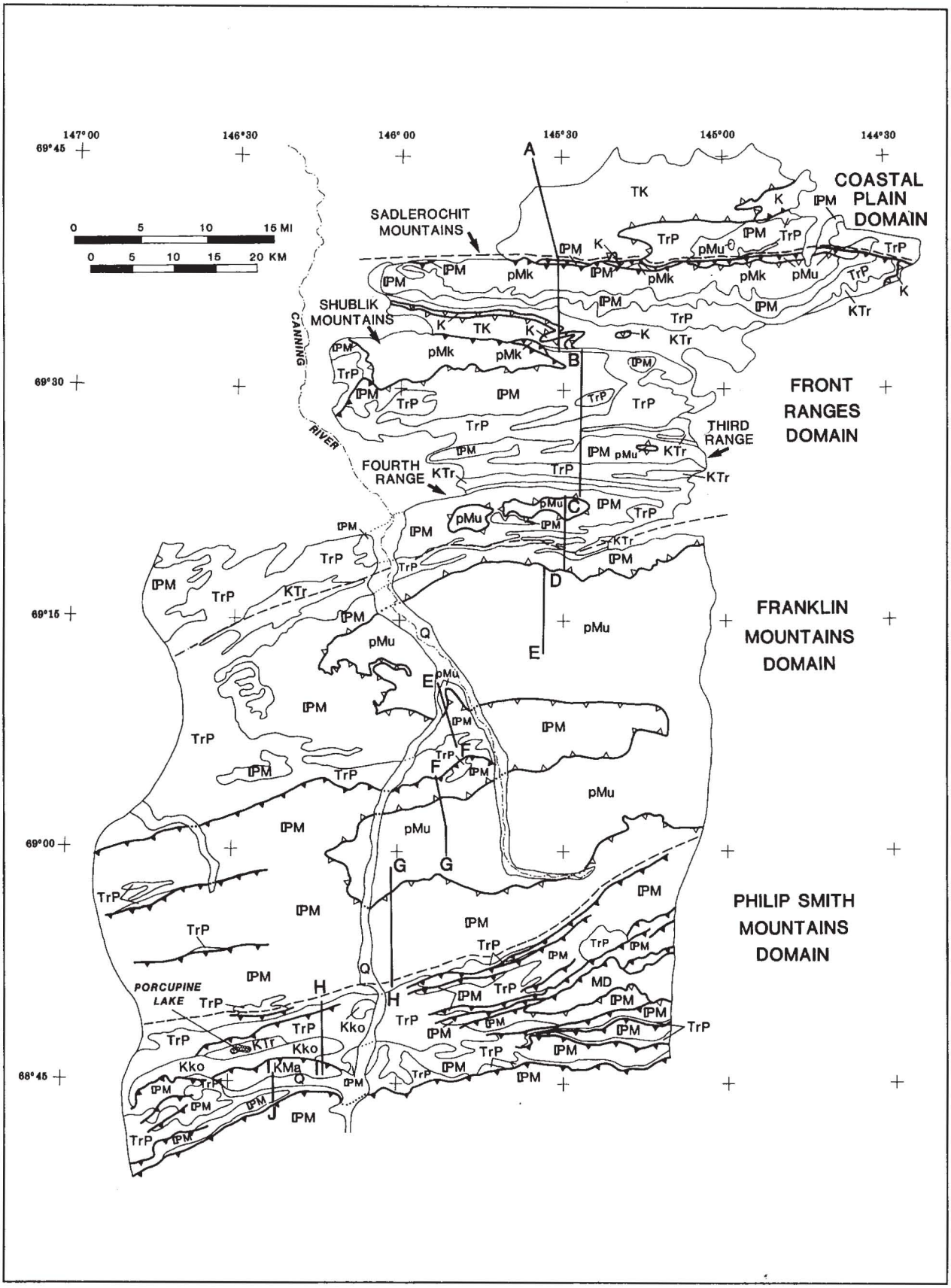
147°00
146°30
146°00
145°30
145°00
144°30
69°45
69°30
69°15
69°00
68°45
0 5 10 15 MI
0 5 10 15 20 KM
SADLEROCHIT MOUNTAINS
SHUBLIK MOUNTAINS
CANNING RIVER
FOURTH RANGE
THIRD RANGE
PORCUPINE LAKE
COASTAL PLAIN DOMAIN
FRONT RANGES DOMAIN
FRANKLIN MOUNTAINS DOMAIN
PHILIP SMITH MOUNTAINS DOMAIN
A
B
C
D
E
F
G
H
I
J
Q
TK
K
KTr
TrP
IPM
pMk
pMu
Kko
KMa
MD

5A

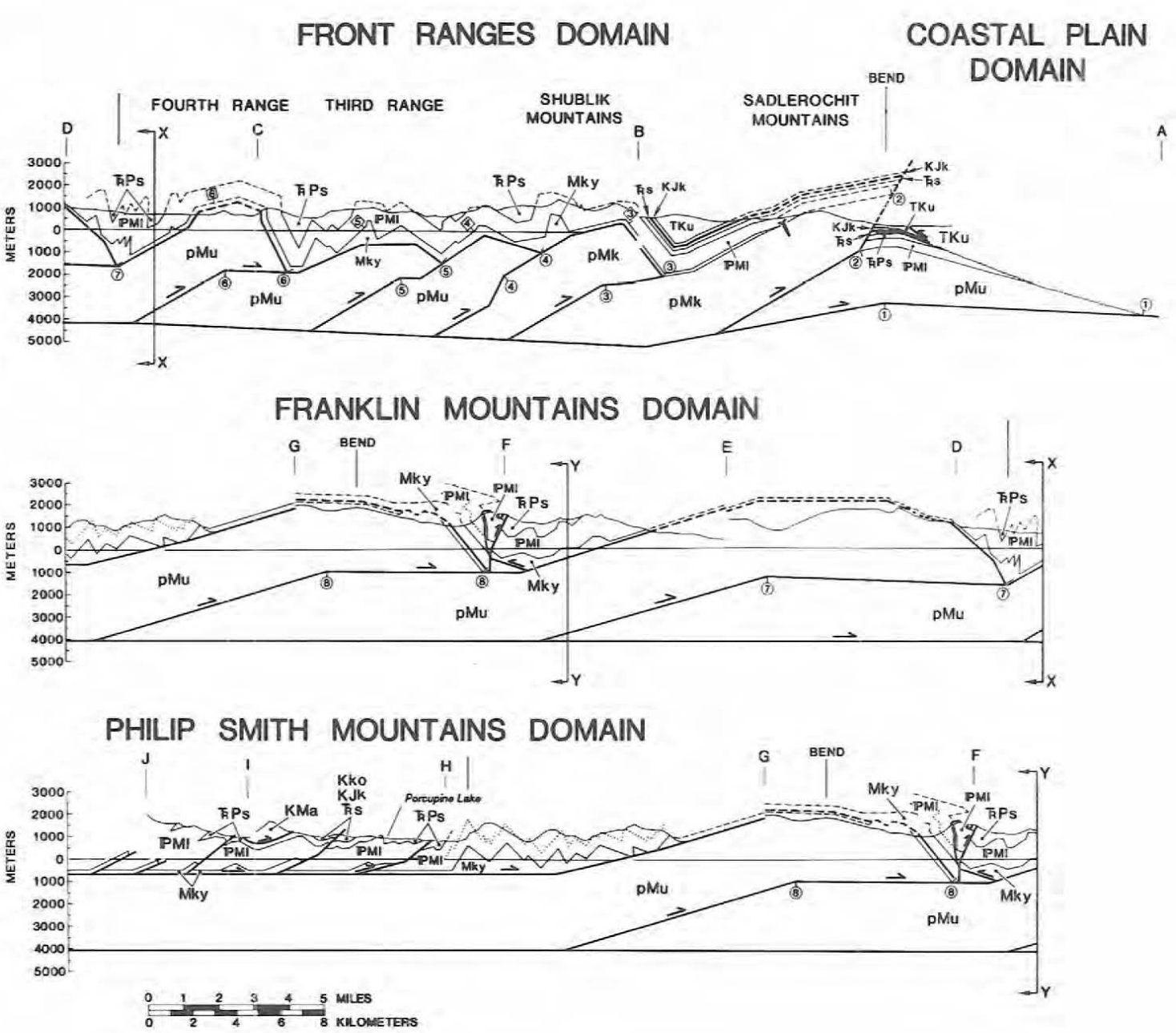
FRONT RANGES DOMAIN
COASTAL PLAIN DOMAIN
FOURTH RANGE
THIRD RANGE
SHUBLIK MOUNTAINS
SADLEROCHIT MOUNTAINS
BEND
D
X
C
B
A
METERS
3000
2000
1000
0
1000
2000
3000
4000
5000
ŦPs
PMI
pMu
Mky
pMk
KJk
Ŧs
TKu
FRANKLIN MOUNTAINS DOMAIN
G
BEND
F
E
D
Y
PHILIP SMITH MOUNTAINS DOMAIN
J
I
H
Kko
KJk
Ŧs
KMa
Porcupine Lake
0 1 2 3 4 5 MILES
0 2 4 6 8 KILOMETERS

5B

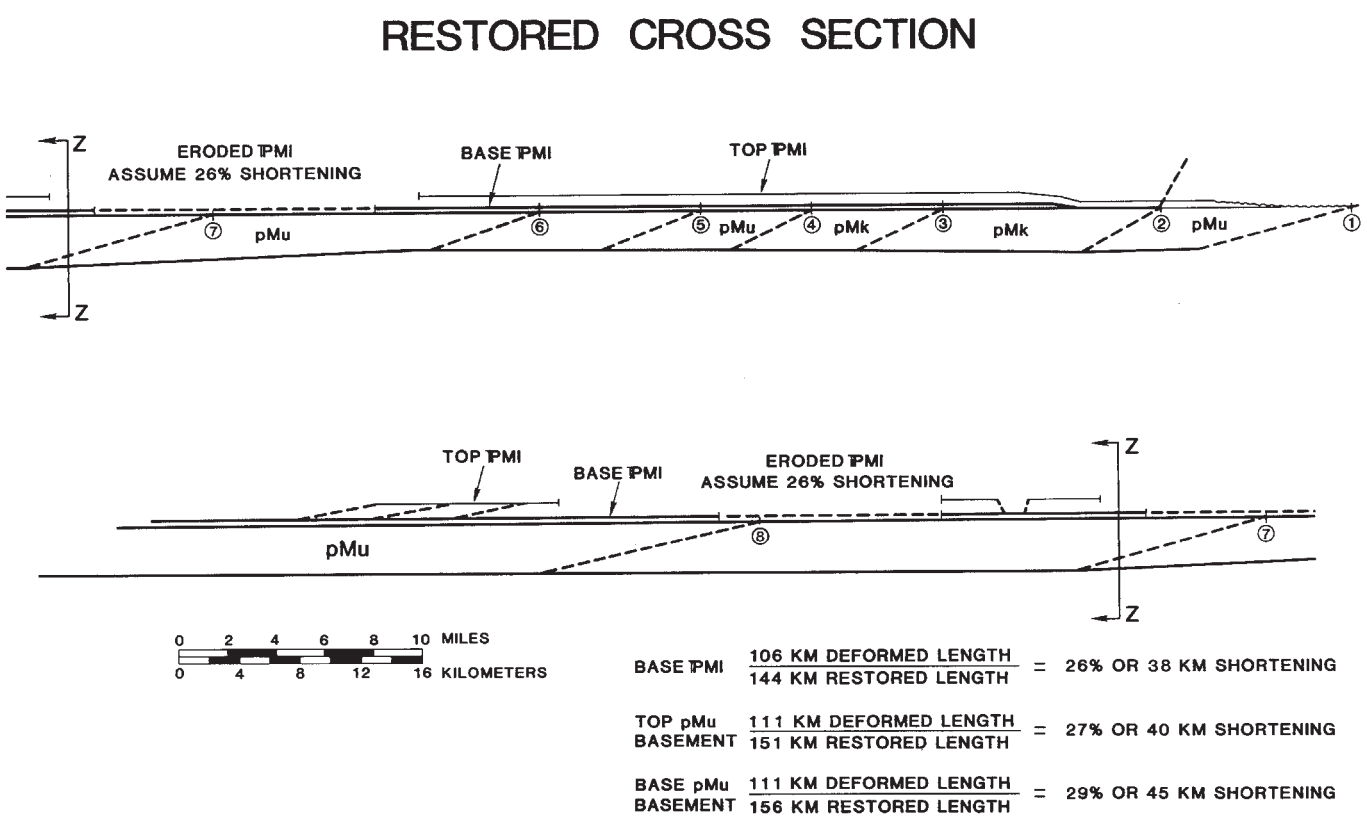

Figure 5. *Balanced cross section across the western structural province of the northeastern Brooks Range. Line of section shown on figure 4. (5A) Deformed section. Section is separated into overlapping parts to illustrate relationships between structures. Numbers indicate the hangingwall cutoff at the leading edge of each horse, the corresponding footwall cutoff, and the point at the base of the Lisburne Group that overlay these cutoffs in the undeformed state (determined from the restored cross section, fig. 5B). (5B) Restored section. Note that restored section is shown at a different scale than the deformed section in order to save space. Numbers indicate the position of the leading edge of each future horse.*

EXPLANATION

TKu	Kemik Sandstone, pebble shale unit, Hue Shale, and Canning Formation (Lower Cretaceous to Lower Tertiary)
KJk	Kingak Shale (Jurassic to Lower Cretaceous)
Trs	Shublik Formation (Triassic)
TrPs	Sadlerochit Group (Permian to Triassic)
IPMI	Lisburne Group (Mississippian to Pennsylvanian)
Mky	Kayak Shale (Mississippian)
pMu	Undifferentiated pre-Mississippian rocks and unconformably overlying Mississippian Kekituk Conglomerate
Units restricted to the north (Sadlerochit and Shublik Mountains)	
pMk	Mafic volcanic rocks, Katakturuk Dolomite, and Nanook Limestone (Proterozoic to Devonian)
Units restricted to the south (Porcupine Lake vicinity)	
KMa	Mount Annette allochthon Mississippian to Lower Cretaceous)
Kko	Kongakut Formation (Lower Cretaceous)
Symbols	
A-J	Offsets in line of section
3	Leading-edge cutoffs (footwall and hanging wall) for each horse numbered from north to south)
3	Point of base of IPMI originally overlying leading-edge cutoffs for each horse

unconformity and within the overlying Kekiktuk Conglomerate (Ziegler, 1989). The rocks above the Kayak Shale detachment are shortened primarily by detachment folds that are significantly smaller than the underlying anticlinoria, display no consistent sense of asymmetry, and are only locally breached by thrust faults (fig. 5, table 1)

Front Ranges Domain

The Front Ranges domain includes structures exposed in the Sadlerochit and Shublik Mountains and Third and "Fourth" Ranges, a series of ranges that form a salient north of the range front of the rest of the northeastern Brooks Range (figs. 4 and 5). This domain is characterized by a series of doubly plunging anticlinoria that are much smaller in strike-length, wavelength, and amplitude than those in the Franklin Mountains domain to the south (table 1). In the southern part of the domain, each anticlinorium is interpreted to reflect a single horse in a regional duplex, as in the Franklin Mountains domain. However, some important structural changes from the rest of the transect are present in the northern part of the domain (northern Shublik Mountains and Sadlerochit Mountains). Here, the sub-Mississippian rocks are dominated by a thick sequence of structurally competent Proterozoic to Devonian carbonate rocks, in contrast with the structurally less competent, lithologically heterogeneous sub-Mississippian rocks to the south. Moderately south-dipping thrust faults truncate the forelimbs of the anticlinoria that define both the Shublik and Sadlerochit Mountains, and mark their northern range fronts (fig. 4). These apparent out-of-sequence faults are unusual in that they cut up-section from sub-Mississippian rocks to Cretaceous and younger rocks, thus cutting across the stratigraphic position of the Kayak Shale. These faults truncate older folds and faults and appear to be the last-formed structures in hindward-propagating thrust sequences localized at the leading edges of the Shublik and Sadlerochit Mountains anticlinoria (Meigs, 1989; McMullen, 1989; Rogers, 1989). Detachment folds in the Lisburne and Sadlerochit Groups are not present in the Sadlerochit Mountains (fig. 5). Instead, these units have deformed with the sub-Mississippian rocks, probably because the Kayak Shale detachment horizon depositionally thins and disappears northward in this area.

Philip Smith Mountains Domain

The Philip Smith Mountains domain is characterized by a lower average structural relief than in the provinces to the north. This is manifested by exposures that consist mainly of Mississippian to Triassic rocks, with relatively few exposures of sub-Mississippian rocks (fig. 4). This decrease in structural relief and exposure of sub-Mississippian rocks reflects an abrupt southward decrease in the importance of the anticlinoria that dominate the northeastern Brooks Range. This change in structure corresponds with the southward appearance below the Kayak Shale detachment horizon of a structural-stratigraphic unit not present to the north: a southward-thickening wedge of Middle Devonian to Lower Mississippian clastic sedimentary rocks, equivalent to those documented farther east by Anderson (1990, 1991a and b). The lack of previous deformation and the different thickness and lithologic character of this structural-stratigraphic unit likely account for the southward appearance of smaller, but largely unexposed, fold-and-thrust structures below the Kayak Shale detachment horizon (table 1).

The dominant exposed structures are strongly asymmetrical, north-overturned anticline-syncline pairs that are breached in their steep, short limbs by thrust faults (fig. 5, table 1). As in the detachment folds to the north, these folds and faults have formed above a detachment in the Kayak Shale. However, the strong asymmetry and abundance of thrust faults represents a significant contrast with the domains to the north. The boundary between the Franklin Mountains and Philip Smith Mountains domains has been referred to as the "continental divide thrust front" (fig. 3) (Wallace and others, 1988). The Cenozoic duplex and detachment folds north of this boundary are younger than the thrust-truncated folds in the Philip Smith Mountains domain, which could have begun forming as early as Late Cretaceous time (Wallace and Hanks, 1990; Wallace and others, in review). The domain boundary is marked by a regionally significant relative structural low in the vicinity of Porcupine Lake (fig. 4). Along the line of section, this low preserves a local remnant of Mississippian to Lower Cretaceous allochthonous rocks (figs. 4 and 5), the Mt. Annette allochthon and related rocks (Churkin and others, 1989), that were displaced a considerable distance (at least 46 km, and probably much more) from the south. The rocks of this klippe were deposited in deeper-water environments than coeval rocks in their footwall, and are similar to allochthonous rocks that are very widespread in the central and western Brooks Range (Mull, 1982; Mayfield and others, 1988). The klippe itself is overprinted by folds and faults formed in the structurally underlying rocks. The presence of this klippe shows that a thrust-emplaced roof once existed over the faulted asymmetrical folds, indicating that they constitute a duplex of fault-truncated folds.

Table 1. *Summary of structural characteristics above and below the Kayak Shale detachment in the three structural domains on the Canning River transect*

	DOMAIN		
	Philip Smith Mountains	**Franklin Mountains**	**Front Ranges**
	Above Kayak Shale detachment		
Structural-stratigraphic unit	Lisburne & Sadlerochit Groups (SU2)	Lisburne & Sadlerochit Groups (SU2)	Lisburne & Sadlerochit Groups (SU2)
Fold type	Thrust-truncated detachment folds	Detachment folds	Detachment folds Absent in Sadl. & Shublik Mts. Commonly combine to form box folds
Interlimb angle	100-30°	100-30°, locally to 0° in synclinoria	130-60°
Wavelength	0.5-2 km	1-2 km	1.5-3 km
Amplitude	≤0.5 km	0.3-1.0 km	0.6-1.0 km
Strike-length	7-19 km	≥10 km	7-25 km
Symmetry	Strongly asymmetrical, short limbs to north	Mostly symmetrical, but variable	Mostly symmetrical, but variable
Thrust faults	North-vergent thrusts truncate fold short limbs	Rare, north-vergent thrusts Mostly out-of-syncline	Rare, north-vergent thrusts Mostly where Kayak absent
	Below Kayak Shale detachment		
Structural-stratigraphic unit	Middle Devonian-Lower Mississippian clastic wedge (SU1D)	Pre-Mississippian, undifferentiated (SU1A)	Pre-Mississippian, undifferentiated (SU1A) Carbonates (SU1B) in Sadl. & Shublik Mts.
Fold type	Possibly fault-bend folds	Fault-bend folds (inferred)	Fault-bend folds (inferred)
Wavelength	~4-12 km	22-24 km	6-15 km
Amplitude	~2.5-3.2 km	3-4 km	1.5-3 km
Strike-length	~25-65 km	90 km	34-66 km
Symmetry	Uncertain, but no strong asymmetry	Short limb to north	Short limb to north
Thrust faults	Exposed north-vergent thrusts locally floor folds Thrusts may underlie fault-bend folds & link floor thrust below clastic wedge to roof thrust in Kayak	North-vergent thrusts inferred to underlie fault-bend folds & link floor thrust in pre-Mississippian to roof thrust in Kayak	North-vergent thrusts inferred to underlie fault-bend folds & link floor thrust in pre-Mississippian to roof thrust in Kayak. Thrusts truncate forelimbs of Sadl. & Shublik Mts. anticlinoria

STRUCTURAL INTERPRETATION

The Kayak Shale serves as a fundamental detachment horizon that separates two distinct sets of structures exposed along the Canning River transect. Large anticlinoria have formed in sub-Mississippian rocks and the Kekiktuk Conglomerate below the detachment, where-as shorter wavelength folds and, to the south, thrust faults, have formed above the detachment. The geometry and kinematics of these two sets of structures are very different, although they quite likely simply represent different modes of accommodating the same shortening and were controlled by differences in structural stratigraphy. The first of the major interpretations discussed below is that the overall structure of the Front Ranges and Franklin Mountains domains is a passive-roof duplex with a roof thrust in the Kayak Shale. The second major interpretation regards the mode of shortening above the Kayak Shale. Shortening in the roof of the passive-roof duplex has been accommodated primarily by symmetrical detachment folds, whereas to the south, in the Philip Smith Mountains domain, detachment folds are strongly asymmetrical and have been truncated by thrust faults.

Passive Roof Duplex

The structural origin of the anticlinoria in the Front Ranges and Franklin Mountains domains must be explained in order to determine how shortening has been accommodated below the Kayak Shale. Two end-member models span a range of possible solutions to this problem (Wallace and Hanks, 1990): the anticlinoria may have formed by large-scale thrust duplication, resulting in formation of fault-bend folds, or by variation across strike in the amount of shortening and thickening that has resulted from some combination of penetrative strain, small-scale folding, and small-scale imbrication. As summarized above, the geometry of the anticlinoria suggests that each is a fault-bend fold formed by displacement of a horse over a ramp that connects a floor thrust in the sub-Mississippian rocks with a roof thrust in the Kayak Shale. If this interpretation is correct, then the backlimb of each anticlinorium reflects the dip of the footwall ramp and the fold geometry constrains the range of possible depths to the floor thrust. The depth to the roof thrust can be inferred directly using the estimated stratigraphic thickness between strata exposed in structural lows and the underlying Kayak Shale detachment. A general lack of structural thickening, detachment, or penetrative strain in the Kekiktuk Conglomerate (for example, Ziegler, 1989) limits the extent to which internal thickening of the unconformably underlying pre-Mississippian rocks can have contributed to formation of the anticlinoria, and thereby places additional limits on the depth to the floor thrust.

Given the geometry of the anticlinoria, various fault-bend fold interpretations are possible depending on the interpretation of the depth to the floor thrust and the degree to which the horse is interpreted to thicken by small-scale internal deformation. The interpretation chosen for the balanced cross section (fig. 5) assumes no internal shortening and the minimum possible depth to the floor thrust because this geometry yields the shortening value which matches most closely that determined above the Kayak Shale. However, this interpretation alone does not account for the difference in elevation between the regional base level of the sub-Mississippian unconformity along the cross section (that is, beneath the synclinoria) and in the subsurface of the coastal plain to the north (as determined, for example, from depth conversions of interpretations of seismic data by Bruns and others (1987)). This discrepancy can most likely be accounted for by additional structural thickening below the basal detachment shown on the cross section.

Regardless of the exact horse geometry chosen, and consequent detachment depth and shortening value, the structure below the detachment in the Kayak Shale is by definition a duplex if it involves thrust duplication. Vann and others (1986) recognized that the duplex in the northeastern Brooks Range is a passive-roof duplex. A "passive-roof duplex" (Banks and Warburton, 1986) or "low-taper triangle zone" (McMechan, 1985) is distinguished from other duplexes by the way shortening is accommodated above the roof thrust. In a passive-roof duplex, forward displacement of each successive horse is accommodated above the duplex by hindward displacement on the roof thrust. This means that the displacement on each horse must be accommodated in the roof sequence by shortening either directly above or behind that horse. This contrasts with the more familiar "active-roof" duplex (for example, Boyer and Elliot, 1982; Mitra, 1986), in which shortening in the roof sequence is accommodated ahead of each horse above forward-displaced thrusts.

In the examples of passive-roof duplexes described by Banks and Warburton (1986) and by McMechan (1985), shortening in the roof is accommodated largely by thrust faults, with either forward or hindward displacement. The duplex in the northeastern Brooks Range differs from these examples in that shortening above the roof thrust is accommodated almost entirely by detachment folds (fig. 5). An idealized example of a single horse in such a duplex is illustrated in figure 6. Shortening below the roof thrust is taken up mainly by displacement on the thrust fault that defines the base of the horse (fig. 6C). An additional relatively small com-ponent of shortening is accommodated by the fault-bend fold formed by

displacement of the horse over the footwall ramp. In contrast, the equivalent shortening in the roof is distributed over the entire horse in multiple detachment folds. In this case, backthrust displacement on the roof thrust increases hindward from the leading edge of the horse to the point in the roof sequence that lay over the leading edge in the undeformed state (fig. 6D). Hindward of this point, backthrust displacement on the roof thrust decreases progressively.

The best evidence for backthrust displacement on the roof thrust of the duplex in the northeastern Brooks Range is found in the Sadlerochit Mountains, at the northern end of the cross section (fig. 5). Here, the stratigraphic horizon that elsewhere serves as the roof thrust, the Kayak Shale, depositionally thins and disappears to the north, thus pinning the roof thrust. Consequently, displacement of the horse immediately to the south, beneath the northern Shublik Mountains, must be accommodated in the roof sequence hindward of the leading edge of the horse, requiring backthrust displacement on the roof thrust. To the west, an out-of-sequence thrust fault cuts from sub-Mississippian rocks across the roof thrust along the northern range front of the Shublik Mountains (fig. 4). However, the displacement on this fault is not sufficient to accommodate all of the displacement of the horse beneath the northern Shublik Mountains, and hence does not preclude backthrust displacement on the roof thrust.

The northward termination of the roof thrust in the Sadlerochit Mountains also serves as a "pin," or reference point for comparison of shortening above and below the roof thrust to the south (fig. 5). Restoration of structures above and below the roof thrust southward from this pin identifies the point in the roof sequence that lay above the leading edge of each horse in the undeformed state (numbered points in restored cross section, fig. 5B). In the deformed state, each of these points lies hindward of the leading edge of its corresponding horse (note separation between numbered leading-edge cutoffs and corresponding points above the roof thrust in the deformed cross section, fig. 5A). Thus, restoration of the duplex suggests backthrust displacement on its roof thrust. Furthermore, the approximately equal values of shortening above and blow the roof thrusts, as indicated by the cross section, is consistent with the passive-roof interpretation.

Detachment Folds

In a detachment fold (Dahlstrom, 1990; Jamison, 1987), folding in a relatively competent rock unit is accommodated by internal deformation of an underlying, relatively incompetent rock unit. This incompetent unit is separated from another underlying competent unit by a surface or zone of displacement (detachment horizon or decollement), reflecting a difference in amount and/or distribution of shortening across the detachment horizon. The model for detachment fold geometry described by Jamison (1987) is for asymmetrical folds, but detachment folds commonly lack a consistent sense of asymmetry, as in examples described from the Jura Mountains (Laubscher, 1977) and the Appalachians (Wiltschko and Chapple, 1977; Davis and Engelder, 1985).

Detachment folds have formed above the roof thrust of the regional-scale duplex in the northeastern Brooks Range (fig. 5). In contrast with the most familiar examples of detachment folds, which have formed above evaporite layers, these detachment folds have formed above a shale unit. The Mississippian Kayak Shale is the incompetent stratigraphic horizon that serves both as the roof thrust of the underlying duplex and the incompetent layer above which detachment folds have formed. The Kayak Shale is a highly fissile black shale that is about 200-400 m thick throughout most of the northeastern Brooks Range. It thins northward to 100 m or less in the Shublik Mountains, and is much thinner to absent in the Sadlerochit Mountains, where it has not served as a detachment horizon. The Kayak Shale is visibly thickened in anticlines, but a lack of appropriate exposures precludes determining whether it is thinned in synclines.

Carbonates of the Mississippian-Pennsylvanian Lisburne Group form the competent structural member that overlies the Kayak Shale. The Lisburne Group is 450-850 m thick, and generally thickens southward. Within the Lisburne Group, the upper Wahoo Formation is the more competent unit and defines the largest folds. The underlying Alapah Formation is thinner-bedded and more argillaceous and commonly is thickened in the cores of anticlines by disharmonic folds that are smaller than those in the Wahoo Formation. Terrigenous clastic rocks of the Permian-Triassic Sadlerochit Group overlie the Lisburne Group. Folds in the Sadlerochit Group are generally controlled by those in the underlying Lisburne Group, although parasitic folds and thrust faults also are present, particularly above a minor detachment horizon in the Kavik Shale (fig. 2).

The detachment folds in the Front Ranges and Franklin Mountains domains are generally open to tight chevron-shaped folds that are upright with respect to the underlying detachment surface. The detachment surface is tilted in the limbs of the regional anticlinoria, so the axial surfaces of the detachment folds may dip steeply north or south depending on their position with respect to the anticlinoria (fig. 5). The geometry of the folds varies depending on the local magnitude of shortening. The folds are tightest in the synclinoria, displaying high amplitude relative to wavelength. Although commonly eroded from the crests of the anticlinoria, detachment folds

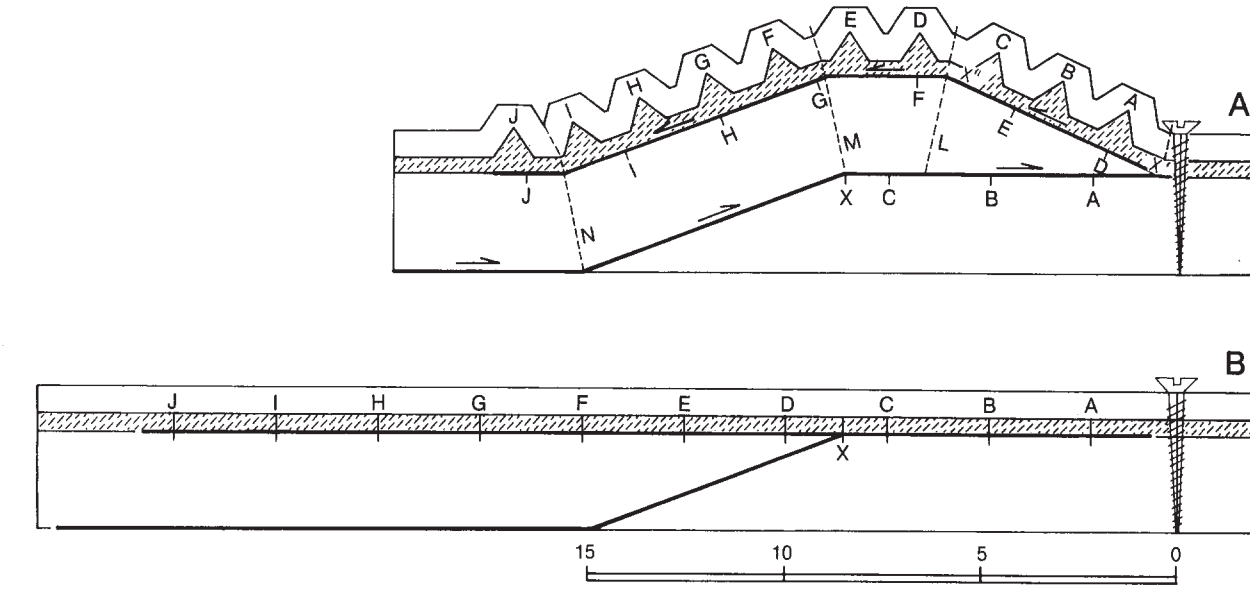

Figure 6. *Schematic cross section and displacement diagrams of idealized passive-roof duplex. Units of distance are arbitrary.(6A.) Accommodation of shortening by displacement of a single horse in a passive-roof duplex and by detachment folding in its roof. A-J indicate positions of detachment fold hinges and the originally underlying points beneath the roof thrust. L-N are hinges in the fault-bend fold. X and X' mark the footwall and hangingwall cutoffs, respectively, of the leading edge of the horse, and X" the originally overlying point above the roof thrust. (6B.) Restoration of A. Letter designations as in A.*

are present over the anticlinoria downplunge. The folds are more open over the anticlinoria, particularly on the long backlimbs and in the Front Ranges domain. These folds display low amplitude relative to wavelength, and box-fold geometries are common. The fact that detachment folds are well developed over the forelimbs and crests of the anticlinoria suggests that the folds did not form entirely ahead of each successively emplaced horse, as might be expected to result from forward displacement on the roof thrust of an active-roof duplex. Instead, it suggests that folds formed directly above each horse as it was emplaced, requiring backthrust displacement of the rocks above the roof thrust. In the Front Ranges and Franklin Mountains domains, shortening of the Lisburne and Sadlerochit Groups is accommodated almost entirely by detachment folds, with rare small-displacement out-of-syncline and fold-breaching thrust faults being present only where the folds are tightest.

Figure 7A illustrates a generalized and hypothetical model for the evolution of symmetrical detachment folds, like those in the Front Ranges and Franklin Mountains domains. It is not the objective of this paper to discuss the geometry and kinematics of detachment folds in detail, but the diagram illustrates some important relevant points. As a detachment fold evolves, it must obey the laws of conservation of bed length and cross-sectional area (Dahlstrom, 1990). In other words, the length of the folded competent bed and the cross-sectional area of both the competent bed and the incompetent detachment unit must be the same in both the undeformed and deformed states (assuming plane strain). This constraint, which is followed in the model, places significant limitations on the possible geometries and kinematic paths of folds; only a single geometric/kinematic path is possible for an ideal symmetrical chevron fold with a fixed detachment depth. The arc-length of the fold (that is, the bed-length encompassed by the fold) must increase with increasing shortening if bed length and area are to be conserved. This requires that at least some hinges migrate as a fold evolves, rather than remaining fixed in their original positions with respect to bedding. As shortening increases, the interlimb angle decreases and the ratio of amplitude to wavelength increases. The natural fold geometries observed along the transect (fig. 5 and table 1) display a similar range in geometric characteristics.

The geometry of folds in the Lisburne and Sadlerochit Groups is quite different in the Philip Smith Mountains domain than in the Front Ranges and Franklin Mountains domains to the north (fig. 5 and table 1). Relatively constant structural relief is reflected by the predominance of

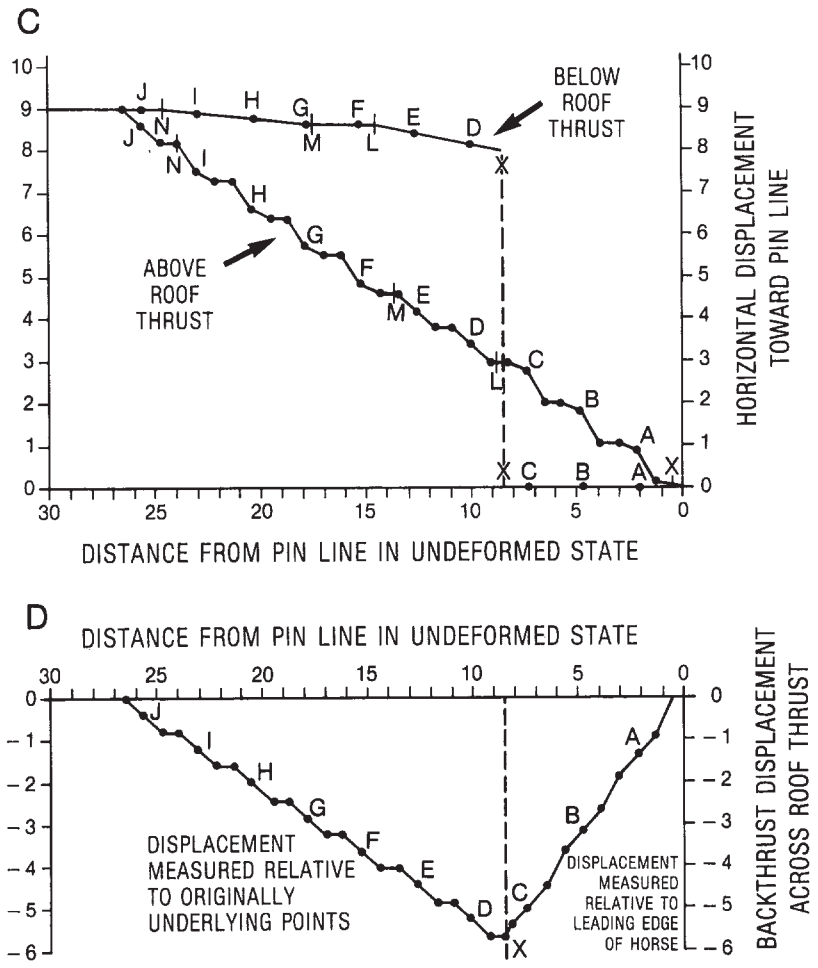

Figure 6C. Distribution of horizontal displacement as a function of original position in undeformed state. Vertical scale is exaggerated for clarity. Letter designations as in A; dashed line marks position of thrust fault at X. Shortening beneath the roof thrust is accommodated mainly by displacement on a single fault, whereas above the roof thrust, the equivalent shortening is distributed over a series of detachment folds.

Figure 6D. Amount of backthrust displacement across the roof thrust as a function of original position in undeformed state. Vertical scale is exaggerated for clarity. Letter designations as in A; dashed line marks position of thrust fault at X. Backthrust displacement increases hindward from the leading edge of the horse to the point above the roof thrust that originally overlay that leading edge. Backthrust displacement decreases progressively hindward of this point.

exposures of Lisburne Group limestones for more than 35 km to the south of a synclinal structural low in the vicinity of Porcupine Lake (fig. 4). Thus, anticlinoria involving sub-Mississippian rocks are not important in this domain, and a passive-roof duplex as seen in the Front Ranges and Franklin Mountains domain either is not present or has had little influence on the structures exposed at the surface. Folds in this domain are strongly asymmetrical, with a consistent northward (forward) vergence. These folds commonly are breached through their steep limbs by thrust faults with northward displacement. These folds are similar in geometry to fault-propagation folds (Suppe, 1985), and are represented as such on the present cross section (fig. 5). However, they differ from fault-propagation folds because in each the fault cuts through the fold, rather than dying out in the fold, and cuts through the steep limb, rather than along its lower hinge (Wallace, field observations, 1991; also observed to the east by Homza, 1992). On average, the geometry of the folds in the Philip Smith Mountains domain is different from that of the detachment folds to the north, although they also formed above a detachment in the Kayak Shale. However, folds representing a complete transition between the end-member geometries are present, suggesting that the asymmetrical, fault-breached folds in the Philip Smith Mountains domain also are detachment folds.

Figure 7B illustrates a generalized and hypothetical model for the evolution and eventual thrust truncation of asymmetrical detachment folds, like those in the Philip Smith Mountains domain. The model obeys the laws of conservation of bed length and cross-sectional area. This places some constraints on the geometries that are possible, although they are not as restrictive as in the case of symmetrical detachment folds. A range of geometries is possible for a given shortening, and the model illustrates only one of the possible kinematic paths. Thrust breakthrough of the steep limbs of folds probably results from geometric and/or mechanical limits to continued fold growth with increasing shortening. It should be noted that in the natural folds, the fault flattens up-section in a detachment horizon in the Sadlerochit Group, resulting in superposition of a fault-bend fold geometry on the truncated asymmetrical detachment-fold geometry.

Possible Controls on Structural Geometry

A passive-roof duplex formed in the Front Ranges and Franklin Mountains domains but apparently did not form in the Philip Smith Mountains domain to the south. Shortening above this duplex was accommodated by generally unfaulted, upright, and symmetrical detachment folds, in contrast with the thrust-truncated, forward-vergent asymmetrical detachment folds of the Philip Smith Mountains domain to the south. It is not clear what factors controlled these structural differences, but comparison of the characteristics of the various domains offers some empirical clues.

A fundamental factor in the formation of the detachment folds and associated thrust faults must have been the structural stratigraphy, particularly the relative thicknesses of, and competency contrast between, the Kayak Shale and the overlying Lisburne Group. The thickness and mechanical weakness of the Kayak Shale was an essential element, as indicated by the lack of detachment folds in the Sadlerochit Mountains, where the Kayak Shale is thin to absent. The shale was sufficiently effective as a detachment horizon to allow formation of a low-taper, weak basal-layer wedge, as described by Davis and Engelder (1985) for a basal layer of salt. They argued that a particular sense of vergence will not predominate in such a wedge, as is the case over the passive-roof duplex in the northeastern Brooks Range.

There is little obvious change in the structural stratigraphy of the Kayak Shale and the Lisburne Group between the Franklin Mountains and the Philip Smith Mountains domains. This is consistent with the interpretation of detachment folding in both areas. However, it does not account for the differences in geometry and faulting, so other factors must be sought to explain them.

The structural stratigraphy and geometry beneath the Kayak Shale detachment differ dramatically between the Franklin Mountains and the Philip Smith Mountains domains. In the Franklin Mountains and Front Ranges domains, the Kayak Shale is underlain by a relatively thin Kekiktuk Conglomerate, which in turn unconformably overlies a polydeformed assemblage of lithologically heterogeneous stratified rocks. The general lack of penetrative strain, detachment, or imbrication in the Kekiktuk Conglomerate indicates that it was structurally attached to, and deformed with, the underlying rocks, and that it and the underlying rocks behaved relatively competently during formation of the passive-roof duplex to form simple, long-wavelength anticlinoria. Given their character, it is not clear why the sub-Kekiktuk rocks behaved so competently during Cenozoic deformation. However, reactivation of favorably oriented pre-Mississippian structures, especially south-dipping faults or bedding, and "structural hardening" as a result of pre-Mississippian shortening could account for the apparently competent behavior of these previously deformed rocks.

A wedge of Middle Devonian to Lower Mississippian clastic sedimentary rocks, equivalent to those documented farther east by Anderson (1990, 1991a and b), thickens southward from near the boundary between the Franklin and Philip Smith Mountains domains (Wallace, field observations, 1991; also observed to the east by R.K. Crowder, T.E. Moore, and C.G. Mull, personal commun., 1992). The sub-Middle Devonian unconformity that defines the base of this wedge is truncated northward by the sub-Mississippian unconformity, which is ultimately succeeded to the south by a conformity in the Endicott Mountains allochthon (Anderson and Wallace, 1991; Brosgé and others, 1988). This wedge has been thickened by folds and thrust faults that are smaller and closer spaced than the anticlinoria in the Franklin Mountains domain to the north (table 1) (Brosgé and Reiser, 1965; Brosgé and others, 1976; Anderson, 1991). If anticlinoria like those in the Franklin Mountains domain exist beneath the wedge, they are much smaller, as indicated by the relatively constant level of structural relief across the Philip Smith Mountains domain.

The change in character of the rocks beneath the Kayak Shale detachment near the boundary between the Franklin Mountains and Philip Smith Mountains domains undoubtedly had a significant influence on the structures that formed in those domains, particularly beneath the detachment. The previously shortened and variably dipping sub-Mississippian rocks to the north behaved relatively competently, forming large fault-bend folds, probably controlled in part by pre-Mississippian structures (Wallace and Hanks, 1990). Differences in the sizes of these anticlinoria are the main distinguishing characteristic between the Front Ranges and Franklin Mountains domains. The size of these structures likely was influenced by pre-Mississippian structures. The best evidence for this is in the Sadlerochit and Shublik Mountains, where a structural repeat of pre-Mississippian stratigraphy is overlapped by the sub-Mississippian unconformity, and hence is of pre-Mississippian origin, and coincides directly with Cenozoic anticlinoria. The northward decrease in the size of the anticlinoria may also be related to a decrease in the depth of the floor thrust.

In the Philip Smith Mountains domain, folds and thrust faults in the Middle Devonian to Lower Mississippian clastic wedge are bounded above by the detachment in the Kayak Shale and below by a probable detachment beneath the clastic wedge, and thus constitute a duplex. The northward increase in structural relief and size of horses between the Philip Smith and Franklin Mountains

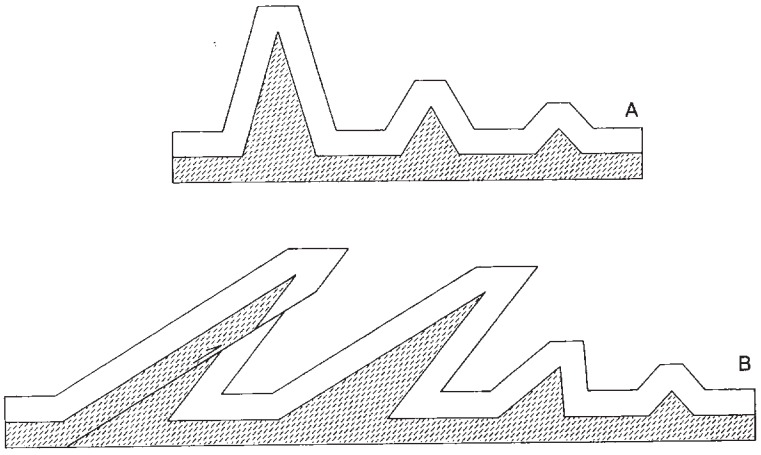

Figure 7. *Hypothetical sequence of evolution of detachment folds. Progressive evolution is shown with a series of arbitrarily spaced structures that accommodate increasing shortening to the left. Bed length and cross-sectional area are conserved in these models. (7A) Series of symmetrical and upright detachment folds that increase in amplitude/wavelength with increasing shortening. Note that for a given thickness of detachment unit, the conservation laws uniquely determine the size and geometry of each fold as a function of the amount of shortening accommodated by that fold. (7B) Series of detachment folds that increase in both asymmetry and amplitude/wavelength with increasing shortening. Additional shortening is ultimately accommodated by thrust breakthrough of the steep limb of a fold. Although the conservations laws restrict the possible geometries for a given thickness of detachment unit and shortening accommodated by a fold, a range of geometries are possible for a given value of shortening. Geometries shown here are arbitrarily chosen to approximate the apparent evolutionary path of observed folds.*

domains corresponds with the northward pinch-out of the previously undeformed Middle Devonian to Lower Mississippian clastic wedge over the previously deformed sub-Mississippian rocks.

The significant difference between the Philip Smith and Franklin Mountains domain in structural topography and in spacing and type of structures below the Kayak Shale detachment corresponds with the change in structure above the detachment. The structures below the detachment likely influenced the geometry of overlying structures, although it is not clear how. The relatively smooth surface defined by the broad, low amplitude-to-wavelength anticlinoria to the north is overlain by upright detachment folds probably formed as a result of backthrust displacement. If displacement on adjacent horses in the passive-roof duplex occurred in part concurrently, as seems likely, then the structural relief of the more forward horse would serve as an impediment to forward displacement of the roof. This would favor the concentration of shortening in the synclinoria and the formation of upright folds. In contrast with the anticlinoria to the north, the shorter-wavelength, lower-amplitude fold-and-thrust structures to the south are overlain by forward-vergent asymmetrical, thrust-truncated folds. These probably formed in a more typical fold-and-thrust wedge characterized by a basal detachment that steps up-section in the forward direction and by thrust faults with a forward displacement sense.

To the west-northwest of the northeastern Brooks Range, beneath the North Slope (fig. 1), a southward-thickening wedge of mid-Cretaceous and younger clastic deposits fills the Colville basin (Bird, 1986; Molenaar and others, 1987), and the sub-Mississippian unconformity dips southward beneath the basin from the Barrow arch (Bird, 1986). A similar pattern probably existed in the northeastern Brooks Range prior to Cenozoic shortening, uplift, and erosion (Wallace and Hanks, 1990), as suggested by projection of the Barrow arch and Colville basin into the northeastern Brooks Range (Bird and Bader, 1987; Molenaar and others, 1987). Thus, a greater depositional overburden of mid-Cretaceous and younger rocks probably existed southward prior to formation of the fold-and-thrust structures considered here. An additional structural overburden extended northward to the Franklin

Mountains-Philip Smith Mountains domain boundary as indicated by the klippe near Porcupine Lake (figs. 4 and 5). The absolute timing of emplacement of this klippe is unknown, but it is analogous to Early Cretaceous allochthons farther west (Mull, 1982, 1985; Mayfield and others, 1988) and it was deformed by underlying asymmetrical folds and thrust faults characteristic of the Philip Smith Mountains domain, indicating it was emplaced before their formation.

Thus, a greater combined tectonic and depositional overburden probably was present in the Philip Smith Mountains domain than to the north. The lesser overburden to the north could have facilitated the upright growth of detachment folds, whereas the greater overburden to the south may instead have favored the formation of asymmetrical folds and thrust faults. Similarly, the lesser overburden to the north may have favored backthrust displacement on the Kayak Shale detachment, as opposed to the forward displacement to the south. The major change between the Philip Smith and Franklin Mountains domains in the character of rocks beneath the Kayak Shale detachment is the most obvious explanation for the corresponding change in the mode of deformation beneath the detachment, but it is also possible that the amount of overburden had some influence.

The Front Ranges and Franklin Mountains domains are characterized by a relatively low average shortening (about 24 percent). The cross section shows only the northernmost part of the Philip Smith Mountains domain, and includes the major structural low in the Porcupine Lake vicinity, which is characterized by less structural relief and, hence, less shortening than is typical for the domain. Thus, the shortening determined for the domain from the cross section (about 27 percent) probably is lower than the average shortening for the domain as a whole, and does not include the major shortening associated with emplacement of the Mt. Annette allochthon. The folds in the Lisburne Group in the Philip Smith Mountains domain are about the same arc-length as to the north, but generally are tighter, overturned, and truncated by thrust faults. Thus, a greater average shortening would be expected in this domain. This difference in shortening quite likely had an influence both on the sense of displacement on the Kayak Shale detachment and on the geometry of overlying structures. A low average shortening may have allowed backthrust displacement and formation of upright folds. However, as shortening and consequent structural thickening increased, it seems likely that structures would have developed a more consistent sense of forward vergence.

SUMMARY AND CONCLUSIONS

A transect across the northeastern Brooks Range in the vicinity of the Canning River displays well-exposed examples of a passive-roof duplex and shale-cored detachment folds. The structural stratigraphy of the region has played a fundamental role in the types of structures that formed. A thick shale unit, the Kayak Shale, has served as a major detachment horizon, which separates structural-stratigraphic units that have deformed quite differently. Carbonates of the Lisburne Group form the dominant competent unit above the Kayak Shale and define the characteristic fold and fault spacing above the detachment. Less competent clastic rocks of the overlying Sadlerochit Group have deformed with the Lisburne Group, but also display closer-spaced folds and thrust faults. Below the Kayak Shale detachment, the structural stratigraphy varies from north to south. In the north, previously complexly deformed sub-Mississippian rocks plus a veneer of Mississippian Kekiktuk Conglomerate have deformed relatively competently, despite their lithologically heterogeneous, well-stratified character. To the south, a southward-thickening wedge of Middle Devonian to Lower Mississippian clastic rocks, including equivalents of the Kekiktuk Conglomerate, apparently constitutes a structural-stratigraphic unit that deformed independently of the pre-Mississippian rocks to the north.

The transect can be divided into three structural domains based on variations in structure. Two domains constitute most of the transect and are characterized by anticlinoria cored by sub-Mississippian rocks with a cover shortened by upright folds formed above the Kayak Shale. The northern, or Front Ranges, domain is characterized by anticlinoria that are smaller in length, width, and amplitude than those in the central, or Franklin Mountains, domain. The southern, or Philip Smith Mountains, domain is characterized by north-vergent asymmetrical folds and thrust faults formed above the Kayak Shale and an absence of anticlinoria.

In the Front Ranges and Franklin Mountains domains, the structure below the Kayak Shale is interpreted to be a duplex with a floor thrust at depth in the sub-Mississippian rocks and a roof thrust in the Kayak Shale. Since the floor and linking thrusts of this duplex are not exposed, the depth to detachment, and hence the amount of shortening accommodated by the duplex, are conjectural. However, the geometry of the upper surface of the horses suggests a fault-bend fold model with a shortening approximately equal to that accommodated above the roof thrust. Other models require a deeper floor thrust for the duplex, with shortening less than that accommodated by the cover. The roof thrust is pinned to the north, requiring that shortening above the duplex must be accommodated by

backthrust displacement on the roof thrust. Thus, the duplex is a passive-roof duplex, regardless of the actual geometry of the underlying horses. Surface observations provide the basis for a balanced cross section showing a subsurface reconstruction of the preferred fault-bend fold geometry for the duplex and representing the detachment folds above its roof thrust. Shortening in the duplex and its cover are approximately equal in this balanced cross section, which supports the viability of the interpretation that the Front Ranges and Franklin Mountains domains are underlain by a passive-roof duplex.

The roof of this duplex is unusual in that it is well-preserved and has been shortened by folding, without significant thrust faulting. The folds in the roof are interpreted to be detachment folds that differ from the most familiar examples of detachment folds in that they are cored by shale, instead of evaporites. On average, the detachment folds in the Front Ranges and Franklin Mountains domains are upright (with respect to the underlying detachment horizon) and symmetrical. Hindward of the duplex, in the Philip Smith Mountains domain, forward-vergent asymmetrical, thrust-breached folds formed above the Kayak Shale and display geometries common in fold-and-thrust belts. These folds are also interpreted to be detachment folds because there is a complete transition in geometry from the documented detachment folds to the north. This suggests that a thrust-truncated-detachment fold model may be applicable to many fault-related folds, although fault-bend and fault-propagation fold models have most typically been applied in recent years.

The factors that control the geometry of the structures and their variations along the transect are uncertain. However, possible controlling factors are suggested by the structural stratigraphy and by variations in rock characteristics that correspond spatially with changes in structural geometry. The presence of the thick and incompetent Kayak Shale allowed detachment between under- and overlying competent units that shortened in different ways. In addition, the thick, incompetent shale was a major, if not the main, factor favoring formation of detachment folds in the overlying competent carbonate rocks of the Lisburne Group. A change from upright, symmetrical detachment folds to the north to forward-vergent, thrust-truncated detachment folds to the south corresponds with (1) a probable increase in depositional and tectonic overburden, (2) an increase in shortening, and (3) a change in underlying structural topography from smooth, high-relief, long-wavelength structures to rougher, lower-relief, shorter-wavelength structures. This southward decrease in the size of fold-and-thrust structures beneath the regional detachment horizon corresponds with, and likely is genetically related to, a southward change from previously highly deformed, lithologically heterogeneous rocks to a previously undeformed, southward-thickening clastic wedge.

ACKNOWLEDGMENTS

ARCO Alaska Inc. provided the support for the initial phases of this study and permission to present the results publicly. ARCO geologists who participated in the mapping during the summers of 1983 and 1984 included myself, J.S. Namson, T.L. Davis, J.A. Helwig, T.E. Moore, M. Churkin, and C.K. Worley. I particularly thank J.S. Namson, both for introducing me to the "Suppe approach" to fold-and-thrust structures and for taking the lead in constructing the cross section. M.D. Mangus also helped greatly by providing an introduction to the geology of the region in 1983.

Many of the interpretations presented here evolved during later phases of the study, which were part of a continuing program of geological research in the northeastern Brooks Range by the University of Alaska Fairbanks (UAF), with field work conducted during the summers of 1986 to 1991. This work was supported by grants from Amoco Production Company, ARCO Alaska, Inc., BP Exploration (Alaska) Inc., Chevron USA, Inc., Conoco Inc., Elf Exploration, Inc., Exxon Company, USA, Japan National Oil Corporation, Mobil Exploration and Producing U.S. Inc., Murphy Exploration and Production Company, Phillips Petroleum Company, Shell Western Exploration & Production Inc., Texaco Inc., and Union Oil Company of California. Additional support was provided by the University of Alaska Fairbanks and by the Petroleum Research Fund (administered by the American Chemical Society). Field work would not have been possible without helicopter and other logistical support provided by the Alaska Division of Geological & Geophysical Surveys (DGGS) during 1986 and 1987, and helicopter support provided at cost by the U.S. Fish and Wildlife Service during 1988 to 1991.

University of Alaska graduate students T.A. Imm, B.S. (Till) McMullen, A.J. Meigs, J.A. Rogers, and J.A. Ziegler have conducted studies in the general area of the transect, and W.R. Camber, C.L. Hanks, T.X. Homza, and A.V. Anderson have conducted studies in areas with features analogous to those of the transect. Although the results of these studies are not reported here, they have contributed to overall understanding of the transect. This work has also benefitted from discussions with J.G. Clough, R.K. Crowder, J. Decker, D.M. Dolberg, C.G. Mull, M.S. Robinson, P. O'Sullivan, and K.F. Watts. I wish to thank Deborah Coccia and Joseph Enzweiler of Photo-Graphics in the Geophysical Institute for their fine drafting, and C.G. Mull and T.E. Moore for their helpful reviews.

REFERENCES

Anderson, A.V., 1990, Middle Devonian to Lower Mississippian clastic depositional cycles, upper Kongakut River, northeastern Brooks Range, Alaska, preliminary results: Alaska Division of Geological & Geophysical Surveys, Public-Data File 90-2B, 8 p., 2 sheets.

_____1991a, Geologic map and cross-sections, headwaters of the Kongakut and Aichilik Rivers, Demarcation Point A-4 and Table Mountain D-4 Quadrangles, eastern Brooks Range, Alaska: Alaska Division of Geological & Geophysical Surveys, Public-Data File 91-3, 24 p., 2 sheets, scale 1:25,000.

_____1991b, Ulungarat Formation: Type section of a new formation, headwaters of the Kongakut River, eastern Brooks Range, Alaska: Alaska Division of Geological & Geophysical Surveys, Public-Data File 91-4, 28 p.

Anderson, A.V., and Wallace, W.K., 1991, Middle Devonian to Early Mississippian stratigraphic record of the formation of a passive continental margin in northeastern Alaska: Geological Society of America Abstracts with Programs, v. 23, no. 5, p. 436.

Banks, C.J., and Warburton, J., 1986, "Passive-roof" duplex geometry in the frontal structures of the Kirthar and Sulaiman mountain belts, Pakistan: Journal of Structural Geology, v. 8, nos. 3 and 4, p. 229-237.

Bird, K.J., 1986, The framework geology of the North Slope of Alaska as related to oil-source rock correlations, *in* Magoon, L.B., and Claypool, G.E., eds., Alaska North Slope oil-rock correlation study: American Association of Petroleum Geologists Studies in Geology no. 20, p. 3-29.

Bird, K.J., and Bader, J.W., 1987, Regional geologic setting and history of petroleum exploration, *in* Bird, K.J., and Magoon, L.B., eds., Petroleum geology of the northern part of the Arctic National Wildlife Refuge, northeastern Alaska: U.S. Geological Survey Bulletin 1778, p. 17-25.

Boyer, S.E., and Elliot, D., 1982, Thrust systems: American Association of Petroleum Geologists Bulletin, v. 66, no. 9, p. 1196-1230.

Brosgé, W.P., and Reiser, H.N., 1965, Preliminary geologic map of the Arctic Quadrangle, Alaska: U.S. Geological Survey Open-File Report 65-22, 1 sheet, scale 1:250,000.

Brosgé, W.P., Reiser, H.N., Dutro, J.T., Jr., and Detterman, R.LK., 1976, Reconnaissance geologic map of the Table Mountain Quadrangle, Alaska: U.S. Geological Survey Open-File Report 76-546, 2 sheets, scale 1:200,000.

Brosgé, W.P., Nilsen, T.H., Moore, T.E., and Dutro, J.T., Jr., 1988, Geology of the Upper Devonian and Lower Mississippian Kanayut Conglomerate in the central and eastern Brooks Range, *in* Gryc, G., ed., Geology and exploration of the National Petroleum Reserve in Alaska, 1974 to 1982: U.S. Geological Survey Professional Paper 1399, p. 299-316.

Bruns, T.R., Fisher, M.A., Leinbach, W.J., Jr., and Miller, J.J., 1987, Regional structure of rocks beneath the coastal plain, *in* Bird, K.J., and Magoon, L.B., eds., Petroleum geology of the northern part of the Arctic National Wildlife Refuge, northeastern Alaska: U.S. Geological Survey Bulletin 1778, p. 249-254.

Churkin, M., Jr., Namson, J.S., and Wallace, W.K., 1989, Mt. Annette allochthon, a klippe of Mississippian-Triassic chert and Cretaceous flysch, northeastern Brooks Range: Geological Society of America Abstracts with programs, v. 21, no. 5, p. 66.

Dahlstrom, C.D.A., 1990, Geometric constraints derived from the law of conservation of volume and applied to evolutionary models for detachment folding: American Association of Petroleum Geologists Bulletin, v. 74, no. 3, p. 336-344.

Davis, D.M., and Engelder, T., 1985, The role of salt in fold-and-thrust belts: Tectonophysics, v. 119, p. 67-88.

Homza, T.X., 1992, A detachment fold-truncation duplex, southwest Bathtub Ridge, northeastern Brooks Range, Alaska: Master of Science thesis, University of Alaska, Fairbanks, 110 p.

Jamison, W.R., 1987, Geometric analysis of fold development in overthrust terranes: Journal of Structural Geology, v. 9, no. 2, p. 207-219.

Laubscher, H.P., 1977, Fold development in the Jura: Tectonophysics, v. 37, p. 337-362.

Mayfield, C.F., Tailleur, I.L., and Ellersieck, I., 1988, Stratigraphy, structure, and palinspastic synthesis of the western Brooks Range, northwestern Alaska, Chapter 7, *in* Gryc, G., ed., Geology and Exploration of the National Petroleum Reserve in Alaska, 1974 to 1982: U.S. Geological Survey Professional Paper 1399, p. 143-186.

McMechan, M.E., 1985, Low-taper triangle-zone geometry: An interpretation of the Rocky Mountain foothills, Pine Pass-Peace River area, British Columbia: Bulletin of Canadian Petroleum Geology, v. 33, no. 1, p. 31-38.

McMullen, B.S., 1989, Structural geometry and evolution of the western Shublik Mountains, northeastern Brooks Range, Alaska: Master of Science thesis, University of Alaska, Fairbanks, 171 p.

Meigs, A.J., 1989, Structural geometry and sequence in the eastern Sadlerochit Mountains, northeastern

Brooks Range, Alaska: Master of Science thesis, University of Alaska, Fairbanks, 220 p.

Mitra, S., 1986, Duplex structures and imbricate thrust systems: Geometry, structural position, and hydrocarbon potential: American Association of Petroleum Geologists Bulletin, v. 70, no. 9, p. 1087-1112.

Molenaar, C.M., Bird, K.J., and Kirk, A.R., 1987, Cretaceous and Tertiary stratigraphy of northeastern Alaska, *in* Tailleur, I.L., and Weimer, P., eds., Alaskan North Slope geology: Pacific section, SEPM and Alaska Geological Society, Book 50, p. 513-528.

Mull, C.G., 1982, Tectonic evolution and structural style of the Brooks Range, Alaska: An illustrated summary, *in* Powers, R.B., ed., Geologic studies of the Cordilleran thrust belt: Rocky Mountain Association of Geologists, Denver, Colorado, v. 1, p.1-45.

Mull, C.G., 1985, Cretaceous tectonics, depositional cycles, and the Nanushuk Group, Brooks Range and Arctic Slope, Alaska, *in* Huffman, A.C., Jr., ed., Geology of the Nanushuk Group and related rocks, North Slope, Alaska: U.S. Geological Survey Bulletin 1614, p. 7-36.

Namson, J.S., and Wallace, W.K., 1986, A structural transect across the northeastern Brooks Range, Alaska: Geological Society of America Abstracts with Programs, v. 18, no. 2, p. 163.

Rattey, R.P., 1985, Northeastern Brooks Range, Alaska: New evidence for complex thin-skinned thrusting: American Association of Petroleum Geologists Bulletin, v. 69, no. 4, p. 676.

Reiser, H.N., Brosgé, W.P., Dutro, J.T., Jr., and Detterman, R.L., 1971, Preliminary geologic map, Mt. Michelson Quadrangle, Alaska: U.S. Geological Survey Open-File Report 71-237, 1 sheet, scale 1:200,000.

Rogers, J.A., 1992, Lateral variation of range-front structures and structural evolution of the central Shublik Mountains and Ignek Valley, northeastern Brooks Range, Alaska: Master of Science thesis, University of Alaska, Fairbanks, 128 p.

Suppe, J., 1983, Geometry and kinematics of fault-bend folding: American Journal of Science, v. 283, p. 684-721.

Suppe, J., 1985, Principles of structural geology: Prentice-Hall, Englewood Cliffs, New Jersey, 537 p.

Vann, I.R., Graham, R.H., and Hayward, A.B., 1986, The structure of mountain fronts: Journal of Structural Geology, v. 8, nos. 3 and 4, p. 215-227.

Wallace, W.K., and Hanks, C.L., 1990, Structural provinces of the northeastern Brooks Range, Arctic National Wildlife Refuge, Alaska: American Association of Petroleum Geologists Bulletin, v. 74, no. 7, p. 1100-1118.

Wallace, W.K., Watts, K.F., and Hanks, C.L., 1988, A major structural province boundary south of Bathtub Ridge, northeastern Brooks Range, Alaska: Geological Society of America Abstracts with programs, v. 20, no. 3, p. 241.

Wiltschko, D.V., and Chapple, W.M., 1977, Flow of weak rocks in Appalachian Plateau folds: American Association of Petroleum Geologists Bulletin, v. 61, no. 5, p. 653-670.

Ziegler, J.A., 1989, A detailed structural analysis across a regional unconformity, forks of the Canning River, Franklin Mountains, northeastern Brooks Range, Alaska: Master of Science thesis, University of Alaska, Fairbanks, 302 p.

CONTENTS OF PREVIOUS SHORT NOTES ON ALASKAN GEOLOGY

Short Notes on Alaskan Geology-1976: **DGGS Geologic Report 51 (out of stock, $3.50 photocopied)**

Short Notes on Alaskan Geology-1977**: DGGS Geologic Report 55 (out of stock, $5.00 photocopied)**

Short Notes on Alaskan Geology-1978**: DGGS Geologic Report 61 ($2.00)**

Short Notes on Alaskan Geology-1979-80**: DGGS Geologic Report 63 ($1.00)**

Short Notes on Alaskan Geology-1981: **DGGS Geologic Report 73 ($3.00)**

Short Notes on Alaskan Geology-1982-83**: DGGS Professional Report 86 ($2.50)**

Short Notes on Alaskan Geology-1991**: DGGS Professional Report 111 ($8.00)**

Thick buried peat layers are laterally extensive beneath the salt marsh at Chickaloon Bay and are exposed in meander banks along the Chickaloon River and other streams crossing the marsh. At location 92-17 (lower photograph), radiocarbon age of 0-259 yr B.P. and was probably submerged and buried as a result of subsidence during the 1964 event. Peat from the top of the second buried peat layer (at shovel tip) has a calibrated age of 761-1,060 yr B.P. and was probably buried as a result of the previous great earthquake. Photos by R.A. Combellick.